Authors' response to referee comment RC1
on manuscript
"Direct links between hygroscopicity and mixing state of ambient aerosols:
Estimating particle hygroscopicity from their single particle mass spectra"

We thank Referee #1 for the comments and suggestions. We have addressed every comment and made significant changes to the paper to improve the paper. Again, the referee's comments are greatly appreciated.

Referee Comments in black bold.

Authors' Response **in** blue.

Changes in manuscript **in** *Red italic.*

Major comments

(1) The authors showed that the temporal variations of the estimated particle hygroscopicity were consistent with the back-trajectory analysis and atmospheric visibility observations. It is hard to believe that hygroscopicity could be simply explained by the back-trajectory analysis, or the observed hygroscopicity could be a major reason for the visibility. A closer look at the discussion revealed that such conclusions were not precisely summarized.

Response:

We agreed that there were some shortcomings in the original discussions. In the original manuscript, the back trajectories and visibility were included to support the estimated hygroscopicity, because of their connections to hygroscopicity. The original manuscript has been rearranged and revised considerably to address the referee's comments. In the revised manuscript, the back trajectories were just used to offer some general descriptions of the meteorological conditions. As suggested in the last comment. The correlations between PM and visibility by either considering the hygroscopicity or not have been added in the revised manuscript to extend the analysis of visibility.

Changes in manuscript:

Line 483-500:

"The temporal variation of particle estimated GF from Sep-12 to Sep-28 was illustrated in Figure 9. Four distinct periods (P1-P4) were identified based on their different hygroscopicity distributions. Generally, the P1 and P3 periods were characterized by elevated MH mode which dominated the ATOFMS particles numbers, while in P2 and P4 the MH particles decreased significantly and sea salt mode was pronounced. Back trajectories during P1-P4 were analyzed using HYSPLIT mode (Draxler, R. R. and Rolph, G. D.,2003) to inspect the airmass that influenced the sampling site (Figure S8). The 24-hour back trajectories suggests that the airmass in P1 period mainly circulated in local regions from northwest direction to Shanghai. The local circulations brought regional aerosol pollution to the sampling site, resulted in elevated concentrations of particles, especially the MH particles. During P2, the airmass originated from the ocean in northeast direction with less continental influence. The cleaner air from the ocean almost wiped out the accumulated particles observed in P1 and the concentrations of sea salt particles increased. In the majority of time during P3, the airmass

stayed over continental areas. The MH particles dominated particle numbers in this period and the sea salt mode were barely present. During Sep-18 to Sep-20 in P3, the LH particles showed increased concentrations and gradually decreased after Sep-20. Similar to P1, the origin of airmass in P4 shifted to the ocean in eastern directions and SS mode emerged again. Both the particle spectra and the back trajectories supported that the GF mode of 1.6 can be mainly attributed to sea salt particles."

Line 603-624:

'An exponential relation between visibility and PM concentrations was found by the previous study (Qu et al., 2015). After applying the exponential fitting to the visibility and particle volume concentrations, we found a moderate correlation for ATOFMS particles (R^2=0.45) and better correlations for $PM_{2.5}$ concentrations (R^2=0.64) (Figure S12). However, the fitting errors were clearly dependent on ambient RH, with larger errors in higher humidity, indicating that hygroscopicity might affect visibility degradations, which were consistent with other studies (Chen et al., 2012;Liu et al., 2012). To further examine the effect of particle hygroscopicity on visibility, we derived particle volumes in different RH using estimated κ values (Petters and Kreidenweis, 2007). The κ values were calculated using the GF of individual particles at 85% RH for ATOFMS data and the average GF of 1.36 for $PM_{2.5}$ volume data. With hygroscopicity being considered, we found notable improvements of the correlations between PM concentrations and visibility, with the improved correlation observed for $PM_{2.5}$ concentrations (R^2=0.82) after applying correction for hygroscopicity (Figure 12). However, this improvement was barely the case for NH particles, probably due to the negligible hygroscopic growth. For the ATOFMS particles in different GF modes, we found the highest R^2 (0.65) for the MH particles. The correlation between SS particles and visibility was distorted due to the visibility reached its limit (10 km) when sea salt mode was pronounced (Figure 9). The R^2 between MH particles and visibility suggests that the variation of MH particles accounted for the major part of visibility changes (65%) during this period, which coincided well with the major contribution of nitrate and sulfate to light extinction (61%) in eastern China areas (Qu et al., 2015). These results indicate the importance of discriminating particles by hygroscopicity in explaining the measured visibility.'

(2) The results indicate that particles with stronger hygroscopicities were more likely to have higher effective densities. Is it suitable for all the observed particle types? Could it be theoretically supported? This is hard to believe. For instance, aging of Dust particles lead to nitrate coatings, which would lower the effective density, but increase the hygroscopicity.
Response:

We agree with the referee's opinion, and decided to remove this part in the revised manuscript. Density is indeed a property related to particle types. We observed smaller ρ_{eff} of EC particles than dust/ash in less hygroscopic range based on our data, suggesting that it is inappropriate to discuss density in a general way without referring particle types. In the original manuscript, the effective density was included for the sake of a complete report of the measured data. As suggested by another referee, the discussions of effective density seem to be out of place, as the main objective of this study is to connect hygroscopicity to composition. We agree with the referee's opinion, since hygroscopicity is depending on

particle composition, rather than density. The presented data only suggested a statistical positive correlation between effective density and GF, but the explanation of the correlation need other information including particle shapes, which also affect ρ_{eff} (Ghazi et al., 2013;Khalizov et al., 2012). On the other hand, the effective densities were not well incorporated into the discussions on estimated hygroscopicity. We note that the hygroscopicity prediction algorithm is just depending on particle mass spectra and the density was not involved in calculation.

Changes in manuscript:

Relevant discussions are removed.

Specific comments:

1. Abstract: "These hygroscopicity estimation results with single particle mass spectra analysis can provide critical information on particulate water content, particle source apportionment, and aging processes." I wonder how hygroscopicity can provide critical information on the source of particles. The authors did not discuss this in the text but only took sea salt particles as an example in Figure 5.

Response:

We agree that the source apportionment was not clearly presented. Particle hygroscopicity can offer some aids in the source apportionment of single particles. An example is the Al-Si particle in Dust/ash type. Although most of the dust/ash particles show considerable hygroscopicity, the Al-Si particles had low hygroscopicity. Thus, we ascribe the sources of Al-Si to soil dust, as some laboratory studies also found soil dust has low hygroscopicity. Without hygroscopicity information, the identification of Al-Si particle source would be difficult, because the Si and Al peaks were also present in ash particles from coal emissions (Xu et al., 2017).

Changes in manuscript:

Line 42-46:

"Based on the combined information on particle composition, hygroscopicity, airmass back trajectories and ambient pollutants concentrations, we inferred that the NH, LH, MH, SS modes were characterized by POA/EC, SOA, SIA and salts compositions, respectively. The proposed method would provide additional information to the study of particle mixing states, source identification and visibility degradation."

Line 268-276:

"Some of the clusters showed characteristic hygroscopicity distributions which offered values in the source apportionment of these particles. As an illustration, we presented the mass spectra and hygroscopicity distribution of the Al-Si cluster in Figure 3. The mass spectra of Al-Si particles showed stronger aluminum (27Al⁺) and silicate (-76SiO₃⁻) peaks in their positive and negative spectra, respectively. Particle number distribution of Al-Si particles suggested that they were detected with the highest probability at GF 1.1. In the preliminary study we identified the similar Al-Si particles exclusively in NH mode (Wang et al., 2014). Based on their hygroscopicity distribution, we assumed the Al-Si particles are soil dusts according to their reported low hygroscopicity (Koehler et al., 2009)."

2. Introduction: "Herich et al. have firstly applied the HTDMA-ATOFMS system to investigate particle composition as a function of hygroscopicity." Some results related to such measurements are missing here.

Response:

We have added discussions on the findings of prior studies.

Changes in manuscript:

Line 96-102:

"Herich et al. firstly applied the tandem HTDMA-ATOFMS system to characterize particle composition of different hygroscopicity (Herich et al., 2008;Herich et al., 2009). A large portion of the less hygroscopic modes were found to be contributed by organics and combustion species in both urban and remote sites, while the sulfates and nitrates were present in almost all particles independent of hygroscopicity. These findings were similarly observed in our previous characterization using HTDMA-ATOFMS in Shanghai city (Wang et al., 2014), except higher nitrate and sulfate intensities were found in hygroscopic particles in our study."

3. Experimental section: what is the accuracy of hygroscopicity determination by the HTDMA? What is the uncertainty in GF prediction?

Response:

We have added relevant information in manuscript as follows.

Changes in manuscript:

Line 219-226:

"The uncertainties in the GF prediction in this method were estimated. The sources of uncertainties may stem from the errors in GF selection in HTDMA and the algorithm itself. After the 0.5 power treatment to peak intensities, the only parameter that can affect the estimated GF would be the matching criteria of particles. We have changed the matching criteria of 95-100% maximum dot products to 90-100% and 98-100% and the variations of GFs were inspected (Figure S5). Based on the distributions of GF variations, we estimated the overall uncertainties in the GF estimations is within ±0.15."

4. Line 148: "The DMAs were kept to select the desired diameters before significant number of particles were chemical analyzed by ATOFMS." What does a significant number refer to?

Response:

Particles with certain GFs (e.g., 1.4) typically have higher concentrations in the downstream of HTDMA, i.e. faster detection of particles in ATOFMS at these GFs. For other GFs (especially near the limits of GF distribution, e.g., 0.9, 1.7) particles had much smaller concentrations. For the sake of the statistical significance, we decided that the number of acquired spectra at each GF much be larger than 200.

Changes in manuscript:

Line 166 -167:

"The HTDMA-ATOFMS system was kept sampling until a sufficient number of particles (> 200) were analyzed by ATOFMS for each GF setting (Table 1)".

5. Line 171: "This problem was relieved by taking the 0.5 power (square root) of peaks intensities." Maybe more information is required to validate such treatments.

Response:

We took 0.5 power of mass peak intensities in the estimation of GF. Similar treatment (logarithm) of ATOFMS spectra was proposed in prior literature (Rehbein et al., 2012). This treatment was applied to both the HTDMA-ATOFMS and ambient particle data before the evaluation of particle similarity. It is known that ATOFMS mass peak intensities are affected not only by composition abundance in particles, but also by their ionization efficiencies in ATOFMS. The ATOFMS is more sensitive to metallic compositions than organics, resulting disproportionate large peaks of metals to reflect their actual concentrations in particles. We suppose the 0.5 power treatment of mass peak areas can partly solve the bias of ATOFMS toward different compositions, since it reduces larger peaks more rapidly than small peaks.

The application of 0.5 power treatment is not just based on speculation. We find it gave better results in the estimated hygroscopicity. We carried two rounds of GF estimations in which the pretreatment was either included or not. In figure S3 the two distributions of estimated GF are compared. As shown in figure, the hygroscopicity distribution without treatment suggests abnormal shape with an extra mode of GF=1.35, which was inconsistent with HTDMA observations in this area. As a comparison, with the 0.5 power treatment to peak intensities and the obtained hygroscopicity distributed regularly with smoother shapes, which agrees well with the HTDMA data of ambient particles. It is noted that in the two estimations the dataset and algorithm are identical with the only difference of the pretreatment. This fact suggests that the 0.5 power treatment could indeed be used to improve hygroscopicity estimation.

As a reply to the referee's concern, we have added relevant information in the revised manuscript.
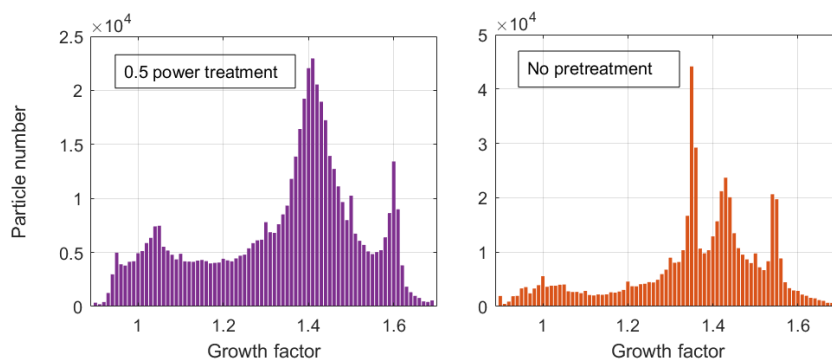
Figure S3. The estimated particle hygroscopicity distribution with (left) and without (right) taking 0.5 power of peak intensities.

Changes in manuscript:

Line 194-196:

"The 0.5 power treatment to peaks intensity was applied because it offered better results in the estimation of hygroscopicity than without it, as discussed in the supplemental information (Figure S3)."

6. Line 239: "About 20% of analyzed particles are classified as Amines-rich". Is there any explanation for such a high fraction of Amine particles?

Response:

Amine particles constitute an important type of particles and were normally detected by single particle techniques in Shanghai area. A previous single particle study suggested that the number fraction of amine particles varies considerably in different seasons (4.4% in summer vs. 23.4% in winter), which can be explained by gas-to-particle partitioning of amines at lower temperatures (Huang et al., 2012). Except temperature variations, relative humidity was also found to promote particulate amine formation through acid–base reactions of amines in high RH periods (Huang et al., 2012;Chen et al., 2019;Zhang et al., 2012). The meteorological data during the HTDMA-ATOFMS experiment indicate low temperatures (3-10 ℃, 6 ℃ in average) and higher relative humidity (50-93%, 78% in average) in this period, which both favor the formation of particulate amines in ambient aerosol. In the preliminary HTDMA-ATOFMS experiment amine particles makes up 20% of particle numbers, a comparable fraction to present study (~25%) (Wang et al., 2014).

Changes in manuscript:

Line 284-287:

"Particulate amine formation was favored in low temperatures and higher humidity conditions (Huang et al., 2012;Zhang et al., 2012). The elevated amine particle fractions may be related to the low temperature (6 ℃) and high humidity (78% RH) condition during this experiment."

7. Lines 251-252: "…CNO peaks, which are present in biomass particles, were absent very weak, suggesting that biomass burning is not their source." Do you mean CN/CNO peaks are necessarily served as markers for biomass burning?

Response:

In the ATOFMS source characterizations, biomass particles produce strong CN/CNO peak in negative spectra (Silva et al., 1999; Zauscher et al., 2013;Pratt and Prather, 2009). This mass spectral feature was also observed by studies in China (Bi et al., 2011) and our laboratory experiment on various biomass particles. We suppose the presence of CN/CNO peak is related to the ubiquity of nitrogen-containing organics in biomass, such as amino acids. Except CN/CNO, other peaks at m/z at -45/-59/-71/-73 can also be used to indicate biomass, although their intensities were typically weaker than CN/CNO. We think it is insufficient to indicate biomass particles just from the presence of CN/CNO, since CN/CNO can also be produced from other sources. The original sentence is inaccurate and we have revised it.

Changes in manuscript:

Line 298-302:

"Additionally, the -26CN and -42CNO peak which are typically present in biomass particles, were found to be weak or absent, suggesting that there are some chemical differences between Ammonium/OC and biomass particles (Silva et al., 1999;Zauscher et al., 2013;Pratt and Prather, 2009)."

8. Line 256: "…characterizations, it is possible that the ammonium/OC particles might be from coal burning sources". There are already some paper published reporting the single particle mass spectra of coal burning particles in China. The author should directly refer to these papers, rather than (Healy et al., 2010). Still, such an assignment might not be appropriate, since it is more likely produced from secondary processes, associated with high

abundance of ammonium sulfate.

Response:

We followed the referee's suggestion and revised the manuscript.

Changes in manuscript:

Line 305-310:

"A prior ATOFMS study identified the Ammonium/OC particles are from agricultural sources, and found most of them were present in higher photochemical oxidation periods (Qin et al., 2012), consistent with the prominent secondary peaks of ammonium found in this study. It is likely the organics in this type is secondary since the GF 1.2 is close to the hygroscopicity of SOA (GF=1.24 at 90% RH) (Gysel et al., 2007;Sjogren et al., 2008). "

9. Line 260: the authors further concluded that "These particles were not likely to be deeply aged particles, because their hygroscopicity was only moderate." It is a little bit confusing, since the aging should be deduced from the mass spectra, not the hygroscopicity. Hygroscopicity could be linked to the chemical compositions, but not particle age.

Response:

We agree that the original statement is inaccurate. We have modified this sentence.

Changes in manuscript:

Line 310-312:

"We inferred that the ammonium was not contributing significant mass fractions to these particles, due to the high hydrophilicity of ammonium salts while Ammonium/OC particles were only moderate hygroscopic ".

10. Line 398: "…higher hygroscopicity could play more important role…" higher correlation cannot infer the higher contribution of aerosol particles with higher hygroscopicity to visibility decrease. Is it possible to estimate the relative contribution based on the combined measurements in this study?

Response:

This comment is very instructive and we attempted to analysis hygroscopicity and visibility in further detail. We acknowledge that the original statement is over simplified since PM concentrations were also contributing to visibility degradation. To evaluate the role of hygroscopicity more explicitly, we compared PM concentrations with visibility in two situations where hygroscopicity was either considered or not. In the revision we only consider particle volume concentrations since hygroscopic growth increase particle volumes rather than particle numbers. The results suggested improved correlations between visibility and particle concentrations of LH, MH, SS, all ATOFMS particles and $PM_{2.5}$ concentrations with hygroscopic growth being considered.

Changes in manuscript:

Line 584-624:

"3.3.4 Comparing the estimated hygroscopicity with visibility

Particle optical properties were closely connected to hygroscopicity (Liu et al., 2012;Qu et al., 2015;Chen et al., 2012). The hygroscopic growth increases particle volumes and cross sections and is contributing to the visibility degradation. With the estimated hygroscopicity of ATOFMS particles, we correlated atmospheric visibility with particle concentrations to study their

contributions to the visibility variation. The ATOFMS particle volume concentrations were calculated for hygroscopicity modes of NH, LH, MH and SS based on ATOFMS particle diameter and numbers. The particle volume concentrations was used because hygroscopic growth change particle sizes rather than numbers (Chen et al., 2012). The visibility data was obtained from (https://www.wunderground.com/) logged in the Hongqiao airport (31°12'N, 121°20'E) and Pudong airport (31°9.3'N, 121°49'E) during the study period (see the map in Figure S5). The temporal variations of visibility in two sites correlated strongly (Figure S5), despite the 45 kilometers distance between two airports. The Fudan site is located roughly between the two airports, and the two sets of visibility data were averaged to represent the study site. In P2 and P4 the site was under the influences from ocean, resulting visibilities larger than 10 km (Figure 9). Apart from ATOFMS particles, contemporary $PM_{2.5}$ volume concentrations were also correlated with visibility. The $PM_{2.5}$ volume concentrations were derived from $PM_{2.5}$ mass concentrations using particle density (1.4 gcm^{-3}). A strong correlation between ATOFMS particle numbers and $PM_{2.5}$ was found (R^2=0.80).

An exponential relation between visibility and PM concentrations was generally found (Qu et al., 2015). With the application of the exponential fitting to the visibility and particle volume concentrations, we found moderate correlation for ATOFMS particles (R^2=0.45) and better correlations for $PM_{2.5}$ concentrations (R^2=0.64) (Figure S12). However, the errors of fittings were clearly dependent on ambient RH conditions, with increased errors in higher humidity This result indicates that hygroscopicity have played its roles in the visibility degradations (Chen et al., 2012;Liu et al., 2012). To account for particle hygroscopicity, we derived particle volumes in different RH using κ values (Petters and Kreidenweis, 2007). The κ values were calculated using the GF of individual particles at 85% RH for ATOFMS data and the average GF of 1.36 for $PM_{2.5}$ volume data. With hygroscopicity being considered, we found notable improvements of the correlations between PM concentrations and visibility, with the best correlation observed for $PM_{2.5}$ concentrations (R^2=0.82) after correction for hygroscopicity (Figure 12). However, this improvement was barely present for NH particles due to the negligible hygroscopic growth. For the ATOFMS particles in different GF modes, we found the highest R^2 (0.65) for the MH particles and gradually loose correlations from MH to NH mode. The low correlation for SS particles is related to the saturated visibility (10 km) when sea salt mode was pronounced (Figure 9). The R^2 of MH particles suggests the MH particles were explaining the major part of visibility variations (65%) in this period, which coincided well with the major contribution of nitrate and sulfate to light extinction (61%) in eastern China areas (Qu et al., 2015). These facts indicate the importance of discriminating particles by hygroscopicity in explaining the measured visibility."

Minor:

References such as "Zelenyuk et al.(Zelenyuk et al., 2008)" is incorrectly formatted.

Response:

We have made correction to this reference.

Changes in manuscript:

Line 93-96:

"Zelenyuk et al. connected a single particle mass spectrometer SPLAT with HTDMA to demonstrate the capability of this system to derive quantitative information on aerosol

hygroscopicity, composition, and effective density (Zelenyuk et al., 2008).”

Line 98: “HTMDA-ATOFMS”

Response:

This mistyping was corrected.

Changes in manuscript:

Line 107-108:

“We conducted a comprehensive HTDMA-ATOFMS experiment with the particle GF varied in a more complete range (0.9~1.7, 85% RH)”.

Line 183: “value from 0.1 to 1.7” is it 0.9-1.7?

Response:

The mistyping was corrected.

Changes in manuscript:

Line 208-209:

“where: GF_{pred}= the estimated GF of ambient particle, GF_i= GF value from 0.9 to 1.7 interspaced by 0.1, F_i= number percentages of the matched particles in each GF bin.”

Line 314: “can be measured on by HTDMA-ATOMFS system”

Response:

The discussions of effective density were removed.

Changes in manuscript:

This sentence was removed after revision.

References

Bi, X. H., Zhang, G. H., Li, L., Wang, X. M., Li, M., Sheng, G. Y., Fu, J. M., and Zhou, Z.: Mixing state of biomass burning particles by single particle aerosol mass spectrometer in the urban area of PRD, China, Atmospheric Environment, 45, 3447-3453, 10.1016/j.atmosenv.2011.03.034, 2011.

Chen, J., Zhao, C. S., Ma, N., Liu, P. F., Gobel, T., Hallbauer, E., Deng, Z. Z., Ran, L., Xu, W. Y., Liang, Z., Liu, H. J., Yan, P., Zhou, X. J., and Wiedensohler, A.: A parameterization of low visibilities for hazy days in the North China Plain, Atmospheric Chemistry and Physics, 12, 4935-4950, 10.5194/acp-12-4935-2012, 2012.

Chen, Y., Tian, M., Huang, R.-J., Shi, G., Wang, H., Peng, C., Cao, J., Wang, Q., Zhang, S., Guo, D., Zhang, L., and Yang, F.: Characterization of urban amine-containing particles in southwestern China: seasonal variation, source, and processing, Atmospheric Chemistry and Physics, 19, 3245-3255, 10.5194/acp-19-3245-2019, 2019.

Ghazi, R., Tjong, H., Soewono, A., Rogak, S. N., and Olfert, J. S.: Mass, Mobility, Volatility, and Morphology of Soot Particles Generated by a McKenna and Inverted Burner, Aerosol Science and Technology, 47, 395-405, 10.1080/02786826.2012.755259, 2013.

Gysel, M., Crosier, J., Topping, D. O., Whitehead, J. D., Bower, K. N., Cubison, M. J., Williams, P. I., Flynn, M. J., McFiggans, G. B., and Coe, H.: Closure study between chemical composition and hygroscopic growth of aerosol particles during TORCH2, Atmospheric Chemistry and Physics, 7, 6131-6144, 2007.

Herich, H., Kammermann, L., Gysel, M., Weingartner, E., Baltensperger, U., Lohmann, U., and Cziczo, D. J.: In situ determination of atmospheric aerosol composition as a function of hygroscopic growth, Journal of Geophysical Research-Atmospheres, 113, D16213
10.1029/2008jd009954, 2008.

Herich, H., Kammermann, L., Friedman, B., Gross, D. S., Weingartner, E., Lohmann, U., Spichtinger, P., Gysel, M., Baltensperger, U., and Cziczo, D. J.: Subarctic atmospheric aerosol composition: 2. Hygroscopic growth properties, Journal of Geophysical Research-Atmospheres, 114, D13204
10.1029/2008jd011574, 2009.

Huang, Y., Chen, H., Wang, L., Yang, X., and Chen, J.: Single particle analysis of amines in ambient aerosol in Shanghai, Environmental Chemistry, 9, 202-210, 10.1071/en11145, 2012.

Khalizov, A. F., Hogan, B., Qiu, C., Petersen, E. L., and Zhang, R. Y.: Characterization of Soot Aerosol Produced from Combustion of Propane in a Shock Tube, Aerosol Science and Technology, 46, 925-936, 10.1080/02786826.2012.683839, 2012.

Koehler, K. A., Kreidenweis, S. M., DeMott, P. J., Petters, M. D., Prenni, A. J., and Carrico, C. M.: Hygroscopicity and cloud droplet activation of mineral dust aerosol, Geophysical Research Letters, 36, L08805
10.1029/2009gl037348, 2009.

Liu, X. G., Zhang, Y. H., Cheng, Y. F., Hu, M., and Han, T. T.: Aerosol hygroscopicity and its impact on atmospheric visibility and radiative forcing in Guangzhou during the 2006 PRIDE-PRD campaign, Atmospheric Environment, 60, 59-67, 10.1016/j.atmosenv.2012.06.016, 2012.

Petters, M. D., and Kreidenweis, S. M.: A single parameter representation of hygroscopic growth and cloud condensation nucleus activity, Atmospheric Chemistry and Physics, 7, 1961-1971, 2007.

Qin, X. Y., Pratt, K. A., Shields, L. G., Toner, S. M., and Prather, K. A.: Seasonal comparisons of single-particle chemical mixing state in Riverside, CA, Atmospheric Environment, 59, 587-596, 10.1016/j.atmosenv.2012.05.032, 2012.

Qu, W. J., Wang, J., Zhang, X. Y., Wang, D., and Sheng, L. F.: Influence of relative humidity on aerosol composition: Impacts on light extinction and visibility impairment at two sites in coastal area of China, Atmospheric Research, 153, 500-511, 10.1016/j.atmosres.2014.10.009, 2015.

Rehbein, P. J. G., Jeong, C.-H., McGuire, M. L., and Evans, G. J.: Strategies to Enhance the Interpretation of Single-Particle Ambient Aerosol Data, Aerosol Science and Technology, 46, 584-595, 10.1080/02786826.2011.650334, 2012.

Sjogren, S., Gysel, M., Weingartner, E., Alfarra, M. R., Duplissy, J., Cozic, J., Crosier, J., Coe, H., and Baltensperger, U.: Hygroscopicity of the submicrometer aerosol at the high-alpine site Jungfraujoch, 3580 m a.s.l., Switzerland, Atmospheric Chemistry and Physics, 8, 5715-5729, 2008.

Wang, X. N., Ye, X. N., Chen, H., Chen, J. M., Yang, X., and Gross, D. S.: Online hygroscopicity and chemical measurement of urban aerosol in Shanghai, China, Atmospheric Environment, 95, 318-326, 10.1016/j.atmosenv.2014.06.051, 2014.

Xu, J., Li, M., Shi, G., Wang, H., Ma, X., Wu, J., Shi, X., and Feng, Y.: Mass spectra features of biomass burning boiler and coal burning boiler emitted particles by single particle aerosol mass spectrometer, Science of The Total Environment, 598, 341-352, https://doi.org/10.1016/j.scitotenv.2017.04.132, 2017.

Zelenyuk, A., Imre, D., Han, J. H., and Oatis, S.: Simultaneous measurements of individual ambient particle size, composition, effective density, and hygroscopicity, Analytical Chemistry, 80, 1401-1407, 10.1021/ac701723v, 2008.

Zhang, G., Bi, X., Chan, L. Y., Li, L., Wang, X., Feng, J., Sheng, G., Fu, J., Li, M., and Zhou, Z.: Enhanced trimethylamine-containing particles during fog events detected by single particle aerosol mass spectrometry in urban Guangzhou, China, Atmospheric Environment, 55, 121-126, 10.1016/j.atmosenv.2012.03.038, 2012.

Authors' response to referee comment RC2
on manuscript
"Direct links between hygroscopicity and mixing state of ambient aerosols:
Estimating particle hygroscopicity from their single particle mass spectra"

We thank Referee#2 for the comments and suggestions. We have addressed every comment and made significant changes to the paper to improve the paper. Again, the referee's comments are greatly appreciated.

Referee Comments in black bold.

Authors' Response **in** blue.

Changes in manuscript **in** *Red italic.*

Major Comments

1. The authors claim that they can predict the growth factor from the mass spectra, but they mainly just showed associations between particle types and growth factors, not that the spectra provide a degree of predictability.

Response:

We thank the reviewer for this comment. We would call it "estimate" rather than "predict". The GF of a particle can be estimated based on HTDMA-ATOFMS data for two reasons. First, different particle types had distinct GF distributions. Second, particles in different bins had different mass spectra. In the revised manuscript, we have added a section to discuss this issue. The discussions of GF estimation were inserted between the discussions of HTDMA - ATOFMS data and estimated GF ambient particles.

Changes in manuscript:

Line 391-407:

"3.2 Predictability of hygroscopicity from particle mass spectra

The GF of a particle can be estimated based on HTDMA-ATOFMS data for two reasons. First, different particle types had distinct GF distributions. Second, particles in different GF bins had different mass spectra. The GF estimation from particle spectra requires that the HTDMA-ATOFMS data is capable to represent the major particle types normally presented in atmosphere, which is evidenced in the preceding discussions. In another aspect, the GF prediction from mass spectra also demands that HTDMA-ATOFMS data are sensitive to reflect the composition differences with GF variations.

To test the sensitivity of HTDMA-ATOFMS data, we evaluated the average spectral similarities between each pair of GF groups. The average similarities were calculated from the similarities between every possible pairs of particles from the two GF groups. The self-comparing of particles within the same GF group were excluded. As shown in Figure 6, we observed a general trend that particles in the same GF bins tend to produce the highest similarities. As the GF differences increase, the mass spectra similarity between two GF bins tended to decrease. This result is an evidence that the particles with different GFs are more likely to have discriminable mass spectra, which suggests that the HTDMA-ATOFMS dataset are capable to estimate hygroscopicity just from particle mass spectra."

2. The authors also did not explore whether ion peak areas such as sulfates and nitrates, which are critical for particle water uptake, were better predictors of growth factors than the particle types themselves.

Response:

We have followed this instructive comment and revise the paper carefully. We have correlated peak intensities of nitrate and sulfate with GF for all particles in the HTDMA-ATOFMS dataset. There were indeed correlations between nitrate and sulfate signals and hygroscopicity in certain GF range but a simple trend applicable to all GF was not found. Another characteristic of peak intensities is that their trends were dependent on particle types. The discussion of peak intensities with GF were added both for HTDMA-ATOFMS data and ambient ATOFMS particles.

Changes in manuscript:

Line 344-390:

"Apart from particle number distributions, the HTDMA-ATOFMS dataset provided another aspect of information regarding peak intensities with GF. In this study, we used relative peak intensities (peak areas normalized by the total areas in spectrum) to investigate its relation to GF. Generally, the responses of peak intensity to GF variation were found to be nonlinear, since they were correlated only within specific GF ranges. A simple trend applicable to whole GF range was not observed.

We presented the statistics of peak intensity of nitrate ($-46NO_2$, $-62NO_3$, $-125H(NO_3)_2$) and sulfate ($-80SO_3$, $-97HSO_4$) which were known to be critical to particle hygroscopicity (Figure 4). As previously observed (Herich et al., 2009;Herich et al., 2008;Wang et al., 2014), the nitrate and sulfate peaks were present in the majority of particles in all GF bins. However, peak intensities of nitrate and sulfate were indeed stronger in hygroscopic particles than hydrophobic particles. In Figure 4 we observed positive correlation between nitrate and sulfate intensities and GF in GF <1.2 range, suggesting contribution of nitrate and sulfate to particle hygroscopicity in low GF range (Figure 4). However, in higher GF range (GF 1.3-1.5), nitrate and sulfate peaks seem to reach a plateau with unclear dependence on GF. Nitrate and sulfate were known to contribute large fractions of particle mass in MH particles (Swietlicki et al., 2008;Laborde et al., 2013;Liu et al., 2014). The unclear trend of nitrate and sulfate with GF seem to suggest that nitrate and sulfate were in stable ratios since nitrate and sulfate peaks were dominating peak areas in negative spectra. For particles of even higher GF, differences were observed between GF 1.3-1.5 and GF 1.5-1.7 range in that stronger nitrate and weaker sulfate peaks were detected in the GF 1.3-1.5 range. Particles classification suggests that this general characteristic is also at variance for different particle types. The same statistics for EC and Dust/ash particles were presented in Figure 4. Compared with EC particles, smaller sulfate and stronger nitrate peaks were found in Dust/ash spectra, and the observed trend in total particles were less obvious in Dust/ash. These facts highlight the nonlinearity between peak intensities and GF and that particle types should also be considered in describing peak intensities.

The analysis of peak intensities with GF can disclose some atmospheric processes happened on aerosol. We take the Sea salt as an illustration. Sea salt particles were known to react with atmospheric nitric acid, with NaCl in fresh sea salt be transformed into NaNO3 in the reacted sea salt (Gard et al., 1998). This composition transformation is indicated in corresponding

changes of NaCl and NaNO$_3$ peak intensities in particle spectra. The unreacted sea salt particles tend to produce larger peaks of Na$_2$Cl$^+$ and NaCl$_2^-$ in spectra (Gaston et al., 2011;Prather et al., 2013). In particle spectra of reacted sea salt, the NaCl peaks (Na$_2$Cl$^+$, NaCl$_2^-$) decrease while NaNO$_3$ peaks (Na$_2$NO$_3^+$, Na(NO$_3$)$_2^-$) increase. We presented peak intensities of sea salt in GF 1.5-1.7 range where sea salt particles were detected with largest numbers (Figure 5). We found that the positive correlation between NaCl peak intensity and GF, and the negative correlation for NaNO$_3$ peaks. Therefore, the HTDMA-ATOFMS data supported that reacted sea salt have reduced hygroscopicity (Herich et al., 2009;Gaston et al., 2018). Laboratory HTDMA study suggested that NaCl and NaNO$_3$ have deliquesced at 85% RH and that the NaNO$_3$ (GF ~1.8) is less hygroscopic than NaCl (GF ~2.2) (Hu et al., 2010). The reduced hygroscopicity of sea salt is in line with the GF of sodium salts. However, the sea salt hygroscopicity (GF 1.5-1.7) was smaller than pure NaNO$_3$ salt (supposing fully reacted), suggested that the chemical transformation alone is not sufficient to account for the observed hygroscopicity of sea salt. We hypothesize that other compositions as organics were mixed into sea salt and contributed to the reduction of sea salt hygroscopicity (Gaston et al., 2011;Randles et al., 2004;Facchini et al., 2008)."

Line 548-583:
"3.3.3 Peak intensity variations with estimated GF
Particle hygroscopicity and peak intensities in particle mass spectra were correlated to show their connections. The correlation was illustrated similarly to the analysis of the HTDMA-ATOFMS dataset, as shown in Figure 11. In addition to the statistics on peak intensities of different GF, the number distributions ATOFMS particles with GF and peak intensities were presented for nitrate (-46NO$_2$, -62NO$_3$, -125H(NO$_3$)$_2$) and sulfate peaks (-97HSO$_4$, -80SO$_3$) in the lower panels in Figure 11. The general trends of peak intensities with GF in HTDMA-ATOFMS dataset was preserved in estimated GF of ambient particles. The trends of nitrate and sulfate peak intensities showed increases from NH to LH range and remained constant in the MH mode. Similar to HTDMA-ATOFMS particles, stronger nitrate peaks were detected in SS particles compared with the MH particles, while an opposite trend was observed for sulfate intensities. These results highlight the nonlinearity between GF and peak intensities of ATOFMS particles.

The nonlinearity of peak intensities with GF was also suggested by the different particle types presented in ATOFMS data. As shown in the lower panels in Figure 11, the distribution of ATOFMS individual particles showed enrichment in different areas in the GF-peak intensity diagram, suggesting the presence of particle groups of different compositions. To illustrate this character, we selected two areas with clear particle enrichments in GF-peak intensity diagram and their particle composition were analyzed (denoted as A and B in lower left panel in Figure 11). Obviously, particles in area A produced much larger nitrate signals than particles in area B. Particle numbers in the two areas suggested that Dust/ash dominated particles in area A (59%) while in area B the Dust/ash only accounted for 14% of particles (Figure S10). As a contrast, particles in area B were dominated by Aged EC type (53%) followed by 25% Dust/ash. Table 2 suggests that Aged EC and Dust/ash are the major types presented in the same MH mode. However, peak intensity responses to GF were indeed different for different particle types, suggesting the importance of particle types in describing peak intensities.

The particle distribution with sulfate intensities showed similar enrichment patterns to nitrate (lower right panel in Figure 11). Sulfate peak intensities were found to correlated with hygroscopicity in GF <1.2 range but in MH range no correlated with GF was observed. We note that except the larger peaks of nitrate and sulfate, some smaller peaks were also found to correlated with GF within specific particle type. We correlated peak intensities of Na_2Cl^+ and NO_3^- with the estimated GF of sea salt particles (Figure S9). The Na_2Cl^+ peaks were positively correlated with GF while the nitrate peaks were negatively correlated with GF. The observed correlation in sea salt particles are consistent with discussed trends in the HTDMA-ATOFMS dataset. These results demonstrate that the GF estimation method have effectively reflected the minor changes in particle mass spectra into the estimated hygroscopicity."

3. This paper is missing critical information about how the ATOFMS data was treated and analyzed and what criteria were used to assign particle types and ascribe a growth factor.

Response:

We agree that the description of ATOFMS data analysis method is necessary. We have added this missing information in the revised manuscript. It is made clear that a single growth factor of particle types was not assigned, since particles in each type were distributed at more than one GF. The hygroscopicity of particle types were calculated based on their number distributions at different growth factors.

Changes in manuscript:

Line 139-146:

"The ATOFMS data was analyzed within the YAADA toolkit (http://www.yaada.org/). Particles with similar composition were grouped into clusters by an adaptive resonance algorithm (ART-2a) (Song et al., 1999). The ART-2a algorithm parameters were set to: vigilance factor = 0.85, learning rate = 0.05 and number of iterations = 20. The clusters generated by the algorithm were regrouped into major types by considering their similar composition and hygroscopicity patterns. The obtained particle types were labelled by consulting previous single particle characterization studies (Spencer et al., 2006;Silva et al., 1999;Sullivan et al., 2007a;Gaston et al., 2011;Qin et al., 2012). "

4. I don't understand the authors' claim regarding particle effective density as a predictor for particle hygroscopicity. Can the authors show a theoretical reason for such a claim?

Response:

In the original manuscript the effective density was prepared for the purpose of a complete report of the measured data, since aerodynamic diameters were measured by ATOFMS. As suggested in another item of comment, the discussions of effective density seem out of place in view of the main objective of this study is to connect hygroscopicity to composition. We accept the referee's opinion since the hygroscopicity are depending on particle composition, rather than particle density. The presented data only suggested a statistical positive correlation between effective density and GF, but a meaningful explanation of this correlation need further information including   particle physical shapes, which also affect ρ_{eff} (Ghazi et al., 2013;Khalizov et al., 2012). On the other hand, effective densities were not well incorporated into the discussions on estimated hygroscopicity. Therefore, the discussion of effective density seems somewhat redundant. In revised manuscript we decided to

concentrate on particle composition and the effective density were not discussed. We note that the hygroscopicity prediction algorithm is just based on particle composition and the density was not involved in calculation.

Changes in manuscript:

This section of information was removed.

Specific Comments

Abstract:

1. Lines 31-32: The authors need to explain why the higher effective density correlates with the hygroscopicity.

Response:

We only suppose that the lower effective densities of NH particles may be caused by the organic compositions. The higher densities of hygroscopic particles are probably related to the increasing fractions of secondary matters in particles. As responded in the major comment 4, this section of discussion was removed.

Changes in manuscript:

This part of information was removed.

2. Lines 32-34: The authors need to revise this statement or revise their work to show a degree of predictability of the GF was achieved.

Response:

As responded in the major comment 1, we re-analyzed the HTDMA-ATOFMS data and made the suggested revisions to the manuscript, in which the discussions on predictability, correlations between peak intensities and GF were added.

Changes in manuscript:

Line 31-33:

"Peak intensities in particle spectra were found nonlinearly correlated with hygroscopicity and the correlations were variant with particle types."

3. Lines 37-39: I don't understand this claim that back-trajectory analysis is consistent with particle hygroscopicity. The authors need to clarify this statement.

Response:

The original statement is problematic. We have revised the manuscript considerably according the referee's suggestions. The original statement is changed as follows.

Changes in manuscript:

Line 42-46:

"Based on the combined information on particle composition, hygroscopicity, airmass back trajectories and ambient pollutants concentrations, we inferred that the NH, LH, MH, SS modes were characterized by POA/EC, SOA, SIA and salts compositions, respectively. The proposed method would provide additional information to the study of particle mixing states, source identification and visibility degradation."

Introduction:

1. Lines 47-49: This sentence is very vague. The authors should discuss heterogeneous and

multiphase reactions that would affect particle hygroscopicity.

Response:

We have revised this sentence and relevant references were added as suggested.

Changes in manuscript:

Line 53-55:

"Aerosol particles provide surfaces for atmospheric heterogeneous reactions to occur and act as the sink for these reactions (Sullivan et al., 2007b;Gard et al., 1998;Qiu and Zhang, 2013), which are of significance to air quality, visibility and human health. "

2. While the coupling of techniques was discussed, the authors need to add discussion of growth factors observed in ambient environments and what has been learned about how composition drives hygroscopicity in tandem experiments.

Response:

As suggested, some discussions on the growth factors had been added, together with the previous findings in these studies.

Changes in manuscript:

Line 79-83:

"The HTDMA measurements suggest that several hygroscopicity modes exist simultaneously, probably due to the external mixing of atmospheric particles. HTDMA hygroscopicity were generally fell into four categories: nearly hydrophobic (NH), less-hygroscopic (LH), more-hygroscopic (MH), and sea-salt mode, with their center GFs (90% RH) lie in 1.0-1.11, 1.11-1.33, >1.33 and >1.8 ranges, respectively (Swietlicki et al., 2008)."

Line 96-102:

"Herich et al. firstly applied the tandem HTDMA-ATOFMS system to characterize particle composition of different hygroscopicity (Herich et al., 2008;Herich et al., 2009). A large portion of the less hygroscopic modes were found to be contributed by organics and combustion species both in the urban and remote site, while the sulfates and nitrates were present in almost all particles independent of hygroscopicity. Similar findings were also observed in our preliminary characterization using HTDMA-ATOFMS in Shanghai city (Wang et al., 2014), except higher nitrate and sulfate intensities were found in hygroscopic particles in our study."

Methods:

1. The data analysis methods for the ATOFMS measurements are missing yet are a critical component of this work. What clustering method was used? Art2a? What vigilance factor, learning rate, and number of iterations were used? How were particle types assigned?

Response:

We agree that the description of ATOFMS data analyzing method is necessary. We have added this missing information in manuscript as follows.

Changes in manuscript:

Line 139-146:

"The ATOFMS data was analyzed within the YAADA toolkit (http://www.yaada.org/). Particles with similar composition were grouped into clusters by an adaptive resonance algorithm (ART-2a) (Song et al., 1999). The ART-2a algorithm parameters were set to: vigilance factor = 0.85,

learning rate = 0.05 and number of iterations = 20. The clusters generated by the algorithm were regrouped into major types by considering their similar composition and hygroscopicity patterns. The obtained particle types were labelled by consulting previous single particle characterization studies (Spencer et al., 2006;Silva et al., 1999;Sullivan et al., 2007a;Gaston et al., 2011;Qin et al., 2012). "

2. What size range did the ATOFMS hit particles? Usually 250 nm is on the lower end of what the instrument can see for certain inlet configurations, what is the detection efficiency of the ATOFMS at this lower size?

Response:

According to instrument manual, the TSI ATOFMS-3800 can analyzes particles in 0.1-3 µm range (the AFL model is 3800-100). Ambient studies in Shanghai verified that most of the ATOFMS particles lie in this size range. Considering that the 250 nm is on the lower end of detection range, we expected the ATOFMS detection efficiency has decreased compared with larger particles. In HTDMA-ATOFMS experiment we selected 250 nm dry particles because the concentrations of larger particles were found to decrease further in the SMPS size distributions. We calculated ATOFMS detection efficiency at 250 nm by referring to the CPC concentration which was measured parallel to ATOFMS. Considering the different flowrates of CPC and ATOFMS, the ATOFMS and CPC data suggest that ATOFMS have detection efficiency of 1.6×10^{-2} in this experiment. The ATOFMS detection efficiency is also subjected to variation with GF as shown in Figure S2. In revised manuscript we added this part of information.

Changes in manuscript:

Line 172-181

"The ATOFMS used in this study detects particles in 100-3000 nm diameter range. The 250 nm dry diameter is near the lower end of ATOFMS detection range, therefore the detection efficiency at this size is expected to be lowered compared with larger particles. This study selected 250 nm particles because the concentrations of larger particles decreases further, as indicated by the SMPS size distributions. Therefore, the selection of D_{dry} = 250nm is a compromise between detection probability and particle concentrations (Wang et al., 2014; Herich et al., 2008). With the measured ATOFMS particle numbers and CPC concentrations, the detection efficiency of ATOFMS were calculated to be ~1.6×10^{-2} at the dry size. In Figure S2 we presented ATOFMS detection efficiencies together with the particle hit rate (hit particles/total sized particles) at different growth factors."

3. What were the hit rates for the different growth factors? This will be important for assessing how representative the observed particles are of each growth factor.

Response:

ATOFMS hit rates for different growth factors is presented in Figure S2. Higher hit rates for particles of low hygroscopicity range (GF <1.3) were observed than more hygroscopic particles (GF >1.4). This variation of hit rate is probably caused by the different particle compositions at different growth factors. In previous ATOFMS study it was verified that the coating of secondary species on particles can reduce the ionization efficiencies and lower the hit rate (Hatch et al., 2014). This is consistent with the HTDMA-ATOFMS observation that more

hygroscopic particles tend to produce stronger secondary peaks. We added this information in revised manuscript.
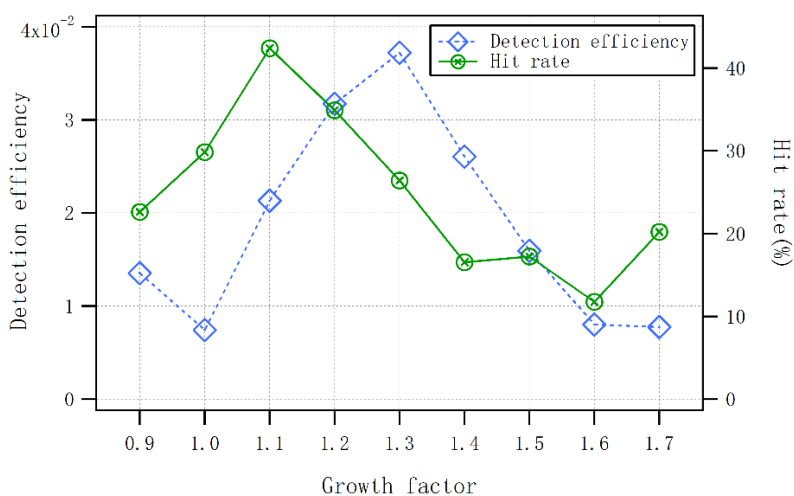
Figure S2. ATOFMS particle detection efficiency and hit rates at different growth factors.

Changes in manuscript:

Line 180-184:

"In Figure S2 we presented ATOFMS detection efficiencies together with the particle hit rate (hit particles/total sized particles) at different growth factors. Generally, the detection efficiencies suggested variations at different GFs. We found higher detection efficiencies in moderate GF range (1.2-1.4) and higher hit rates in GF<1.3 range, which is probably caused by variations of compositions with GF (Hatch et al., 2014)."

4. Lines 166-167; Lines 191-194: the authors mentioning assigning a GF for ambient particles that match particles observed during HTDMA-ATOFMS spectra. What was the criteria for matching particles and assessing their similarity? Was a threshold dot product used to assess similarity as was done for prior ATOFMS studies (e.g., [Pratt and Prather, 2009]).

Response:

We matched the HTDMA-ATOFMS particles with ambient particles by the criteria of mass spectral similarity. The similarity was calculated in the same way as that in ART-2a algorithm, that is, the dot products between the normalized mass spectra. In this preliminary study, we set a threshold dot product in matching particles. The similarities of the matched particles were recorded by the algorithm during calculation. The distribution of similarities suggests that the majority of particles (79.4%) have matching dot products in >0.8 (average dot product 0.86). We note that the 0.5 power treatment to peak intensities was applied before the calculation of similarity. To certain extend this exponentiation of peak intensities lowered the dot products between ATOFMS and HTDMA-ATOFMS mass spectra (96% of matching dot products >0.8, average dot product 0.94), because peaks of smaller intensities increased their weights in the evaluation of similarity. The figure S4 shows the distribution of the matching similarities. We have added the missing information in manuscript.
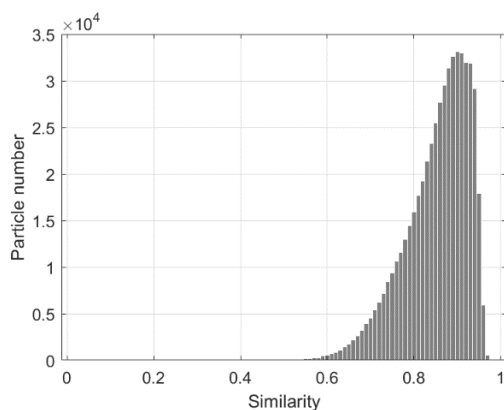
Figure S4. The distribution of matching similarities in the estimation of hygroscopicity.

Changes in manuscript:

Line 199-202:

"In this study we set a threshold similarity (0.7 dot product) in matching particles, as was required in ART-2a algorithm (Song et al., 1999). Ambient particles with matching dot products <0.7 were excluded from analysis of the estimated GF. The similarity data suggests that 96.2% of the matching similarities are > 0.7 and 79% of them are >0.8 (Figure S4)."

5. Lines 171-174: I have not heard of treating ATOFMS data this way. It is well-known that the instrument is sensitive to ionization potential energies ([Gross et al., 2000]) and usually relative intensities are used to work with such spectra. The authors' method of arbitrarily reducing the intensity of metals so that organics are relatively enhanced requires significant justification.

Response:

We took 0.5 power of mass peak intensities in the estimation of GF. This treatment was applied to both the HTDMA-ATOFMS and ambient particle data before the evaluation of particle similarity. As noted by the referee, ATOFMS mass peak intensities are affected not only by composition abundance in particles, but also by their ionization efficiencies in ATOFMS. The ATOFMS is known to be sensitive to metallic compositions than organics, resulting disproportionate large peaks of metals to reflect their actual concentrations in particles. We suppose the 0.5 power treatment of mass peak areas can partly solve the bias of ATOFMS toward different compositions, since this treatment reduce larger peaks more rapidly than smaller peaks. Similar treatment (take the logarithm of peak areas) of ATOFMS data was proposed in prior literature (Rehbein et al., 2012). In ATOFMS data analysis the peak relative intensities were also used. Relative intensities are the normalized intensities by the total peak area in spectrum. However, the normalization only removes the amplitude of mass spectra but the overall shape of the spectra is not changed.

The application of 0.5 power treatment is not just based on speculation. We find it gave better results in the estimated hygroscopicity. We carried two rounds of GF estimations in which the pretreatment was either included or not. In figure S3 the two distributions of estimated GF using 0.5 power treatment or not are compared. As shown in figure, the hygroscopicity distribution without treatment shown abnormal shape with an extra mode of GF=1.35, which was inconsistent with HTDMA observations in this area. As a comparison, we applied the 0.5

power treatment to peak intensities and the obtained hygroscopicity were distributed regularly with smoother shapes, which agrees well with the HTDMA data of ambient particles. We note that in the two estimations the dataset and algorithm are identical with the only difference of pretreatment. This fact suggests that the 0.5 power treatment could indeed be used to improve hygroscopicity estimation.

To reply to the referee's concern, we have added relevant information in manuscript.
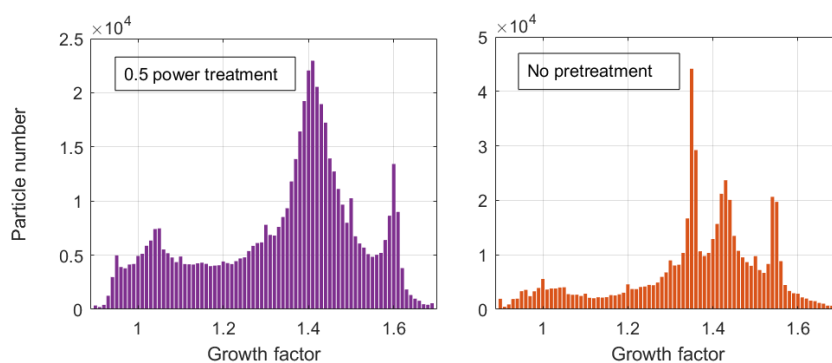
Figure S3. The estimated particle hygroscopicity distribution with (left) and without (right) taking 0.5 power of peak intensities.

Changes in manuscript:

Line 194-196:

"The 0.5 power treatment to peaks intensities was applied because it offered better results in the estimation of hygroscopicity, as discussed in the supplemental information."

6. The authors used candidate particle types to explain hygroscopicity, but did they ever simply compare sulfate and nitrate peak areas to the growth factor data to see if those soluble compounds could explain their results better than different particle types?

Response:

We have considered the referee's suggestions carefully and have added relevant discussions in revisions.

Changes in manuscript:

Line 344-390:

"3.1.2 Peak intensity variations with GF

Apart from particle number distributions, the HTDMA-ATOFMS dataset provided another aspect of information regarding peak intensities with GF. In this study we used relative peak intensities (peak areas normalized by the total areas in spectrum) to study its relations to GF. Generally, the responses of peak intensity to GF variation were found nonlinear since they were correlated within specific GF ranges but a simple trend applicable to all GF was not observed. To demonstrate this character, we presented the statistics of peak intensity of nitrate ($-46NO_2$, $-62NO_3$, $-125H(NO_3)_2$) and sulfate ($-80SO_3$, $-97HSO_4$) which were known to be critical to particle hygroscopicity (Figure 4). As previously observed (Herich et al., 2009;Herich et al., 2008;Wang et al., 2014), the nitrate and sulfate peaks were present in the majority of particles in all GF bins. However, peak intensities of nitrate and sulfate were indeed stronger in hygroscopic particles than hydrophobic particles. In Figure 4 we observed positive correlation between

nitrate and sulfate intensities and GF in GF <1.2 range, suggesting contribution of nitrate and sulfate to particle hygroscopicity in low GF range (Figure 4). However, in higher GF range (GF 1.3-1.5), nitrate and sulfate peaks seem to reached a plateau with unclear dependence on GF. Nitrate and sulfate were known to contribute large fractions of particle mass in MH particles (Swietlicki et al., 2008;Laborde et al., 2013;Liu et al., 2014). The unclear trend of nitrate and sulfate with GF seem to suggest that nitrate and sulfate were in stable ratios since nitrate and sulfate peaks were dominating peak areas in negative spectra. For particles of even higher GF, differences were observed between GF 1.3-1.5 and GF 1.5-1.7 range in that stronger nitrate and weaker sulfate peaks were detected in the GF 1.3-1.5 range. Particles classification suggests that this general characteristic is also at variance for different particle types. The same statistics for EC and Dust/ash particles were presented in Figure 4. Compared with EC particles, smaller sulfate and stronger nitrate peaks were found in Dust/ash spectra, and the observed trend in total particles were less obvious in Dust/ash. These facts highlight the nonlinearity between peak intensities and GF and that particle types should also be considered in describing peak intensities.

The analysis of peak intensities with GF can disclose some atmospheric processes happened on aerosol. We take the Sea salt as an illustration. Sea salt particles were known to react with atmospheric nitric acid, with NaCl in fresh sea salt be transformed into $NaNO_3$ in the reacted sea salt (Gard et al., 1998). This composition transformation is indicated in corresponding changes of NaCl and NaNO3 peak intensities in particle spectra. The unreacted sea salt particles tend to produce larger peaks of Na_2Cl^+ and $NaCl_2^-$ in spectra (Gaston et al., 2011;Prather et al., 2013). In particle spectra of reacted sea salt, the NaCl peaks (Na$_2$Cl+, NaCl$_2$-) decrease while NaNO3 peaks ($Na_2NO_3^+$, $Na(NO_3)_2^-$) increase. We presented peak intensities of sea salt in GF 1.5-1.7 range where sea salt particles were detected with largest numbers (Figure 5). We found that the positive correlation between NaCl peak intensity and GF, and the negative correlation for $NaNO_3$ peaks. Therefore, the HTDMA-ATOFMS data supported that reacted sea salt have reduced hygroscopicity (Herich et al., 2009;Gaston et al., 2018). Laboratory HTDMA study suggested that NaCl and NaNO3 have deliquesced at 85% RH and that the $NaNO_3$ (GF ~1.8) is less hygroscopic than NaCl (GF ~2.2) (Hu et al., 2010). The reduced hygroscopicity of sea salt is in line with the GF of sodium salts. However, the sea salt hygroscopicity (GF 1.5-1.7) was smaller than pure $NaNO_3$ salt (supposing fully reacted), suggested that the chemical transformation alone is not sufficient to account for the observed hygroscopicity of sea salt. We hypothesize that other compositions as organics were mixed into sea salt and contributed to the reduction of sea salt hygroscopicity (Gaston et al., 2011;Randles et al., 2004;Facchini et al., 2008;Herich et al., 2009). "

Results:

1. The particle statistics mentioned in Section 3.1.1 are really hard to follow and put into context. I suggest just keeping this section focused on particle types, then moving Section 3.2.1 up and providing better statistics for the particle types that contributed to each growth factor including a description of the percentage of each particle type observed for each growth factor and what the hit rates were on the ATOFMS for each growth factor.

Response:

We accepted the referee's suggestions and have made corresponding rearrangements of text

in manuscript. The changes include removing the statistics on particle contribution of HTDMA-ATOFMS particles and adding new statistics on particle contributions in hygroscopicity modes based on ATOFMS particles. Since the GF were estimated only for hit particles, we cannot derive the hit rates at different GF for ATOFMS particles. As an alternative, we provided the hit rates information with GF based on the HTDMA-ATOFMS data in Figure S2.

Changes in manuscript:

Line 463-481:

"In Table 2 we made the statistics on average number contributions of particle types to the NH, LH, MH and SS mode. The presented statistics were based on the temporal contributions of each particle types in daily resolution. It is noted that particle number contributions presented in Table 2 may be different from HTDMA-ATOFMS dataset (Figure 2). For example, the Cooking particles contributions to NH mode was significantly lower in the ATOFMS dataset (3%) than HTDMA-ATOFMS dataset (19%). This result is understandable because particle concentrations are variant with particle size and HTDMA-ATOFMS only analyzed a narrow size bin from the total particle size distribution. For each hygroscopicity mode, there were multiple particle types contributing significant number fractions, suggesting that even within the same hygroscopicity mode there were still some heterogeneity in particle composition. Particles in the same hygroscopicity mode may share some common features in compositions but their differences are distinguishable in single particle data. In another respect, the contributions of each type also suggest the existence of a predominant type that accounts for major fractions in respective modes compared with other types, such as Aged EC in MH mode, Ammonium/OC in LH mode. The comparison between Table 2 and Figure 2 suggests that, although their absolute contributions may be different, the hygroscopicity patterns of particle types in the two datasets are in good agreement. Based on this fact, we concluded that the composition-hygroscopicity connections contained in HTDMA-ATOFMS dataset was successfully reflected into the predicted GF."

2. Line 207: add the following references for ATOFMS detection of biomass burning aerosol: [Pratt et al., 2010; Zauscher et al., 2013].

Response:

This suggestion is accepted.

Changes in manuscript:

Line 241-243:

"The Biomass particles produced characteristic peaks of -26(CN), -42(CNO), -59($C_2H_3O_2$), -73($C_3H_5O_2$) and dominant peak at 39K and related peaks at 113(K_2Cl) or 213(K_3SO_4) (Silva et al., 1999;Zauscher et al., 2013;Pratt and Prather, 2009).

3. Lines 214-215 describing EC particles require a reference to prior work [Ault et al., 2010; Spencer et al., 2006; Toner et al., 2008].

Response:

This suggestion is accepted.

Changes in manuscript:

Line 250-251:

"The EC particles were detected by a series of elemental carbon peaks at C_n (n=1, 2, 3 …) in the

negative and positive spectra (Ault et al., 2010;Spencer et al., 2006;Toner et al., 2008)."

4. Line 217: define NH and MH.

Response:

The NH and MH were defined in the text.

Changes in manuscript:

Line 251-253:

"EC particles distributed broadly from nearly-hydrophobic (NH) mode to more-hygroscopic (MH) mode."

5. Lines 223-225: I suggest adding Figure S2 to the main text.

Response:

The peak intensity trends in Figure S2 was presented only for EC particles. To embody the referee's opinion, we transmitted the information in Figure S2 to a new figure to show the peak intensities of EC, Dust/ash and all particles, as seen in Figure 4 in the main text.

Changes in manuscript:

Line 903-906:

"
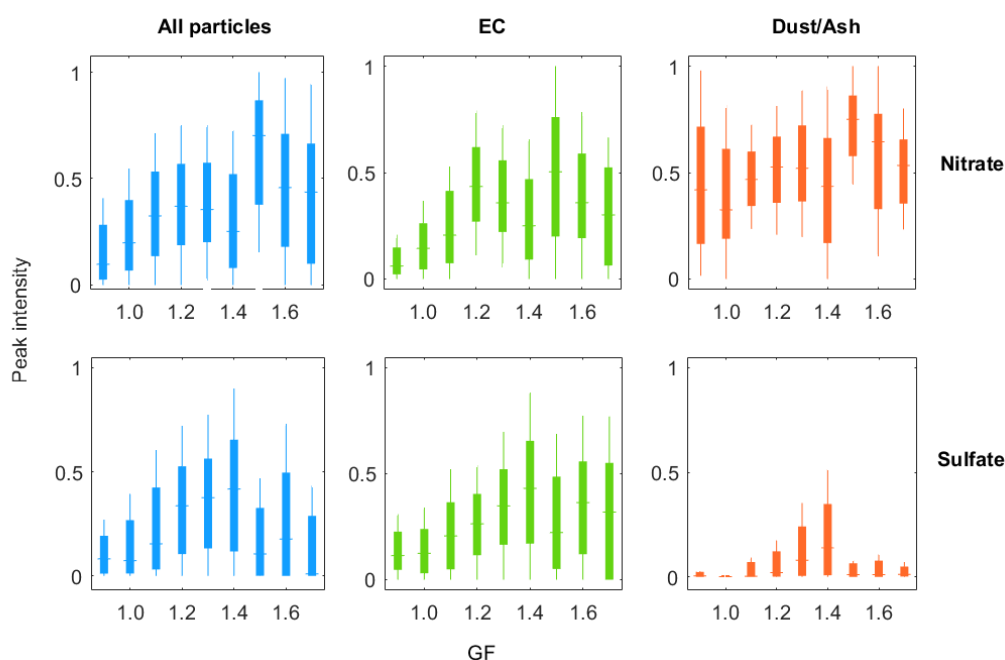
Figure 4. Statistics of nitrate and sulfate peak intensities (minimum, 25th percentile, median, 75th percentile, maximum) with GF in HTDMA-ATOFMS experiment. The intensity statistics were calculated for All particles, EC particles and Dust/Ash particles separately."

6. Lines 226-227: please add [Ault et al., 2011; Gaston et al., 2017; Sullivan et al., 2007].

Response:

This suggestion is accepted.

Changes in manuscript:

Line 264-265:

"Dust/ash type particles produced inorganic peaks of salts and metals (Gaston et al., 2017;Ault

et al., 2011;Sullivan et al., 2007a)."

7. I suggest also adding Figure S3 to the main text.

Response:

We have moved Figure S3 to the main text with relevant discussions.

Changes in manuscript:

Line 900-901:

"
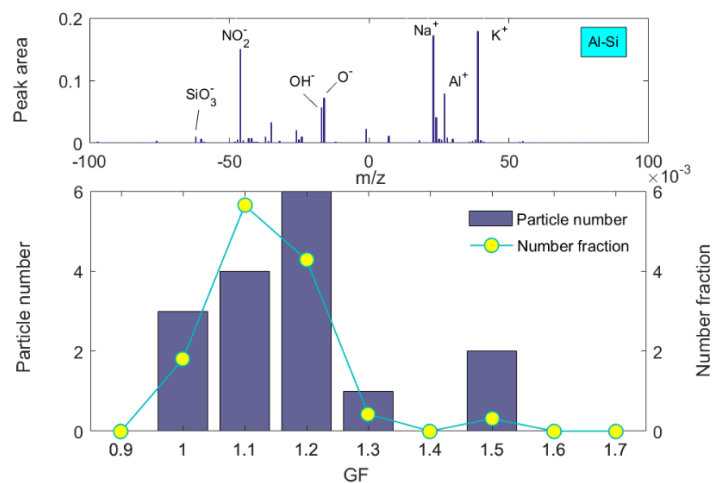
Figure 3. Average mass spectra and hygroscopicity distribution of Al-Si particles. "

8. Lines 255-257: there are other ATOFMS studies showing ammonium/OC particles associated with agricultural emissions [Qin et al., 2012]. The authors should also consider that source for their observations.

Response:

We followed the suggestions of the reviewer and made following changes.

Changes in manuscript:

Line 305-312:

"Prior ATOFMS study attribute similar Ammonium/OC particles to agricultural sources and found they were enriched in higher photochemical oxidation periods (Qin et al., 2012). The secondary nature of Ammonium/OC is also consistent with the pronounced ammonium peak. It is likely that the organics in Ammonium/OC particles are also generated from secondary processes since the GF 1.2 approximate to the hygroscopicity of SOA (GF=1.24 at 90% RH) (Gysel et al., 2007;Sjogren et al., 2008). We inferred that ammonium was not contributing major fractions to Ammonium/OC particles, since ammonium salts was very hydrophilic while Ammonium/OC demonstrate only moderate hygroscopicity."

9. Lines 260-261: aging does not always translate to high hygroscopicity.

Response:

We admit that original statement is not accurate, because aging does not necessarily promote hygroscopicity of all particles. We have revised it accordingly.

Changes in manuscript:

Line 310-312:

"We inferred that ammonium was not contributing major fractions to Ammonium/OC particles,

since ammonium salts was very hydrophilic while Ammonium/OC demonstrate only moderate hygroscopicity.

10. Line 275: please also cite [Pratt and Prather, 2009]
Response:
This suggestion is accepted.
Changes in manuscript:
Line 323-324:
"This phenomenon was also observed for other organic particles (Shi et al., 2012;Pratt and Prather, 2009)."

11. Line 282-283: please site [Gaston et al., 2011]
Response:
This suggestion is accepted.
Changes in manuscript:
Line 332-333:
"Sea salt mass spectra contain dominant sodium peak +23Na and other sodium cluster peaks at +62Na$_2$O, +63Na$_2$OH, +81Na$_2$Cl (Gaston et al., 2017)."

12. The authors mention that only a few sea salt particles were observed, yet this was the only particle type where a thorough investigation linking the particle composition to the GF was performed. Why was this type of analysis or discussion not included for other particle types?
Response:
We analyzed sea salt particles in more detail mainly because they constitute a separated mode without interferences from other types and clearer trends was observed in sea salt. However, this treatment seems insufficient by neglecting other particles. To embody the referee's concern, in the revision we also include analysis of particles for Ammonium/OC particles in LH mode. In discussions of peak intensities, we also included discussions on Dust/ash and EC particles which made major contributions to MH mode.
Changes in manuscript:
Line 561-583:
"The nonlinearity of peak intensities with GF was also suggested by the different particle types presented in ATOFMS data. As shown in the lower panels in Figure 11, the distribution of ATOFMS individual particles showed enrichment in different areas in the GF-peak intensity diagram, suggesting the presence of particle groups of different compositions. To illustrate this character, we selected two areas with clear particle enrichments in GF-peak intensity diagram and their particle composition were analyzed (denoted as A and B in lower left panel in Figure 11). Obviously, particles in area A produced much larger nitrate signals than particles in area B. Particle numbers in the two areas suggested that Dust/ash dominated particles in area A (59%) while in area B the Dust/ash only accounted for 14% of particles (Figure S10). As a contrast, particles in area B were dominated by Aged EC type (53%) followed by 25% Dust/ash. Table 2 suggests that Aged EC and Dust/ash are the major types presented in the same MH mode. However, peak intensity responses to GF were indeed different for different

particle types, suggesting the importance of particle types in describing peak intensities.
The particle distribution with sulfate intensities showed similar enrichment patterns to nitrate (lower right panel in Figure 11). Sulfate peak intensities were found to correlated with hygroscopicity in GF <1.2 range but in MH range no correlated with GF was observed. We note that except the larger peaks of nitrate and sulfate, some smaller peaks were also found to correlated with GF within specific particle type. We correlated peak intensities of Na_2Cl^+ and NO3- with the estimated GF of sea salt particles (Figure S9). The Na_2Cl^+ peaks were positively correlated with GF while the nitrate peaks were negatively correlated with GF. The observed correlation in sea salt particles are consistent with discussed trends in the HTDMA-ATOFMS dataset. These results demonstrate that the GF estimation method have effectively reflected the minor changes in particle mass spectra into the estimated hygroscopicity."

13. Lines 301-302: please cite [Gaston et al., 2011; Prather et al., 2013]

Response:

This suggestion is accepted.

Changes in manuscript:

Line 375-377:

"The unreacted sea salt particles tend to produce larger peaks of Na_2Cl^+ and $NaCl_2^-$ in spectra (Gaston et al., 2011;Prather et al., 2013)."

14. Lines 306-307: please cite [Gaston et al., 2018] who found a similar result using ATOFMS data.

Response:

This suggestion is accepted.

Changes in manuscript:

Line 381-382:

"Therefore, the HTDMA-ATOFMS data supported that reacted sea salt have reduced hygroscopicity (Herich et al., 2009;Gaston et al., 2018)."

15. I had a hard time following lines 305-310, the authors need to clarify whether aged sodium nitrate contributed to the lower GF or whether other factors were responsible.

Response:

The hygroscopicity of sea salt particles was not clearly presented originally. According to HTDMA GF characterization of pure salts, the salt $NaNO_3$ (GF ~1.8) is less hygroscopic than NaCl (GF ~2.2) at 85% RH (D_{dry} 250nm) (Hu et al., 2010). The transformation of NaCl into $NaNO_3$ could reduce particle hygroscopicity, but the transformation alone could not account for the observed hygroscopicity since the observed GF of sea salt (1.5-1.7) were lower than pure $NaNO_3$ (supposing fully transformed). Therefore, we hypothesized that other factors including organics were contributing to the further reduction of sea salt hygroscopicity.

Changes in manuscript:

Line 371-390:

"The analysis of peak intensities with GF can disclose some atmospheric processes happened on aerosol. We take the Sea salt as an illustration. Sea salt particles were known to react with atmospheric nitric acid, with NaCl in fresh sea salt be transformed into $NaNO_3$ in the reacted

sea salt (Gard et al., 1998). This composition transformation is indicated in corresponding changes of NaCl and NaNO3 peak intensities in particle spectra. The unreacted sea salt particles tend to produce larger peaks of Na_2Cl^+ and $NaCl_2^-$ in spectra (Gaston et al., 2011;Prather et al., 2013). In particle spectra of reacted sea salt, the NaCl peaks (Na_2Cl^+, $NaCl_2^-$) decrease while NaNO3 peaks ($Na_2NO_3^+$, $Na(NO_3)_2^-$) increase. We presented peak intensities of sea salt in GF 1.5-1.7 range where sea salt particles were detected with largest numbers (Figure 5). We found that the positive correlation between NaCl peak intensity and GF, and the negative correlation for NaNO3 peaks. Therefore, the HTDMA-ATOFMS data supported that reacted sea salt have reduced hygroscopicity (Herich et al., 2009;Gaston et al., 2018). Laboratory HTDMA study suggested that NaCl and $NaNO_3$ have deliquesced at 85% RH and that the $NaNO_3$ (GF ~1.8) is less hygroscopic than NaCl (GF ~2.2) (Hu et al., 2010). The reduced hygroscopicity of sea salt is in line with the GF of sodium salts. However, the sea salt hygroscopicity (GF 1.5-1.7) was smaller than pure $NaNO_3$ salt (supposing fully reacted), suggested that the chemical transformation alone is not sufficient to account for the observed hygroscopicity of sea salt. We hypothesize that other compositions as organics were mixed into sea salt and contributed to the reduction of sea salt hygroscopicity (Gaston et al., 2011;Randles et al., 2004;Facchini et al., 2008)."

16. Section 3.1.2 seems out of place. While it is an interesting finding that the effective density showed a trend with the GF, the authors need to explain this finding a bit more.
Response:

In the original manuscript the effective density was included for the purpose of a complete presenting of the measured data, since aerodynamic diameters were measured by ATOFMS. The discussions of effective density seem out of place in view of the main objective of this study is to connect hygroscopicity to composition. We accept the referee's opinion since the hygroscopicity are depending on particle composition, rather than particle density. The presented data only suggested a statistical positive correlation between effective density and GF, but a meaningful explanation of this correlation need further information including particle physical shapes, which also affect ρ_{eff}. On the other hand, effective densities were not well incorporated into the discussions on estimated hygroscopicity. Therefore, in revised manuscript we decided to concentrate on particle composition and the effective density were not discussed.

Changes in manuscript:
The discussions were removed.

17. Section 3.2.1 needs some statistics to show that the authors can predict the GF from the spectra alone.
Response:

We accepted the referee's suggestion to include some particle statistics to the ambient particles. In Table 2 we have presented such information on the contributions of particle types to different hygroscopicity modes. The calculate contributions were based on ATOFMS numbers of ambient particles and offer better statistics than HTDMA-ATOFMS particles. The relevant information on HTDMA-ATOFMS particle contributions in original version were removed.

Changes in manuscript:

Line 887-890:

"Table 2. Statistics on particle number contributions of ATOFMS particle types to different GF modes. The statistics are the average contributions and variation ranges (in brackets) based on temporal data in daily resolution.

Contribution (%)	NH (GF <1.1)	LH (GF 1.1-1.3)	MH (GF 1.3-1.5)	SS (GF >1.5)
Fresh EC	14 (7-17)	2 (1-4)	0 (0-3)	0 (0-1)
Cooking	3 (0-7)	1 (0-3)	0 (0-0)	0 (0-0)
Biomass	18 (7-35)	9 (2-17)	0 (0-1)	0 (0-0)
HMOC	40 (30-68)	8 (2-15)	0 (0-1)	0 (0-0)
Ammonium/OC	11 (3-21)	32 (20-45)	2 (1-5)	0 (0-0)
Aged EC	2 (1-5)	12 (5-20)	47 (15-72)	13 (1-42)
Dust/ash	3 (1-6)	13 (9-22)	27 (13-53)	26 (4-44)
Amine-rich	3 (1-5)	12 (2-41)	13 (4-39)	11 (1-44)
Sea salt	0 (0-1)	0 (0-1)	1 (0-4)	40 (7-78)

"

18. Lines 441-442: this suggests that the authors should try comparing their GF data to peak area intensities of sulfate and nitrate.

Response:

We have added discussions on the correlations between peak intensity and estimated GF of ambient particles.

Changes in manuscript:

Line 548-583:

"3.3.3 Peak intensity variations with estimated GF

Particle hygroscopicity and peak intensities in particle mass spectra were correlated to show their connections. The correlation was illustrated similarly to the analysis of the HTDMA-ATOFMS dataset, as shown in Figure 11. In addition to the statistics on peak intensities of different GF, the number distributions ATOFMS particles with GF and peak intensities were presented for nitrate ($-46NO_2$, $-62NO_3$, $-125H(NO_3)_2$) and sulfate peaks ($-97HSO_4$, $-80SO_3$) in the lower panels in Figure 11. The general trends of peak intensities with GF in HTDMA-ATOFMS dataset was preserved in estimated GF of ambient particles. The trends of nitrate and sulfate peak intensities showed increases from NH to LH range and remained constant in the MH mode. Similar to HTDMA-ATOFMS particles, stronger nitrate peaks were detected in SS particles compared with the MH particles, while an opposite trend was observed for sulfate intensities. These results highlight the nonlinearity between GF and peak intensities of ATOFMS particles.

The nonlinearity of peak intensities with GF was also suggested by the different particle types presented in ATOFMS data. As shown in the lower panels in Figure 11, the distribution of ATOFMS individual particles showed enrichment in different areas in the GF-peak intensity diagram, suggesting the presence of particle groups of different compositions. To illustrate this character, we selected two areas with clear particle enrichments in GF-peak intensity diagram and their particle composition were analyzed (denoted as A and B in lower left panel in Figure 11). Obviously, particles in area A produced much stronger nitrate signals than

particles in area B. Particle numbers in the two areas suggested that Dust/ash dominated particles in area A (59%) while in area B the Dust/ash only accounted for 14% of particles (Figure S10). As a contrast, particles in area B were dominated by Aged EC type (53%) followed by 25% Dust/ash. Table 2 suggests that Aged EC and Dust/ash are the major types presented in the same MH mode. However, peak intensity responses to GF were indeed different for different particle types, suggesting the importance of particle types in describing peak intensities.

The particle distribution with sulfate intensities showed similar enrichment patterns to nitrate (lower right panel in Figure 11). Sulfate peak intensities were found to correlated with hygroscopicity in GF <1.2 range but in MH range no correlated with GF was observed. We note that except the larger peaks of nitrate and sulfate, some smaller peaks were also found to correlated with GF within specific particle type. We correlated peak intensities of Na_2Cl^+ and NO_3^- with the estimated GF of sea salt particles (Figure S9). The Na_2Cl^+ peaks were positively correlated with GF while the nitrate peaks were negatively correlated with GF. The observed correlation in sea salt particles are consistent with discussed trends in the HTDMA-ATOFMS dataset. These results demonstrate that the GF estimation method have effectively reflected the minor changes in particle mass spectra into the estimated hygroscopicity."

References

Ault, A. P., Gaston, C. J., Wang, Y., Dominguez, G., Thiemens, M. H., and Prather, K. A.: Characterization of the Single Particle Mixing State of Individual Ship Plume Events Measured at the Port of Los Angeles, Environmental Science & Technology, 44, 1954-1961, 10.1021/es902985h, 2010.

Ault, A. P., Williams, C. R., White, A. B., Neiman, P. J., Creamean, J. M., Gaston, C. J., Ralph, F. M., and Prather, K. A.: Detection of Asian dust in California orographic precipitation, Journal of Geophysical Research-Atmospheres, 116, 10.1029/2010jd015351, 2011.

Engelhart, G. J., Hennigan, C. J., Miracolo, M. A., Robinson, A. L., and Pandis, S. N.: Cloud condensation nuclei activity of fresh primary and aged biomass burning aerosol, Atmospheric Chemistry and Physics, 12, 7285-7293, 10.5194/acp-12-7285-2012, 2012.

Facchini, M. C., Rinaldi, M., Decesari, S., Carbone, C., Finessi, E., Mircea, M., Fuzzi, S., Ceburnis, D., Flanagan, R., and Nilsson, E. D.: Primary submicron marine aerosol dominated by insoluble organic colloids and aggregates, Geophysical Research Letters, 35, 2008.

Gard, E. E., Kleeman, M. J., Gross, D. S., Hughes, L. S., Allen, J. O., Morrical, B. D., Fergenson, D. P., Dienes, T., Galli, M. E., Johnson, R. J., Cass, G. R., and Prather, K. A.: Direct observation of heterogeneous chemistry in the atmosphere, Science, 279, 1184-1187, 10.1126/science.279.5354.1184, 1998.

Gaston, C. J., Furutani, H., Guazzotti, S. A., Coffee, K. R., Bates, T. S., Quinn, P. K., Aluwihare, L. I., Mitchell, B. G., and Prather, K. A.: Unique ocean-derived particles serve as a proxy for changes in ocean chemistry, Journal of Geophysical Research: Atmospheres, 116, 10.1029/2010jd015289, 2011.

Gaston, C. J., Pratt, K. A., Suski, K. J., May, N. W., Gill, T. E., and Prather, K. A.: Laboratory Studies of the Cloud Droplet Activation Properties and Corresponding Chemistry of Saline Playa Dust, Environmental Science & Technology, 51, 1348-1356, 10.1021/acs.est.6b04487, 2017.

Gaston, C. J., Cahill, J. F., Collins, D. B., Suski, K. J., Ge, J. Y., Barkley, A. E., and Prather, K. A.: The Cloud Nucleating Properties and Mixing State of Marine Aerosols Sampled along the Southern California Coast, Atmosphere, 9, 52, 2018.

Ghazi, R., Tjong, H., Soewono, A., Rogak, S. N., and Olfert, J. S.: Mass, Mobility, Volatility, and Morphology of Soot Particles Generated by a McKenna and Inverted Burner, Aerosol Science and Technology, 47, 395-405, 10.1080/02786826.2012.755259, 2013.

Gysel, M., Crosier, J., Topping, D. O., Whitehead, J. D., Bower, K. N., Cubison, M. J., Williams, P. I., Flynn, M. J., McFiggans, G. B., and Coe, H.: Closure study between chemical composition and hygroscopic growth of aerosol particles during TORCH2, Atmospheric Chemistry and Physics, 7, 6131-6144, 2007.

Hämeri, K., Väkevä, M., Aalto, P. P., Kulmala, M., Swietlicki, E., Zhou, J., Seidl, W., Becker, E., and O'dowd, C. D.: Hygroscopic and CCN properties of aerosol particles in boreal forests, Tellus B: Chemical and Physical Meteorology, 53, 359-379, 10.3402/tellusb.v53i4.16609, 2001.

Hatch, L. E., Pratt, K. A., Huffman, J. A., Jimenez, J. L., and Prather, K. A.: Impacts of Aerosol Aging on Laser Desorption/Ionization in Single-Particle Mass Spectrometers, Aerosol Science and Technology, 48, 1050-1058, 10.1080/02786826.2014.955907, 2014.

Herich, H., Kammermann, L., Gysel, M., Weingartner, E., Baltensperger, U., Lohmann, U., and Cziczo, D. J.: In situ determination of atmospheric aerosol composition as a function of hygroscopic growth, Journal of Geophysical Research-Atmospheres, 113, D16213
10.1029/2008jd009954, 2008.

Herich, H., Kammermann, L., Friedman, B., Gross, D. S., Weingartner, E., Lohmann, U., Spichtinger, P., Gysel, M., Baltensperger, U., and Cziczo, D. J.: Subarctic atmospheric aerosol composition: 2. Hygroscopic growth properties, Journal of Geophysical Research-Atmospheres, 114, D13204 10.1029/2008jd011574, 2009.

Hu, D., Qiao, L., Chen, J., Ye, X., Yang, X., Cheng, T., and Fang, W.: Hygroscopicity of Inorganic Aerosols: Size and Relative Humidity Effects on the Growth Factor, Aerosol and Air Quality Research, 10, 255-264, 10.4209/aaqr.2009.12.0076, 2010.

Khalizov, A. F., Hogan, B., Qiu, C., Petersen, E. L., and Zhang, R. Y.: Characterization of Soot Aerosol Produced from Combustion of Propane in a Shock Tube, Aerosol Science and Technology, 46, 925-936, 10.1080/02786826.2012.683839, 2012.

Laborde, M., Crippa, M., Tritscher, T., Juranyi, Z., Decarlo, P. F., Temime-Roussel, B., Marchand, N., Eckhardt, S., Stohl, A., Baltensperger, U., Prevot, A. S. H., Weingartner, E., and Gysel, M.: Black carbon physical properties and mixing state in the European megacity Paris, Atmospheric Chemistry and Physics, 13, 5831-5856, 10.5194/acp-13-5831-2013, 2013.

Liu, H. J., Zhao, C. S., Nekat, B., Ma, N., Wiedensohler, A., van Pinxteren, D., Spindler, G., Muller, K., and Herrmann, H.: Aerosol hygroscopicity derived from size-segregated chemical composition and its parameterization in the North China Plain, Atmospheric Chemistry and Physics, 14, 2525-2539, 10.5194/acp-14-2525-2014, 2014.

Prather, K. A., Bertram, T. H., Grassian, V. H., Deane, G. B., Stokes, M. D., DeMott, P. J., Aluwihare, L. I., Palenik, B. P., Azam, F., Seinfeld, J. H., Moffet, R. C., Molina, M. J., Cappa, C. D., Geiger, F. M., Roberts, G. C., Russell, L. M., Ault, A. P., Baltrusaitis, J., Collins, D. B., Corrigan, C. E., Cuadra-Rodriguez, L. A., Ebben, C. J., Forestieri, S. D., Guasco, T. L., Hersey, S. P., Kim, M. J., Lambert, W. F., Modini, R. L., Mui, W., Pedler, B. E., Ruppel, M. J., Ryder, O. S., Schoepp, N. G., Sullivan, R. C., and Zhao, D.: Bringing the ocean into the laboratory to probe the chemical complexity of sea spray aerosol, Proceedings of the National Academy of Sciences, 201300262, 10.1073/pnas.1300262110, 2013.

Pratt, K. A., and Prather, K. A.: Real-Time, Single-Particle Volatility, Size, and Chemical Composition Measurements of Aged Urban Aerosols, Environmental Science & Technology, 43, 8276-8282, 10.1021/es902002t, 2009.

Qin, X. Y., Pratt, K. A., Shields, L. G., Toner, S. M., and Prather, K. A.: Seasonal comparisons of single-particle chemical mixing state in Riverside, CA, Atmospheric Environment, 59, 587-596, 10.1016/j.atmosenv.2012.05.032, 2012.

Qiu, C., and Zhang, R. Y.: Multiphase chemistry of atmospheric amines, Physical Chemistry Chemical Physics, 15, 5738-5752, 10.1039/c3cp43446j, 2013.

Randles, C. A., Russell, L. M., and Ramaswamy, V.: Hygroscopic and optical properties of organic sea salt aerosol and consequences for climate forcing, Geophysical Research Letters, 31, 10.1029/2004gl020628, 2004.

Rehbein, P. J. G., Jeong, C.-H., McGuire, M. L., and Evans, G. J.: Strategies to Enhance the Interpretation of Single-Particle Ambient Aerosol Data, Aerosol Science and Technology, 46, 584-595, 10.1080/02786826.2011.650334, 2012.

Shi, Y., Ge, M., and Wang, W.: Hygroscopicity of internally mixed aerosol particles containing benzoic acid and inorganic salts, Atmospheric Environment, 60, 9-17, 2012.

Silva, P. J., Liu, D. Y., Noble, C. A., and Prather, K. A.: Size and chemical characterization of individual particles resulting from biomass burning of local Southern California species, Environmental Science & Technology, 33, 3068-3076, 10.1021/es980544p, 1999.

Sjogren, S., Gysel, M., Weingartner, E., Alfarra, M. R., Duplissy, J., Cozic, J., Crosier, J., Coe, H., and Baltensperger, U.: Hygroscopicity of the submicrometer aerosol at the high-alpine site Jungfraujoch, 3580 m a.s.l., Switzerland, Atmospheric Chemistry and Physics, 8, 5715-5729, 2008.

Song, X. H., Hopke, P. K., Fergenson, D. P., and Prather, K. A.: Classification of single particles analyzed by ATOFMS using an artificial neural network, ART-2A, Analytical Chemistry, 71, 860-865, 10.1021/ac9809682, 1999.

Spencer, M. T., Shields, L. G., Sodeman, D. A., Toner, S. M., and Prather, K. A.: Comparison of oil and fuel particle chemical signatures with particle emissions from heavy and light duty vehicles, Atmospheric Environment, 40, 5224-5235, 10.1016/j.atmosenv.2006.04.011, 2006.

Sullivan, R. C., Guazzotti, S. A., Sodeman, D. A., and Prather, K. A.: Direct observations of the atmospheric processing of Asian mineral dust, Atmospheric Chemistry and Physics, 7, 1213-1236, 2007a.

Sullivan, R. C., Guazzotti, S. A., Sodeman, D. A., Tang, Y. H., Carmichael, G. R., and Prather, K. A.: Mineral dust is a sink for chlorine in the marine boundary layer, Atmospheric Environment, 41, 7166-7179, 10.1016/j.atmosenv.2007.05.047, 2007b.

Swietlicki, E., Hansson, H. C., Hameri, K., Svenningsson, B., Massling, A., McFiggans, G., McMurry, P. H., Petaja, T., Tunved, P., Gysel, M., Topping, D., Weingartner, E., Baltensperger, U., Rissler, J., Wiedensohler, A., and Kulmala, M.: Hygroscopic properties of submicrometer atmospheric aerosol particles measured with H-TDMA instruments in various environments - a review, Tellus Series B-Chemical and Physical Meteorology, 60, 432-469, 10.1111/j.1600-0889.2008.00350.x, 2008.

Toner, S. M., Shields, L. G., Sodeman, D. A., and Prather, K. A.: Using mass spectral source signatures to apportion exhaust particles from gasoline and diesel powered vehicles in a freeway study using UF-ATOFMS, Atmospheric Environment, 42, 568-581, 10.1016/j.atmosenv.2007.08.005, 2008.

Vakeva, M., Kulmala, M., Stratmann, F., and Hameri, K.: Field measurements of hygroscopic properties and state of mixing of nucleation mode particles, Atmospheric Chemistry and Physics, 2, 55-66, 2002.

Varutbangkul, V., Brechtel, F. J., Bahreini, R., Ng, N. L., Keywood, M. D., Kroll, J. H., Flagan, R. C., Seinfeld, J. H., Lee, A., and Goldstein, A. H.: Hygroscopicity of secondary organic aerosols formed by oxidation of cycloalkenes, monoterpenes, sesquiterpenes, and related compounds, Atmospheric Chemistry and Physics, 6, 2367-2388, 2006.

Wang, X. N., Ye, X. N., Chen, H., Chen, J. M., Yang, X., and Gross, D. S.: Online hygroscopicity and chemical measurement of urban aerosol in Shanghai, China, Atmospheric Environment, 95, 318-326, 10.1016/j.atmosenv.2014.06.051, 2014.

Zauscher, M. D., Wang, Y., Moore, M. J. K., Gaston, C. J., and Prather, K. A.: Air Quality Impact and Physicochemical Aging of Biomass Burning Aerosols during the 2007 San Diego Wildfires, Environmental Science & Technology, 47, 7633-7643, 10.1021/es4004137, 2013.

Direct links between hygroscopicity and mixing state of ambient aerosols: Estimating particle hygroscopicity from their single particle mass spectra

Xinning Wang[1], Xingnan Ye[1], Jianmin Chen[1], Xiaofei Wang*[1,2] and, Xin Yang*[1,2,3], Tzung-May Fu[3], Lei Zhu[3], Chongxuan Liu[3]

[1] Shanghai Key Laboratory of Atmospheric Particle Pollution and Prevention, Department of Environmental Science and Engineering, Fudan University, Shanghai 200433, China

[2] Shanghai Institute of Pollution Control and Ecological Security, Shanghai 200092, China

[3] School of Environmental Science and Engineering, Southern University of Science and Technology, Shenzhen, China

Atmospheric Chemistry and Physics Discussions

December 23, 2019

April 2nd, 2020

*To whom correspondence should be addressed.

Correspondence to:

Xiaofei Wang

: Email: xiaofeiwang@fudan.edu.cn Tel: +86-21-31242526

25   Xin Yang

26   : Email: yangxin@fudan.edu.cn Tel: +86-21-31245272

27

28 ***ABSTRACT***

29 Hygroscopicity plays ~~a~~ crucial ~~role~~roles in determining aerosol optical properties and aging

30 processes in the atmosphere. We investigated submicron aerosol hygroscopicity and

31 composition by connecting an aerosol time-of-flight mass spectrometer (ATOFMS) ~~to the~~

32 ~~downstream of~~in series to a hygroscopic tandem differential mobility analyzer (HTDMA), to

33 ~~simultaneously~~ characterize ~~hygroscopicities~~hygroscopicity and ~~chemical~~

34 ~~compositions~~composition of ambient aerosols in Shanghai, China. ~~Major~~The HTDMA-

35 ATOFMS data suggested that particle types, including biomass burning, EC, Dust/Ash,

36 organics particles, cooking particles and sea salt, were shown to have distinct hygroscopicity

37 distributions. ~~It is also found that particles with stronger hygroscopicities were more likely to~~

38 ~~have higher effective densities.~~Peak intensities in particle spectra were found nonlinearly

39 correlated with hygroscopicity and the correlations were variant with particle types. Based on

40 the measured hygroscopicity-composition relations, we developed a statistical method to

41 estimate ambient particle hygroscopicity just from their mass spectra. ~~This~~The method was

42 applied to another ambient ATOFMS dataset sampled ~~from~~during September 12nd to 28th, 2012

43 in Shanghai~~, and it is found~~. The estimated hygroscopicity suggested that ambient particles

44 were present in three ~~major~~apparent hygroscopicity modes, whose growth factors ~~at relative~~

45 ~~humidity 85%~~peaked at 1.05, 1.42 and 1.60~~,~~ (85% RH), respectively. The ~~temporal variations~~

46 ~~of the~~ estimated ~~particle hygroscopicity~~GF were ~~consistent with the back trajectory~~

47 ~~analysis~~divided into four bins as <1.1, 1.1-1.3, 1.3-1.5 and >1.5 to represent the nearly-

48 hydrophobic (NH), less-hygroscopic (LH), more-hygroscopic (MH) and ~~atmospheric visibility~~

49 ~~observations. These~~sea salt (SS) mode. Number contributions of particle types to

50 hygroscopicity ~~estimation~~modes showed consistent results with ~~single particle mass spectra~~

51 ~~analysis can provide critical~~the HTDAM-ATOFMS experiment. Based on the combined

52 information on ~~particulate water content,~~particle composition, hygroscopicity, airmass back

53 trajectories and ambient pollutants concentrations, we inferred that the NH, LH, MH, SS modes

54 were characterized by POA/EC, SOA, SIA and salts compositions, respectively. The proposed

55 method would provide additional information to the study of particle mixing states, source

56 ~~apportionment and aging processes~~identification and visibility degradation.

1. INTRODUCTION

Atmospheric particles have critical influences on climate and the environment. They affect climate by directly interacting with sunlight and changing the energy balance of earth's atmosphere (Facchini et al., 1999;Lohmann and Feichter, 2005). Additionally, they act as cloud condensation nuclei or ice nuclei and impact cloud formation (Lohmann et al., 2007). Aerosol particles also participate many important atmospheric reactions (Gard et al., 1998;Qiu and Zhang, 2013). The climate relevant properties and chemical reactivity of aerosols are largely determined by their hygroscopic property. In the ambient condition the hygroscopic growth of particles introduce aqueous surface to particles and their optical effects are importantly altered (Cheng et al., 2008;Titos et al., 2014), which exerts impacts on atmospheric aging processes of particles and visibility degradation (Qu et al., 2015;Liu et al., 2012;Qiu and Zhang, 2013;Wang et al., 2009;Chen et al., 2012;Li et al., 2018).

Atmospheric particles are a mixture of a complicated variety of chemical compounds. The bulk chemical composition of particulate matter (PM) usually refers to its dry composition (Li et al., 2016;Herich et al., 2011).Atmospheric particles have critical impacts on climate and the environment. They affect climate by directly interacting with sunlight and changing the energy balance of earth's atmosphere (Facchini et al., 1999;Lohmann and Feichter, 2005). Aerosol particles also act as cloud condensation nuclei or ice nuclei and impact cloud formation (Lohmann and Feichter, 2005). Aerosol particles provide surfaces for heterogeneous reactions to occur and act as the sink for many atmospheric reactions (Gard et al., 1998;Qiu and Zhang, 2013), which are of significance to air quality, visibility and human health. The climate-relevant and other properties of aerosols are largely determined by their hygroscopicity. In atmospheric conditions the hygroscopic growth transform particles into micro droplets and their optical effects are altered importantly (Cheng et al., 2008;Qu et al., 2015), which further impacts particle aging processes and visibility degradation (Qu et al., 2015;Liu et al., 2012;Qiu and

83 Zhang, 2013;Chen et al., 2012).

84 Atmospheric particles are a mixture of a complicated variety of chemical compounds. The bulk

85 chemical composition of particulate matter (PM) usually refers to its dry composition. However,

86 in ambient ~~condition~~conditions the particulate water is also an important constitution of PM

87 which has not been accounted for in conventional gravitational analysis. The mass of particulate

88 water may be ~~times higher~~much larger than the total mass of dried PM at elevated RHs

89 ~~(Swietlicki et al., 2008).~~(Swietlicki et al., 2008). The factors that affect water contents in

90 particles include the particle hygroscopicity, the particle size distributions and ambient RH.

91 ~~Particle~~The hygroscopicity parameter determines the particle's ability to ~~hygroscopic~~growth.

92 ~~It direclty~~ in their sizes in humidity environment, which is directly relates to particle

93 composition and size. To accurately predict particulate water content, a detailed knowledge on

94 ~~both of~~particle hygroscopicity and composition is needed ~~(Gysel et al., 2007;Sjogren et al.,~~

95 ~~2008;Laborde et al., 2013;Healy et al., 2014).~~(Gysel et al., 2007;Sjogren et al., 2008;Laborde

96 et al., 2013;Healy et al., 2014).

97 ~~Aerosol hygroscopicity could be determined quantitatively by techniques such as the~~

98 ~~Hygroscopic Tandem Differential Mobility Analyzer (HTDMA) (Swietlicki et al., 2008).~~

99 ~~Previous studies have obtained particle hygroscopicity and chemical composition in the same~~

100 ~~time by deploying HTDMA and chemical composition measurements in parallel (Gysel et al.,~~

101 ~~2007;Sjogren et al., 2008;Laborde et al., 2013). The measured hygroscopicity was compared~~

102 ~~with the reconstructed values using the mixing rules of variant compositions (Gysel et al., 2007).~~

103 ~~The hygroscopicity reconstructed in this way is representing the averaged hygroscopicity of~~

104 ~~ensembled particles and therefore could not reflect the mixing states of particles (Healy et al.,~~

105 ~~2014). Ambient studies suggested that atmospheric aerosols were commonly externally mixed,~~

106 ~~as shown by the separated modes in hygroscopicity distributions (Swietlicki et al.,~~

107 ~~2008;Massling et al., 2007;Liu et al., 2011). The alternative way to obtain simultaneous~~

6

108 ~~information on hygroscopicity and composition is connecting the HTDMA with particle~~

109 ~~composition measurement techniques in tandem (Buzorius et al., 2002;Zelenyuk et al.,~~

110 ~~2008;Herich et al., 2008;Laborde et al., 2013). In this configuration, the HTDMA acts as~~

111 ~~hygroscopicity selector, with hygroscopicity segregated particles being analyzed subsequently~~

112 ~~by other techniques. More direct connection between hygroscopicity and composition could be~~

113 ~~established in this way. For particle composition measurement, sensitive methods such as single~~

114 ~~particle mass spectrometers are preferred since they can analyze particles in low concentrations~~

115 ~~in the outflow of HTDMA (Herich et al., 2008;Herich et al., 2009). The merit of single particle~~

116 ~~techniques is that particle mixing state is preserved during analysis (Healy et al., 2014).~~

117 ~~Only a few previous~~ Aerosol hygroscopicity can be quantitatively measured by techniques such

118 as the Hygroscopic Tandem Differential Mobility Analyzer (HTDMA) (Swietlicki et al., 2008).

119 Previous studies measured aerosol hygroscopicity and chemical composition simultaneously

120 by deploying HTDMA and chemical composition measurements in parallel (Gysel et al.,

121 2007;Sjogren et al., 2008;Laborde et al., 2013). The measured hygroscopicity was compared

122 with the reconstructed values using the mixing rules of variant compositions (Gysel et al., 2007).

123 The hygroscopicity reconstructed in this way is representing the averaged hygroscopicity of

124 ensembled particles and therefore could not reflect the mixing states of particles (Healy et al.,

125 2014). However, the HTDMA measurements suggested that several hygroscopicity modes exist

126 simultaneously, which evidenced the external mixing state of atmospheric particles. HTDMA

127 hygroscopicity modes were generally fell into four categories: nearly hydrophobic (NH), less-

128 hygroscopic (LH), more-hygroscopic (MH), and sea-salt mode, with their center GFs (90% RH)

129 lie in 1.0-1.11, 1.11-1.33, >1.33 and >1.8 ranges, respectively (Swietlicki et al., 2008). To

130 investigate the chemical nature of these hygroscopicity modes, it is better to connect HTDMA

131 and composition measurement techniques in tandem, since more direct connection between

132 hygroscopicity and composition could be established in this way (Buzorius et al.,

133 2002;Zelenyuk et al., 2008;Herich et al., 2008;Laborde et al., 2013). For composition

measurement techniques, single particle mass spectrometers are preferred since they are sensitive to analyze particles of low concentrations in the HTDMA outflow (Herich et al., 2008;Herich et al., 2009), and that the particle mixing state information is preserved during analysis (Healy et al., 2014).

Only a few studies have reported simultaneous characterization of hygroscopicity and composition using the tandem method (Herich et al., 2008;Herich et al., 2009;Buzorius et al., 2002;Zelenyuk et al., 2008). Zelenyuk et al.(Zelenyuk et al., 2008)(Herich et al., 2008;Herich et al., 2009;Buzorius et al., 2002;Zelenyuk et al., 2008). Zelenyuk et al. connected HTDMA and a single particle mass spectrometer SPLAT in serieswith HTDMA to perform multiple measurementdemonstrate the capability of this system to derive quantitative information on aerosol composition, hygroscopicity-, composition, and effective density. Herich et al. have (Zelenyuk et al., 2008). Herich et al. firstly applied the tandem HTDMA-ATOFMS system to investigate particle composition as a function of hygroscopicity in Switzerland (Herich et al., 2008) and then in a subarcticcharacterize particle composition of different hygroscopicity (Herich et al., 2008;Herich et al., 2009). A large portion of the less hygroscopic modes were found to be contributed by organics and combustion species both in the urban and remote site (Herich et al., 2009). In a, while the sulfates and nitrates were present in almost all particles independent of hygroscopicity. Similar findings were also observed in our preliminary study, we appliedcharacterization using HTDMA-ATOFMS to characterize chemical compositions of ambient particles with a few hygroscopicities (Wang et al., 2014). However, this obtainedin Shanghai city (Wang et al., 2014), except higher nitrate and sulfate intensities were found in hygroscopic particles in our study. However, the preliminary dataset iswas not sufficiently large to provide a hygroscopicity distribution for each aerosol particle type. Therefore, thesince only a few GF were characterized in that study (GF 1.05-1.1, 1.3, 1.4 and 1.5 at 85% RH). The primary objective of the present study is to establish thorough more complete connections between hygroscopicity and single particle signatures, which could be further utilized to predict hygroscopicity of ambient particles. Here weWe conducted a comprehensive HTMDAHTDMA-ATOFMS characterization experiment with the particle GF varied in a more complete GF range (GF 0.9~1.7, 85% RH), which accountsaccounted for athe main number

8

163 fraction of atmospheric particles in urban atmosphere ~~(Liu et al., 2014;Liu et al., 2011;Ye et al.,~~

164 ~~2013) . Moreover, we~~(Liu et al., 2014;Liu et al., 2011;Ye et al., 2013) . Based on the HTDMA-

165 ATOFMS data, we further developed and tested a method ~~that utilize the established dataset~~ to

166 estimate the hygroscopicity of ambient particles analyzed by ATOFMS.

2. EXPERIMENTAL SECTION

2.1. HTDMA

169 The custom-built HTDMA ~~(Ye et al., 2009;Angelino et al., 2001) consists of two DMAs and a~~

170 ~~humidifier~~(Ye et al., 2009) consists of two DMAs and a humidifier connected in series (Figure

171 1). Aerosol was dried before entering HTDMA (RH ~10%) by a diffusional silica gel tube. The

172 dried aerosol reached ~~its~~ charge equilibrium in a Kr-85 neutralizer. The DMA1 (Model 3081,

173 TSI Inc.) selected particles ~~based on their~~ by electrical mobility size as D_{dry}. ~~Then, the~~The

174 monodisperse particles from DMA1 grew in a Nafion humidifier (RH=85%). The sizes of

175 humidified particles D_{RH} was ~~scanned~~determined by the second DMA ~~and~~connected by a CPC

176 to measure their concentrations. The sheath flow rate in DMA2 (3 l/min) was regulated by mass

177 flow controller. The RH of the DMA2 sheath flow was managed to match the humidifier (85%

178 RH~~) by adjusting the water saturated air.~~). The ~~DMAs, the humidifier and other parts~~HTDMA

179 were installed in thermostatic chamber in which temperature was controlled to $25\pm0.1℃$. The

180 total aerosol flow was 0.4 L/min (the sum flow rate of the CPC, 0.3 L/min and the ATOFMS,

181 0.1 L/min). Aerosol residence time in humidifier was ~10 s. PSL spheres of known size and

182 $(NH_4)_2SO_4$ salt were used to calibrate the HTDMA. The HTDMA uncertainty in GF

183 determination is ±0.05 (Ye et al., 2009;Swietlicki et al., 2008).

2.2. ATOFMS

185 The ~~principle functional parts~~schematic of ATOFMS (Model 3800-100, TSI. Inc) is illustrated

186 in Figure 1. ~~After particles entered the inlet~~Particles were drawn into ATOFMS through a

187 0.1mm orifice ~~of ATOFMS, they were~~and focused into narrow beam through successive

188 expansions and contractions in the aerodynamic focusing Lens (AFL). Particles leaving the

189 AFL ~~have drifting~~obtain velocities ~~which are depended~~depending on their ~~vacuum~~

190 aerodynamic sizes. In the ATOFMS sizing region ~~the~~ particles pass through two orthogonally

191 oriented continuous lasers (Nd: YAG, 532 nm) ~~to scatter~~and laser light~~.~~ was scattered. The

192 scattered light generates ~~two~~ pulses in two photomultiplier tubes (PMT) and the signal delay

193 between the two pulses is used to calculate particle velocity ~~considering the distance between~~

194 ~~two lasers is known.~~. Particle velocity ~~information~~ was also used to trigger ionization laser (Nd:

195 YAG, 266 nm) at ~~appropriate~~exact time to ionize ~~individual~~particles. The negative and positive

196 ions generated from particles. ~~The ions~~ are recorded by a dual polar time-of-flight mass

197 spectrometer ~~to generate positive and negative mass spectra for each particle.~~. More details of

198 ATOFMS were described elsewhere ~~(Gard et al., 1997;Su et al., 2004).~~(Su et al., 2004).

199 The ATOFMS data was analyzed within the YAADA toolkit (http://www.yaada.org/). Particles

200 showing similar composition were classified by the adaptive resonance theory-based clustering

201 algorithm (ART-2a) (Song et al., 1999). The ART-2a algorithm parameters were set to: vigilance

202 factor = 0.85, learning rate = 0.05 and number of iterations = 20. The clusters generated by the

203 ART-2a were manully regrouped into major types by considering their common composition

204 patterns. The obtained particle types were labelled by refering previous single particle

205 characterization studies (Spencer et al., 2006;Silva et al., 1999;Sullivan et al., 2007;Gaston et

206 al., 2011;Qin et al., 2012).

207 **2.3. ~~Field sampling~~Sampling description**

208 ~~During Feb 26 to Mar 7, 2014, the~~ The HTDMA-ATOFMS characterization was

209 ~~performed~~carried out at the building of department of environmental science and technology in

210 Fudan university (31°18'N, 121°29'E~~).~~) from Feb-26 to Mar-7, 2014. Aerosol inlet was installed

211 at the building roof about 6 m above the ground. The Fudan campus was influenced by local

212 emissions sources from transportation, residential, business and cooking activities from

213 surrounding areas which can be viewed as ~~an~~urban environment. A period of ambient ATOFMS

214 data, which persisted from Sep-12 to Sep-28, 2012, was ~~obtained~~recorded at the same site in

215 Fudan campus. Ambient air quality data of pollutants concentrations ($PM_{2.5}$, O_3, and SO_2) in

216 Shanghai city were provided by Shanghai Environmental Monitoring Center (SEMC).

217 ~~The sampling procedure was similar to our previous study (Wang et al., 2014). The HTDMA~~

218 ~~GF distributions obtained during sampling intermittence usually show two hygroscopicity~~

10

219 modes. The first mode centered at GF ~ 1.05 and the second mode at GF ~ 1.45 at RH 85%,

220 which will be termed as Near Hydrophobic (NH) and More Hygroscopic (MH) mode,

221 respectively. These modes were also typically found in other types of environment (Liu et al.,

222 2011;Swietlicki et al., 2008). The majority of particles (>97 %) were shown to have growth

223 factors in 0.9-1.7 range. Therefore, in this study we preselected particles with GFs from 0.9 to

224 1.7 (0.1 GF step) in HTDMA for ATOFMS characterizations.

225 To set the desired GFs, the two DMAs in HTDMA system were maintained at fixed diameters

226 D_{dry}, D_{RH} according to GF=D_{RH}/D_{dry}. The DMAs were kept to select the desired diameters

227 before significant number of particle were chemical analyzed by ATOFMS. In this study the

228 DMA1 (D_{dry}) was set to 250 nm, while the DMA2 (D_{RH}) was set to diameters as shown in Table

229 1, where the length of sampling duration, the number analyzed particles are given. The number

230 of particles analyzed by ATOFMS was affected by the ambient particle number concentrations.

231 Because the particle concentrations in the outflow of HTDMA are generally low and even lower

232 at some GFs, longer sampling time was planned to obtain statistically significant particle

233 numbers (See the CPC concentrations in Figure S1). Usually the ATOFMS has lower detection

234 efficiencies at smaller than 250 nm range due to the reduced scattering efficiency, while larger

235 particles usually have less number concentrations. Therefore, the selection of D_{dry} as 250nm is

236 a compromise between the two issues (Wang et al., 2014;Herich et al., 2008;Herich et al., 2009).

237

238 The sampling procedure was similar to our previous study (Wang et al., 2014). The typical

239 HTDMA GF distributions in this site showed two separated hygroscopicity modes. In 85% RH

240 condition, the two modes were present with respective center GF of 1.05 and 1.45, which were

conventionally classified as Near-Hydrophobic (NH) and More-Hygroscopic (MH) modes, respectively (Swietlicki et al., 2008). These modes were normally present elsewhere in China and other areas (Liu et al., 2011;Swietlicki et al., 2008). The HTDMA data suggest that the majority of particles (>97 %) were of GF in 0.9-1.7 range. Consequently, particles in this GF range were characterized by HTDMA-ATOFMS with a GF step of 0.1.

To characterize the desired GFs, the two DMAs in HTDMA were set at certain diameters D_{dry} and D_{RH} according to GF=D_{RH}/D_{dry}. The HTDMA-ATOFMS system was kept sampling until a sufficient number of particles (> 200) were analyzed by ATOFMS for each GF setting (Table 1). We fixed the DMA1 (D_{dry}) diameter to 250 nm, while the DMA2 diameter (D_{RH}) was set as shown in Table 1. The number of particle spectra in ATOFMS was affected by ambient particle concentrations of certain GF. Since particle concentrations in the downstream of HTDMA were very low, longer sampling were maintained to record sufficient number of spectra in ATOFMS (See the CPC concentrations in Figure S1). The ATOFMS instrument used in this study has size detection range of 100-3000 nm. Considering this, the detection efficiency for 250 nm is expected to be low, as 250 nm is on the lower end of ATOFMS detection range. However, in HTDMA-ATOFMS experiment we selected 250 nm particles, because the concentrations of larger particles were found to decrease further in SMPS size distributions. Therefore, the selection of D_{dry} as 250 nm is a compromise between detection efficiency and particle concentrations (Wang et al., 2014;Herich et al., 2008). With the measured ATOFMS particle numbers and CPC concentrations, the detection efficiency of ATOFMS were calculated to be ~1.6×10^{-2} at the dry size. In Figure S2 we presented ATOFMS detection efficiencies together with the particle hit rate (hit particles/total sized particles) at different growth factors. Generally, the detection efficiencies suggested variations at different GFs. We found higher detection efficiencies in moderate GF range (1.2-1.4) and higher hit rates in GF<1.3 range, which is probably caused by variations of compositions with GF (Hatch et al., 2014).

Table 1. Statistics of the DRH, GF, sampling duration and the number of chemically analyzed particles by ATOFMS (D_{dry} = 250 nm, RH = 85%).

D_{RH} (nm)	225	250	275	300	325	350	375	400	425

Growth Factor	0.9	1.0	1.1	1.2	1.3	1.4	1.5	1.6	1.7
Duration (hours)	42	67	11	20	8	11	34	20	11
Number of spectra detected	742	1665	709	1401	2330	4469	6399	723	262

2.4. Estimation of ambient particle hygroscopicity

When inspecting particle mass spectra obtained from HTDMA-ATOFMS experiment, it is recognized that most of produced spectra were also frequently present in ATOFMS ambient characterizations. This fact forms the basis of the idea to assign similar GF to ambient particles if they have similar composition as in HTDMA-ATOFMS experiment.

To estimate hygroscopicity of ambient single particles, we compare the ambient particle mass spectra with those obtained in HTDMA-ATOFMS experiment similarly as in ART-2a algorithm (Song et al., 1999). In ATOFMS particle spectra, some metal (such as Na, K, Fe) were producing inappropriately large peaks due to higher ionization efficiencies. This problem was relieved by taking the 0.5 power (square root) of peaks intensities. After this treatment the relative intensities of largest peaks were suppressed the while smaller peaks (such as organic peaks) increased relatively in the evaluation of spectra similarities. Then we searched the candidate particles in HTDMA-ATOFMS data which produced the highest similarities with the atmospheric particle (similarities in the range of 95% to 100% maximum similarity). Since each item of mass spectra acquired by HTDMA-ATOFMS was associated with a GF, we obtained a collection of discrete GF values (from 0.9 to1.7 spaced by 0.1) that were the most probable candidate GFs. The estimated GF of the atmospheric particle was determined to be the weighted mean of the candidate GFs, with weights being the number percentages of candidate particles happened in each discrete GF groupsParticles in HTDMA-ATOFMS dataset is comparable to ambient ATOFMS particles. Particle types typically present in HTDMA-ATOFMS study were also preset in ambient ATOFMS studies. Therefore, it is possible to assign similar GF to ambient

particles if they have similar composition. The estimation method was firstly performed by evaluating spectra similarities between ATOFMS and HTDMA-ATOFMS dataset (dot products of normalized spectra). The ATOFMS is known to have higher detection efficiencies toward some metals (such as Na, K, Fe), resulting inappropriately large peaks in particle spectra. We solved the bias by taking the 0.5 power treatment to peaks intensities (Rehbein et al., 2012). In this treatment the larger peaks were suppressed in some degree while smaller peaks increased their weigh relatively. The 0.5 power treatment to peaks intensity was applied because it offered better results in the estimation of hygroscopicity than without it, as discussed in the supplemental information (Figure S3). In the second step we searched matched particles from the HTDMA-ATOFMS dataset showing the best similarities with the ambient particle (dot products in 95-100% range of the maximum dot product). In this study we set a threshold similarity (0.7 dot product) in matching particles, as was required in ART-2a algorithm (Song et al., 1999). Ambient particles with matching dot products <0.7 were excluded from analysis of the estimated GF. The similarity data suggests that 96.2% of the matching similarities are > 0.7 and 79% of them are >0.8 (Figure S4). Since each of the matched particles in HTDMA-ATOFMS dataset was associated with a GF, we obtained a collection of the matching GFs (0.9 -1.7 in 0.1 step). The estimated GF of the ambient particle was determined to be the weighted average of the matched GFs, with the weights being the number percentage of matched particles in each GF bins:

$$GF_{pred} = \frac{\sum GF_i \cdot F_i}{\sum F_i}$$

where: GF_{pred} = the estimated GF of ~~atmospheric~~ambient particle, GF_i = GF value from 0.~~1~~9 to 1.7 interspaced by 0.1, F_i = number percentages of the ~~candidate~~matched particles in each GF ~~group~~bin.

~~From the descriptions above, this method is a~~ The estimation process relied on statistical approach ~~to find~~ in estimating the most probable ~~hydroscopicity~~hygroscopicity for ~~each single particle, rather than estimating chemical compositions in individual particles and then predicting~~ambient particles, rather than by inferring particle compositions of single particles (Healy et al., 2014). The latter method derived quantitative concentrations of various

compositions from peak intensities, which were then applied to predict particle hygroscopicity using the assumed composition, as previously applied by (Healy et al., 2014). The latter approach is based on Zdanovskii-Stokes-Robinson mixing roles, and it needs to assume a chemical composition for each single aerosol particle, which might not be reliable due to the qualitative nature of ATOFMS analysis. However, the new approach developed in this study infer particlerules. Some assumptions including material densities were needed in that method. As a comparison, we inferred hygroscopicity by comparing the mass spectra of ambientmatching particles with particles whose hygroscopicity has already been experimentally determined by HTDMA. ATOFMS particles of known hygroscopicity. Therefore, this method derives GFthe estimated GFs were derived from the measured GF values and the possible artifacts caused by assumptions of composition densities and detection sensitivities in ATOFMS are obviated.

The uncertainties in the GF prediction in this method were estimated. The uncertainties in eventual GF may stem from the intrinsic uncertainties in HTDMA-ATOFMS techniques. For the estimation algorithm itself, only few parameters exist that are capable to affect the estimated GF. With the 0.5 power treatment to peak intensities, the only parameter that could influence the estimated GF would be the matching criteria of particles. We have adjusted the matching criteria of 95-100% maximum dot products to 90-100% and 98-100% and the variations in particle GFs were inspected (Figure S5). Based on the variations of the obtained GF, we estimated that the uncertainty in GF estimation is within ±0.15.

3. RESULTS AND DISCUSSIONS

3.1. Single particle composition and hygroscopicity in HTDMA-ATOFMS experiment

3.1.1 Hygroscopicity distribution of particle types

The sampled aerosols with similar mass spectra are grouped together to form many **different particle types.**

The particles in the HTDMA-ATOFMS dataset were classified into major types based on their mass spectra. The ART-2a algorithm was applied to particle clustering and then similar clusters

15

were combined. The majority of ~~analyzed~~ particles were eventually ~~grouped~~classified into 9

types~~, namely~~ including Biomass, Fresh EC, Aged EC, Dust/Ash, HMOC, Amine-rich,

Ammonium/OC, Cooking and Sea salt ~~types.~~. In Figure 2 ~~presents~~we present the average ~~mass~~

spectra~~, particle~~ of each type and their numbers detected ~~at different GF stages for each types.~~

~~Since the numbers of analyzed particle~~ in each GF bin ~~are~~. Since the total number of detected

particles in GF bins were not ~~a constant~~equal (Table 1), ~~the~~ we also present the particle numbers

normalized ~~particle numbers~~ by the total ~~particle~~ numbers to indicate their detection probability

in each GF bin ~~were calculated to show their occurrence probability (Fig. 2).~~(Figure. 2). The

hygroscopicity of particle types showed different distribution patterns with GF. The

hygroscopicity characters of Biomass, EC, Dust/ash, HMOC and Amine-rich types were

described previously and their hygroscopicity have shown consistent trend with the previous

characterization (Wang et al., 2014).

~~3.1.1. Particle types and GF distributions~~

~~As illustrated in Fig. 2,~~ The Biomass ~~type~~ particles ~~have~~produced characteristic peaks ~~at~~of -

26(CN), -42(CNO), -59($C_2H_3O_2$), -73($C_3H_5O_2$) ~~in negative spectra~~ and dominant ~~potassium~~

peak at 39K and ~~clusters~~related peaks at 113(K_2Cl) or 213(K_3SO_4) ~~(Silva et al., 1999). During~~

~~this study, the HTDMA-ATOFMS system detected 547 biomass~~(Silva et al., 1999;Zauscher et

al., 2013;Pratt and Prather, 2009). Biomass particles ~~which account for 2.9% of total analyzed~~

~~particles. Despite the small number, the hygroscopicity of biomass particles is~~ displayed low ~~in~~

~~that the~~hygroscopicity since majority of ~~biomass particles (87%)~~them were ~~detected~~present in

GF <1.2 range. ~~On average the biomass particle type contribute 2.9% of analyzed particle~~

~~numbers in this GF range,~~. with the peak ~~number fraction occurred at GF 1.1 (19%), as shown~~

~~in Figure 2 (a). Similar hygroscopicity pattern of biomass particles is reported previously~~

~~(Rissler et al., 2006;Martin et al., 2013).~~detection probability at GF 1.1 (Figure 2 (a)). The

hygroscopicity of Biomass particles is consistent with other HTDMA measurement of biomass

particles (Rissler et al., 2006;Laborde et al., 2013). The hygroscopicity of biomass particles in

ambient environment were similarly detected in the HTDMA-SP2, which suggested the center

GF of 1.1~1.2 of biomass particles (at 90% RH), corresponding to the GF of 1.06-1.13 at 85%

373 RH (Laborde et al., 2013).

374 EC type particles are characterized by a series of elemental carbon peaks at C_n (n=1, 2, 3 …) in

375 the negative and positive spectra. EC is a dominant particle type which accounts for 37.5%

376 (7020 particles) of the analyzed particle number in this study. EC particles distributed broadly

377 from NH to MH range. However, the particle compositions are different in NH and MH

378 hygroscopicity range, where fresh and aged EC dominate, respectively (Figure 2 b-c). Fresh

379 EC particles have not experienced significant aging, with weak or no secondary peaks (-62NO_3^-,

380 -97HSO_4^-, 18NH_4^+) in their spectra. Therefore, most of them were in hydrophobic mode

381 (Weingartner et al., 1997). The mass spectra of aged EC showed the internal mixing of

382 secondary matters (nitrate, sulfate, ammonium), which is consistent with their hygroscopic

383 property. The peak intensity variations (-62NO_3^-, -97HSO_4^-, 18NH_4^+ and other relevant peaks)

384 in EC spectra were a function of GF. A gradual increase of secondary peak intensities in GF 0.9

385 -1.2 range was observed (Figure S2).

386 Dust/ash type particles have inorganic peaks of salts and metals oxides (Wang et al.,

387 2019;Zhang et al., 2009;Dall'Osto et al., 2008). About 7.4% of analyzed particles were

388 classified into this type. Most of dust/ash particles (>85%) were detected in hygroscopic range

389 (GF > 1.3). However, Dust/ash particles with Al-Si signals were clearly enriched in NH mode

390 (Wang et al., 2014), with the highest detection probability at GF 1.1, as shown in Figure S3.

391 The Al-Si particles are assumed to be soil dusts according to their reported low hygroscopicity

392 (Koehler et al., 2009).

393 The EC particles were detected by a series of elemental carbon peaks at C_n (n=1, 2, 3 …) in the

394 negative and positive spectra (Ault et al., 2010;Spencer et al., 2006;Toner et al., 2008). EC

395 particles distributed broadly from nearly-hydrophobic (NH) mode to more-hygroscopic (MH)

396 mode. However, the mass spectra of hydrophobic and hygroscopic EC particles were different

397 in their mass spectra. As shown in Figure 2 (b-c), The mass spectra of hygroscopic EC particles

398 produced stronger secondary peaks ($-62NO_3^-$, $-97HSO_4^-$, $18NH_4^+$) than hydrophobic EC

399 particles, consistent with the significant fractions of secondary matters in hygroscopic EC

400 (Laborde et al., 2013). According to their hygroscopicity distributions, the general EC type was

401 divided into Fresh EC and aged EC type. The mass spectra of Fresh EC suggested they were

402 freshly emitted without significant secondary coatings (Weingartner et al., 1997;Laborde et al.,

403 2013;Herich et al., 2009). Peak intensity trends of $62NO_3^-$, $-97HSO_4^-$, $18NH_4^+$ and other related

404 peaks at different GF were summarized for EC particles (Figure S6). Based on the statistics of

405 peak intensities, we found clear increasing trends of secondary peak intensities in GF 0.9-1.2

406 range, but not in all GFs (Laborde et al., 2013;Herich et al., 2008).

407 Dust/ash type particles produced inorganic peaks of salts and metals (Gaston et al., 2017;Ault

408 et al., 2011;Sullivan et al., 2007). Most of dust/ash particles were detected in hygroscopic range

409 (GF>1.3). Most of Dust/ash particles were internally mixed with nitrate. Within the general

410 Dust/ash type there are many sub-clusters according to specific association of metal peaks in

411 particle spectra. Some of the clusters showed characteristic hygroscopicity distributions which

412 offered values in the source apportionment of these particles. As an illustration, we presented

413 the mass spectra and hygroscopicity distribution of the Al-Si cluster in Figure 3. The mass

414 spectra of Al-Si particles showed stronger aluminum ($27Al^+$) and silicate ($-76SiO_3^-$) peaks in

415 their positive and negative spectra, respectively. Particle number distribution of Al-Si particles

416 suggested that they were detected with the highest probability at GF 1.1. In the preliminary

417 study we identified the similar Al-Si particles exclusively in NH mode (Wang et al., 2014).

418 Based on their hygroscopicity distribution, we assumed the Al-Si particles are soil dusts

419 according to their reported low hygroscopicity (Koehler et al., 2009).

420 The spectra of HMOC ~~type~~ particles ~~contain~~showed obvious organic peaks in higher m/z range

421 (>150). ~~This type accounts for 2.6% of total number of analyzed particles. Within the HMOC~~

422 ~~type, 10% particles have identifiable~~Some HMOC particles produce obvious polycyclic

423 aromatic hydrocarbons (PAH) peaks in ~~their~~ positive spectra and ~~7% produce~~ high mass signals

18

424 in negative spectra (Denkenberger et al., 2007). Most of HMOC particles (95%) showed . The

425 mass spectra of HMOC suggested they were generated from combustion including traffic

426 emissions (Dall'Osto et al., 2013;Toner et al., 2008). The majority of HMOC particles displayed

427 low hygroscopicity (GF<1.2), with peak number fractions of 15% at GF 1.0.) (Wang et al.,

428 2014;Herich et al., 2008).

429 Amine-rich type particles produceproduced amine peaks at +59(C_3H_9N), +86($C_5H_{12}N$) and

430 +101($C_6H_{15}N$) (Angelino et al., 2001;Pratt et al., 2009). About 20% of analyzed particles are

431 classified in this type. As found previously (Wang et al., 2014), Amine-rich particles are

432 generally very hydrophilic (Angelino et al., 2001;Pratt et al., 2009). Particulate amine formation

433 was favored in low temperatures and higher humidity conditions (Huang et al., 2012;Zhang et

434 al., 2012). The elevated amine particle fractions may be related to the low temperature (6 °C)

435 and high humidity (78% RH) condition during this experiment. Both the preliminary and

436 present study identified the hydrophilicity of Amine-rich particles, with the highest detection

437 probability occurred within GF>1.5 range. number contributions to GF>1.5 range (Wang et al.,

438 2014). Short alkyl chain aliphatic amines are basic andknown to have relatively high vapor

439 pressures, therefore and basic in nature, their presence in particles indicates they are most likely

440 occur in the form of aminium salts, whose formation is greatly favored in the presence of

441 particulate water (Angelino et al., 2001;Chen et al., 2019). It is found that 77% Amine-rich

442 particles(Angelino et al., 2001;Chen et al., 2019). Mass spectra of Amine-rich particles suggest

443 that 77% of them were internally mixed with sulfate or nitrate.

444 Ammonium/OC type particles demonstrate some similarities to biomass particles, since a

445 strong, dominant potassium peak ^{39}K exist in positive spectra and organic peaks present in

446 lower mass range (45-80). However, this type of particles also produced much more intense

447 ammonium peak at $^{18}NH_4^+$ and significant sulfate peak ($^{-97}HSO_4$). In addition, the $^{-26}$CN or $^-$

448 ^{42}CNO peaks, which are present in biomass particles, were absent or very weak, suggesting that

449 biomass burning is not their source. The hygroscopicity pattern of ammonium/OC particles was

450 quite unique. As shown in Fig. 2 (g), ammonium/OC particles are contributing significantly to

451 ~~moderate hygroscopicity range (GF 1.1-1.3), with maximum number contribution of 25% at~~

452 ~~GF 1.2, a GF at the trough between NH and MH mode. Based on their mass spectral signature~~

453 ~~and the published ATOFMS characterizations, it is possible that the ammonium/OC particles~~

454 ~~might be from coal burning sources (Healy et al., 2010). The organics in ammonium/OC~~

455 ~~particles could be probably produced from inefficient combustion of coal (Wang et al., 2013).~~

456 ~~The strong ammonium peak in this particle type may be generated in SCR denitration process~~

457 ~~since the ammonia is usually added in such process. These particles were not likely to be deeply~~

458 ~~aged particles, because their hygroscopicity was only moderate.~~

459 With the expanded GF range and sampling durations, we identified other particle types of

460 specific hygroscopic patterns, including Ammonium/OC, Cooking and Sea salt particles in this

461 study. The Ammonium/OC particles demonstrated some similarities with biomass particles.

462 There was predominant potassium peak ^{39}K and many organic peaks in the positive mass

463 spectra, as shown in Figure 2. Additionally, stronger $18NH_4^+$ peaks for ammonium and sulfate

464 ($-97HSO_4$) were also present in these particles. The typical $-26CN^-$ and $-42CNO^-$ peaks

465 observed for biomass particles were absent or very weak, suggesting the composition

466 differences between Ammonium/OC and biomass particles (Silva et al., 1999;Zauscher et al.,

467 2013;Pratt and Prather, 2009). The hygroscopicity of the Ammonium/OC particles was unique

468 since they have the largest contributions to moderate GF range (GF 1.1-1.3), with the maximum

469 contribution found at GF=1.2. The GF of Ammonium/OC particles suggests that they can be

470 categorized as LH mode (Swietlicki et al., 2008). A prior ATOFMS study identified that

471 Ammonium/OC particles were from agricultural sources, and found most of them were present

472 in higher photochemical oxidation periods (Qin et al., 2012), consistent with the prominent

473 secondary peaks of ammonium found in this study. It is likely the organics in this type is

474 secondary since the GF 1.2 is close to the hygroscopicity of SOA (GF=1.24 at 90% RH) (Gysel

475 et al., 2007;Sjogren et al., 2008). We inferred that ammonium was not contributing major

476 fractions to Ammonium/OC particles, since ammonium salts was very hydrophilic while

477   Ammonium/OC demonstrate only moderate hygroscopicity.

478 Cooking is ~~a significant~~an important source of primary organic aerosol (POA) in urban regions

479 ~~(Crippa et al., 2013;Robinson et al., 2006). Zhang et al.~~(Crippa et al., 2013;Dall'Osto and

480 Harrison, 2012). Zhang et al. estimated that up to 35% of POA are attributed to cooking aerosol

481 during meal hours ~~(Zhang et al., 2007).~~(Zhang et al., 2007). Cooking particles around the site

482 was likely to be significant considering that the Fudan campus is located in a heavily populated

483 area. The ATOFMS characterization of cooking particles have been performed previously

484 ~~(Silva, 2000;Dall'Osto et al., 2013). The markers~~(Dall'Osto et al., 2013). The marker peaks at

485 -255($C_{16}H_{32}O_2$, palmitic~~),~~) and -281 ($C_{17}H_{34}O_2$, oleic acid) in the negative spectra were used to

486 identify Cooking ~~type of particles (Dall'Osto and Harrison, 2012;Silva, 2000). We identified~~

487 ~~861 (%4.6 of total) cooking particles.~~particles (Dall'Osto and Harrison, 2012;Silva, 2000). As

488 shown in Figure 2(h), ~~this particle type had extreme~~Cooking particles demonstrated very low

489 hygroscopicity and ~~99% of them~~ were detected exclusively in GF<1.1 range. ~~Based on the~~

490 ~~ATOFMS particle number, cooking particles contribute 19% particle concentrations of NH~~

491 ~~mode, with its peak contribution occurred at GF 0.9 (49%).~~ It is noted that GF 0.9 does not

492 necessarily indicate a particle shrinkage in ~~diameter~~85% RH. Cooking particles might become

493 more spherical in elevated RH, resulting in smaller mobility diameters. This phenomenon was

494 ~~also~~observed for other organic particles ~~(Shi et al., 2012).~~(Shi et al., 2012;Pratt and Prather,

495 2009). The low hygroscopicity of cooking particles is consistent with ~~their~~the enriched organic

496 ~~composition~~as indicated by the fatty acids (-171, -255, -279~~, -~~, -281) and HOA (+55, +57) peaks

497 in the spectra. The detection of cooking particles in NH mode ~~is a complement to the~~

498 ~~assumption that combustion sources are the major source of NH particles (Swietlicki et al.,~~

499 ~~2008;Laborde et al., 2013;Herich et al., 2009).~~complemented to the conclusion that combustion

500 processes are mainly responsible for NH particles (Swietlicki et al., 2008;Laborde et al.,

501 2013;Herich et al., 2009).

502 ~~Sea salt particle type is an important type of particles in ambient air in coastal areas(Herich et~~

503 ~~al., 2009;Gard et al., 1998). Their mass spectra contain a major peak at $^{+23}$Na and other peaks~~

504 ~~at $^{+62}$Na$_2$O, $^{+63}$Na$_2$OH, $^{+81}$Na$_2$Cl. The hygroscopicity of sea salt is of interest since it is critical~~

Formatted: Line spacing: 1.5 lines

505 in the aerosol cloud interactions in marine and coastal areas (Andreae and Rosenfeld,

506 2008;Massling et al., 2007). Although only 314 sea salt particles (1.7 %) were detected in this

507 study, their hygroscopicity pattern is rather clear that they were mostly present in the largest

508 GF range (>1.5). The large hygroscopicity of sea salt is also indicated by increased number

509 fractions from 2.6% at GF 1.5 to 19% at GF 1.7, as show in Figure 2 (i). The obtained result

510 here is consistent with HTDMA characterizations in marine environment (Swietlicki et al.,

511 2008;Massling et al., 2007), where sea salt particles made up a clear hygroscopicity mode of

512 the largest GF. The hygroscopicity of sea salt in this study is somewhat different compared with

513 the previous characterization in a subarctic region, where sea salt particles were mainly detected

514 in GF 1.3-1.5 range at 82% RH using HTMDA-ATOFMS (Herich et al., 2009). Therefore sea

515 salt particle properties are variant with locations and other factors (organics in seawater, marine

516 microbiological conditions, aging) should be considered (Facchini et al., 2008;Randles et al.,

517 2004).

518 The impact of aging on sea salt hygroscopicity was investigated. Spectra analysis was

519 performed by correlating sea salt peak intensities with GF. It is known that NaCl in fresh sea

520 salt could react with nitric acid in the atmosphere, with the $NaNO_3$ formed in particles and HCl

521 released (Gard et al., 1998). This chemical transformation is reflected in corresponding change

522 in the sea salt mass spectra. Fresh sea salt produce stronger peaks of positive peak Na_2Cl^+ and

523 negative peak $NaCl_2^-$ in their spectra. With the atmospheric transformation, NaCl is transformed

524 into $NaNO_3$, $Na_2NO_3^+$ and $Na(NO_3)_2^-$ peaks emerge and grow stronger, while NaCl related

525 peaks Na_2Cl^+ and $NaCl_2^-$ decrease or vanish. The statistics of sea salt peak intensities at different

526 GF are shown in Figure 3. Obviously, sea salt particles with smaller GF tend to produce stronger

527   NaNO₃ related peaks and weaker NaCl related peaks. This result is an evidence that aged sea

528   salt have reduced hygroscopicity (Herich et al., 2009). The transformation of NaCl into NaNO₃

529   could not generate the observed reduction in GF. Similar result was observed in the subarctic

530   site (Herich et al., 2009). It is likely that organics condensed on Sea salt particles and lowered

531   their hygroscopicity.

532   **3.1.2. Particle effective density and hygroscopicity**

533   Simultaneous information on particle effective density and hygroscopicity is rarely reported

534   (Zelenyuk et al., 2008). Fortunately, the particle effective densities and chemical composition

535   can be measured on by HTDMA-ATOMFS system (Figure 4). Obviously, the particles with

536   lower GF had lower effective densities, while the particles with higher GF had a larger effective

537   density, which was finally approaching to ~ 1.5 g cm⁻³ and had much smaller range of effective

538   density deviation, suggesting that a main fraction of particles with high GF were more likely to

539   be aged aerosols that mainly comprised of a mixture of secondary species, such as ammonium

540   sulfate (density: 1.77 g/cm³) and ammonium nitrate (density: 1.73 g/cm³). Condensation of

541   ammonium sulfate/nitrate on existing organic carbon aerosols and black carbon aerosols would

542   increase their density. In addition, the densities of ammonium sulfate and ammonium nitrate

543   are similar. Thus, particles with higher mass fraction of ammonium sulfate/nitrate tend to have

544   more similar density, consistent with Figure 4, which shows that the effective density of

545   particles with higher GF had smaller deviation of effective densities.

546   **3.2. Estimating**With particles of higher GF being analyzed in this experiment, we also

547   identified the Sea salt particle which constitutes an important particle type in ambient air in

548   coastal areas (Herich et al., 2009;Gard et al., 1998). Sea salt mass spectra contain dominant

549 sodium peak $23Na^+$ and other sodium cluster peaks at $62Na_2O^+$, $63Na_2OH^+$, $81Na_2Cl^+$ (Gaston
550 et al., 2017). The hydrophilicity of Sea salt is clear that they were mostly detected in the largest
551 GF bins (>1.5), with their number fractions increased from GF 1.5 to 1.7 (Figure. 2). HTDMA
552 studies in marine environment shown that sea salt particles constitute a separated
553 hygroscopicity mode of the largest GF (Swietlicki et al., 2008), which is generally consistent
554 with the observed GF range in the experiment. However, the observed sea salt particle
555 hygroscopicity is somewhat different from the HTDMA-ATOFMS characterization in a
556 subarctic region, where sea salt particles were found mainly detected in GF 1.3-1.5 range at 82%
557 RH (Herich et al., 2009). We inferred that sea salt hygroscopicity properties are variant with
558 locations and other factors (organics in seawater, marine microbiological conditions, aging)
559 should be considered (Facchini et al., 2008;Randles et al., 2004).

560 **3.1.2 Peak intensity variations with GF**

561 Apart from particle number distributions, the HTDMA-ATOFMS dataset provided another
562 aspect of information regarding peak intensities with GF. In this study, we used relative peak
563 intensities (peak areas normalized by the total areas in spectrum) to investigate its relation to
564 GF. Generally, the responses of peak intensity to GF variation were found to be nonlinear, since
565 they were correlated only within specific GF ranges. A simple trend applicable to whole GF
566 range was not observed.

567 We presented the statistics of peak intensity of nitrate ($46NO_2^-$, $62NO_3^-$, $125H(NO_3)_2^-$) and
568 sulfate ($80SO_3^-$, $97HSO_4^-$) which were known to be critical to particle hygroscopicity (Figure
569 4). As previously observed, the nitrate and sulfate peaks were present in the majority of particles
570 in all GF bins (Herich et al., 2009;Herich et al., 2008;Wang et al., 2014). However, peak
571 intensities of nitrate and sulfate were indeed stronger in hygroscopic particles than hydrophobic
572 particles. In Figure 4 we observed positive correlation between nitrate and sulfate intensities
573 and GF in GF <1.2 range, suggesting contribution of nitrate and sulfate to particle
574 hygroscopicity in low GF range (Figure 4). However, in higher GF range (GF 1.3-1.5), nitrate
575 and sulfate peaks seem to reach a plateau with unclear dependence on GF. Nitrate and sulfate
576 were known to contribute large fractions of particle mass in MH particles (Swietlicki et al.,

577 2008;Laborde et al., 2013;Liu et al., 2014). The unclear trend of nitrate and sulfate with GF

578 seem to suggest that nitrate and sulfate were in stable ratios since nitrate and sulfate peaks were

579 dominating peak areas in negative spectra. For particles of even higher GF, differences were

580 observed between GF 1.3-1.5 and GF 1.5-1.7 range in that stronger nitrate and weaker sulfate

581 peaks were detected in the GF 1.3-1.5 range. Particles classification suggests that this general

582 characteristic is also at variance for different particle types. The same statistics for EC and

583 Dust/ash particles were presented in Figure 4. Compared with EC particles, smaller sulfate and

584 stronger nitrate peaks were found in Dust/ash spectra, and the observed trend in total particles

585 were less obvious in Dust/ash. These facts highlight the nonlinearity between peak intensities

586 and GF and that particle types should also be considered in describing peak intensities.

587 The analysis of peak intensities with GF can disclose some atmospheric processes happened on

588 aerosol. We take the Sea salt as an illustration. Sea salt particles were known to react with

589 atmospheric nitric acid, with NaCl in fresh sea salt be transformed into $NaNO_3$ in the reacted

590 sea salt (Gard et al., 1998). This composition transformation is indicated in corresponding

591 changes of NaCl and $NaNO_3$ peak intensities in particle spectra. The unreacted sea salt particles

592 tend to produce larger peaks of Na_2Cl^+ and $NaCl_2^-$ in spectra (Gaston et al., 2011;Prather et al.,

593 2013). In particle spectra of reacted sea salt, the NaCl peaks (Na_2Cl^+, $NaCl_2^-$) decrease while

594 $NaNO_3$ peaks ($Na_2NO_3^+$, $Na(NO_3)_2^-$) increase. We presented peak intensities of sea salt in GF

595 1.5-1.7 range where sea salt particles were detected with largest numbers (Figure 5). We found

596 that the positive correlation between NaCl peak intensity and GF, and the negative correlation

597 for $NaNO_3$ peaks. Therefore, the HTDMA-ATOFMS data supported that reacted sea salt have

598 reduced hygroscopicity (Herich et al., 2009;Gaston et al., 2018). Laboratory HTDMA study

599 suggested that NaCl and $NaNO_3$ have deliquesced at 85% RH and that the $NaNO_3$ (GF ~1.8) is

600 less hygroscopic than NaCl (GF ~2.2) (Hu et al., 2010). The reduced hygroscopicity of sea salt

601 is in line with the GF of sodium salts. However, the sea salt hygroscopicity (GF 1.5-1.7) was

602 smaller than pure $NaNO_3$ salt (supposing fully reacted), suggested that the chemical

603 transformation alone is not sufficient to account for the observed hygroscopicity of sea salt. We

604 hypothesize that other compositions as organics were mixed into sea salt and contributed to the

605 reduction of sea salt hygroscopicity (Gaston et al., 2011;Randles et al., 2004;Facchini et al.,

606 2008).

3.2 Predictability of hygroscopicity from particle mass spectra

608 The GF of a particle can be estimated based on HTDMA-ATOFMS data for two reasons. First,
609 different particle types had distinct GF distributions. Second, particles in different GF bins had
610 different mass spectra. The GF estimation from particle spectra requires that the HTDMA-
611 ATOFMS data is capable to represent the major particle types normally presented in atmosphere,
612 which is evidenced in the preceding discussions. In another aspect, the GF prediction from mass
613 spectra also demands that HTDMA-ATOFMS data are sensitive to reflect the composition
614 differences with GF variations.

615 To test the sensitivity of HTDMA-ATOFMS data, we evaluated the average spectral similarities
616 between each pair of GF groups. The average similarities were calculated from the similarities
617 between every possible pairs of particles from the two GF groups. The self-comparing of
618 particles within the same GF group were excluded. As shown in Figure S7, we observed a
619 general trend that particles in the same GF bins tend to produce the highest similarities. As the
620 GF differences increase, the mass spectra similarity between two GF bins tended to decrease.
621 This result is an evidence that the particles with different GFs are more likely to have
622 discriminable mass spectra, which suggests that the HTDMA-ATOFMS dataset are capable to
623 estimate hygroscopicity just from particle mass spectra.

3.3 Estimated hygroscopicity of ambient particles

625 Prediction of ambient particle hygroscopicity requires that the HTDMA-ATOFMS dataset have
626 good particle representation and coverage. As discussed in the preceding section, particle types
627 which are normally present during ambient ATOFMS sampling have been characterized in this
628 HTDMA-ATOFMS experiment. Therefore, the HTDMA-ATOFMS dataset in this study can be
629 used to estimate particle hygroscopicity for the majority of ambient particles detected by
630 ATOFMS. In this section, we illustrate an estimation of particle hygroscopicity from a period

631 of ambient ATOFMS data (Sep-12 to Sep-28, 2012), which was collected at Fudan campus, the

632 same site for the HTDMA-ATOFMS experiment.

633 3.2A case study of the hygroscopicity estimation were carried out based on a period of ambient

634 ATOFMS measurement. The ATOFMS data was collected at the same Fudan site from Sep-12

635 to Sep-28, 2012. During this period the ATOFMS recorded 538,983 mass spectra of individual

636 particles. With the described estimation method, the GF value (corresponding to 85% RH) was

637 generated for each particle based on individual particle mass spectra. A fraction of the estimated

638 GF (4%) were excluded from analysis since their maximum similarities failed to exceed the

639 threshold value (dot_product > 0.7) between ATOFMS and HTDMA-ATOFMS particles.

640 Particle mixing states in this period were analyzed by clustering particles using ART-2a

641 algorithm (Song et al., 1999). After merging the clusters of similar composition and temporal

642 trends, the majority of particles were finally grouped into the same general types as discussed

643 in HTDMA-ATOFMS dataset (Fresh EC, Aged EC, Dust/Ash, HMOC, Amine-rich,

644 Ammonium/OC, Cooking and Sea salt), which account for 90.8% of the total analyzed particles

645 in this period.

646 **3.3.1 Hygroscopicity modes** ~~in estimated GF~~**and contributions from particle types** | Formatted: Line spacing: 1.5 lines

647 There were 538,983 particles chemically analyzed by ATOFMS during Sep-12 to Sep-28, 2012.

648 The mass spectra in this period was utilized to predict the GF (85% RH) of each individual

649 particle based on the previously described method. With the estimated hygroscopicity of

650 individual particles, several hygroscopicity modes were observed. Figure 5 shows the temporal

651 variation of particle estimated GF. Apparently, at least three hygroscopicity modes were present,

652 with their respective GF peaked at ~ 1.05, 1.42, and 1.6. The temporal variation of

653 hygroscopicity suggested that the entire period can be roughly divided into four distinct periods

654 of P1, P2, P3 and P4 (as indicated in Figure 5) which have different GF distribution patterns.

655 During P1, the particle numbers were dominated by GF 1.42 mode, while during P2, the GF1.42

656 ~~mode disappeared and GF 1.05 and GF 1.6 modes appeared. The hygroscopicity patter during~~

657 ~~P3 is similar to P1, but with more distinct GF 1.05 mode. During P4, all three hygroscopicity~~

658 ~~modes were present.~~

659 ~~The three hygroscopicity modes derived from ATOFMS data were compared with the GF~~

660 ~~distributions that obtained from some HTDMA studies (Ye et al., 2013;Ye et al., 2011;Liu et al.,~~

661 ~~2011;Swietlicki et al., 2008). Previous HTDMA characterizations of particle hygroscopicity in~~

662 ~~Shanghai shows a near hydrophobic mode with center GF in 1.05~1.1 range at RH 85% (Ye et~~

663 ~~al., 2011), which is consistent with our estimated hydrophobic GF mode peaked at 1.05. The~~

664 ~~more hygroscopic mode measured by HTDMA usually centered at GF at 1.43~1.47, while in~~

665 ~~the estimated GF data, the maximum number occurred at GF around 1.42. The mass spectra of~~

666 ~~GF 1.6 mode suggest that they usually have high sodium peaks (Figure S2), which were~~

667 ~~probably sea salt particles. The sea salt mode were reported to be very hygroscopic, with~~

668 ~~average GF around 2.0 at 90% RH for freshly generated sea salt particles in marine areas~~

669 ~~(Swietlicki et al., 2008).~~

670 ~~Since~~The estimation method determined that the GF of ATOFMS particles were restricted

671 within the GF range in HTDAM-ATOFMS dataset (0.9-1.7). Within this GF range, the

672 ATOFMS particle GF distribution suggested several hygroscopicity modes similar to the

673 HTDMA measurement. As shown in Figure 6, three hygroscopicity modes were clear in the

674 GF-number distributions, with particle GF centered at about 1.05, 1.42, and 1.6, respectively

675 (85% RH). Prior HTDMA studies suggested the regular presence of the nearly-hydrophobic

676 mode with center GF in 1.05~1.1 range in Shanghai area (Ye et al., 2011), consistent with the

677 GF 1.05 mode in this study. The second mode at GF 1.42 mode in ATOFMS particles

678 corresponds to the MH mode (GF 1.43~1.47) in Shanghai and other sites using HTDMA (Ye et

679 al., 2013;Ye et al., 2011;Liu et al., 2011). The sea salt mode in HTDMA GF distribution is not

always clear because of the larger size of sea salt particles. However, the sea salt particles were readily detected by ATOFMS because of the detection range of ATOFMS. The particles in GF 1.6 mode contained rich sodium content and their mass spectra suggest typical sea salt peaks (Figure S2). In marine areas the sea salt particles were found to constitute hygroscopicity mode of the largest GF (about 2.0 at 90% RH, corresponding to 1.76 at 85% RH) (Swietlicki et al., 2008).

The ATOFMS measured particle aerodynamic diameters simultaneously for eachindividual particles. Together with the estimated GF, we presentinspected particle number distribution as a bivariate function of the estimated GF and particle diameter (aerodynamic diameter measured by ATOFMS) in , d_{va}) (Figure 6.7). The three particlehygroscopicity modes were also apparentclearer in the GF-d_{va} diagram. We also noticed the gradually increased GF of larger particles, which is , which suggest the increasing trend of particle diameter with increasing GF, a very consistent with HTDMA observations (Ye et al., 2011;Ye et al., 2013).result with HTDMA studies (Ye et al., 2011;Ye et al., 2013). Healy et.al. have applied a different method to estimate particle hygroscopicity from single particle data using ZSR mixing rule (Healy et al., 2014). In that study(Healy et al., 2014). The particle aerodynamic diameter d_{va} was transformed to equivalent mobility diameter d_m by assuming a particle density. Despite in that study. Although the differences in methodmethods are different, the estimated GF and their distributions are comparable for NH and MH mode particles. However,identified hygroscopicity modes were similar between the presence oftwo studies, except the sea salt mode which was absent innot found by Healy et al., (Healy et al., 2014). (Healy et al., 2014).

Based on the GF of hygroscopicity modes, prior HTDMA studies conventionally classified the observed modes into categories as nearly-hydrophobic (NH), less-hygroscopic (LH), more-hygroscopic (MH) and sea salt (SS) modes respectively (Swietlicki et al., 2008;Liu et al., 2011;Sjogren et al., 2008). However, the chemical nature of these hygroscopicity modes was not clear since the HTDAM technique is based on particle numbers and the particle composition information was not obtainable. With the ATOFMS single particle data, particle composition and hygroscopicity was connected directly. To facilitate comparison, we similarly divide the estimated GF into four bins (<1.1, 1.1-1.3, 1.3-1.5 and >1.5) to roughly represent the NH, LH,

709 MH, SS particles according to the conventional classification of hygroscopicity modes

710 (Swietlicki et al., 2008). As shown in Figure 6, particle types were distributed differently in GF

711 modes. For example, the organic particles including HMOC, Biomass and Freshly emitted EC

712 particles were mainly enriched in NH mode, which suggests directly that combustion sources

713 are mainly responsible for NH particles in the ambient (Herich et al., 2008;Herich et al.,

714 2009;Ye et al., 2011).

715 In Table 2 we made the statistics on average number contributions of particle types to the NH,

716 LH, MH and SS mode. The presented statistics were based on the temporal contributions of

717 each particle types in daily resolution. It is noted that particle number contributions presented

718 in Table 2 may be different from HTDMA-ATOFMS dataset (Figure 2). For example, the

719 Cooking particles contributions to NH mode was significantly lower in the ATOFMS dataset

720 (3%) than HTDMA-ATOFMS dataset (19%). This result is understandable because particle

721 concentrations are variant with particle size and HTDMA-ATOFMS only analyzed a narrow

722 size bin from the total particle size distribution. For each hygroscopicity mode, there were

723 multiple particle types contributing significant number fractions, suggesting that even within

724 the same hygroscopicity mode there were still some heterogeneity in particle composition.

725 Particles in the same hygroscopicity mode may share some common features in compositions

726 but their differences are distinguishable in single particle data. In another respect, the

727 contributions of each type also suggest the existence of a predominant type that accounts for

728 major fractions in respective modes compared with other types, such as Aged EC in MH mode,

729 Ammonium/OC in LH mode. The comparison between Table 2 and Figure 2 suggests that,

730 although their absolute contributions may be different, the hygroscopicity patterns of particle

731 types in the two datasets are in good agreement. Based on this fact, we concluded that the

732 composition-hygroscopicity connections contained in HTDMA-ATOFMS dataset was

733 successfully reflected into the predicted GF.

734 **3.3.2. Temporal variations of estimated hygroscopicity**

735 The temporal variation of particle estimated GF from Sep-12 to Sep-28 was illustrated in Figure

736 8. Four distinct periods (P1-P4) were identified based on their different hygroscopicity

distributions. Generally, the P1 and P3 periods were characterized by elevated MH mode which dominated the ATOFMS particles numbers, while in P2 and P4 the MH particles decreased significantly and sea salt mode was pronounced. Back trajectories during P1-P4 were analyzed using HYSPLIT mode (Draxler, R. R. and Rolph, G. D., ~~As illustrated in Figure 5, different mixing states were observed during P1-P4 periods. Taking the P4 period as an example, the sea salt mode in this period was persistent during this period, while the concentrations of NH mode particles were intermittent with abrupt changes in temporal trend, consistent with the characteristic of local emissions. The number concentrations of MH mode particles increased during nighttime (Figure 5), which probably related to the mixing layers fluctuations. These facts indicate that the estimated hygroscopicity could help to investigate particles' sources, formation mechanisms, and their possible atmospheric aging pathways (Healy et al., 2014;Li et al., 2018;Laborde et al., 2013;Kamilli et al., 2014;Swietlicki et al., 2008).~~

~~3.2.2 Hygroscopicity and~~ 2003) to inspect the airmass that influenced the sampling site (Figure S9). The 24-hour back trajectories suggests that the airmass in P1 period mainly circulated in local regions from northwest direction to Shanghai. The local circulations brought regional aerosol pollution to the sampling site, resulted in elevated concentrations of particles, especially the MH particles. During P2, the airmass originated from the ocean in northeast direction with less continental influence. The cleaner air from the ocean almost wiped out the accumulated particles observed in P1 and the concentrations of sea salt particles increased. In the majority of time during P3, the airmass stayed over continental areas. The MH particles dominated particle numbers in this period and the sea salt mode were barely present. During Sep-18 to Sep-20 in P3, the LH particles showed increased concentrations and gradually decreased after Sep-20. Similar to P1, the origin of airmass in P4 shifted to the ocean in eastern directions and SS mode emerged again. Both the particle spectra and the back trajectories supported that the GF mode of 1.6 can be mainly attributed to sea salt particles.

762   Except meteorological conditions, other differences exist in the temporal trends for each

763   hygroscopicity modes. Generally, the NH mode showed relatively stable trends irrespective of

764   different periods of P1-P4, as indicated in Figure 8. Closer inspection of NH particles suggests

765   a notable feature that obvious sharp spikes were present in NH particle temporal concentrations

766   (Figure 8). This character is typical for particles from local emission sources, with undissipated

767   plumes at the time of detection. With the combined information from particle composition in

768   Table 2, we inferred that the NH particles were fresh emitted particles from local sources with

769   high organic or elemental carbon content (Laborde et al., 2013;Herich et al., 2008;Weingartner

770   et al., 1997). The mass spectra of NH particles indicated low nitrate and sulfate signals,

771   suggesting that secondary matters have not accumulated significantly on these particles,

772   consistent with negligible coating thickness on NH particles (Laborde et al., 2013). We tend to

773   ascribe the organics in NH particles to be primary organic carbons (POA) considering their

774   relatively fresh emission state (Sjogren et al., 2008;Liu et al., 2011;Gysel et al., 2007).

775   Some characters of LH particles were noticed. Similar to the particles in MH range, the LH

776   particles mainly presented in continent influenced periods (P1 and P3) (Figure 8). However, the

777   temporal concentrations trends suggested differences between LH and MH particles. For

778   example, MH mode dominated particle numbers in the entire P3, while the LH particles were

779   only pronounced from Sep-17 to Sep-21, with peak concentrations observed on Sep-19. The

780   particle contributions showed that Ammonium/OC is the main contributor to NH particles

781   (Table 2). This conclusion is also correct in temporal basis since the Ammonium/OC

782   contributions to LH range were always much larger than other types of particles in all the

783   studied period. We investigated the nature of the Ammonium/OC particles by comparing its

784   concentration with ambient pollutants levels. As shown in Figure 9, the number fractions of

785   Ammonium/OC particles showed strong connections to ambient O_3 concentrations. During

786   Sep-17 to Sep-21 there were daily oscillations of O_3 levels, which were followed by the same

787   pattern of Ammonium/OC particles with lags of several hours. The maximum O_3 concentrations

788   was found on Sep-19 (219 μgm^{-3}) in the period, the same day when the highest Ammonium/OC

789   particle contribution was observed. HTDMA studies suggested that LH mode became

790   pronounced in new particle formation (NPF) periods with high atmospheric reactivity

32

791 (Swietlicki et al., 2008). Based on these facts, we think the Ammonium/OC particles were

792 related to the oxidation processes of organics vapors by oxidants such as O_3 (Varutbangkul et

793 al., 2006). The moderate hygroscopicity of Ammonium/OC agrees with the hygroscopicity of

794 ambient secondary organic aerosol (SOA) (Gysel et al., 2007;Sjogren et al., 2008). During

795 periods of higher Ammonium/OC contributions (Sep-17 to Sep-21), increased SO_2 levels were

796 also encountered, which coincided with high sulfate signals in mass spectra of Ammonium/OC

797 (Figure 2). Compared with the organic compositions, the sulfate was inferred to have minor

798 contributions to mass fractions because of the moderate hygroscopicity of Ammonium/OC.

799 Particles in MH mode dominated the particle numbers for the majority of time in P1 and P3

800 (60%) compared with the average fraction of 25% in P2 and P4. Inspection of the temporal

801 trends of MH particles also suggest some diurnal variations with higher concentrations in

802 nighttime (Figure 8). As illustrated in Figure 4 and Figure S6, mass spectra of MH particles

803 were dominated by sulfate, nitrate peaks, suggested that MH particles were mixed with

804 significant fraction of secondary inorganic matters (SIA). The coating thickness of the

805 secondary matters was determined by HTDAM-SP2 at different GF (Laborde et al., 2013). The

806 coating thickness of secondary coating was measured to 40-80 nm (D_{dry}=265 nm) in GF 1.2-

807 1.7 range, being equivalent to 55-76% of hygroscopic particle volume was attributed to

808 secondary matters (Laborde et al., 2013;Healy et al., 2014).

809 **3.3.3 Peak intensity variations with estimated GF**

810 Particle hygroscopicity and peak intensities in particle mass spectra were correlated to show

811 their connections. The correlation was illustrated similarly to the analysis of the HTDMA-

812 ATOFMS dataset, as shown in Figure 10. In addition to the statistics on peak intensities of

813 different GF, the number distributions ATOFMS particles with GF and peak intensities were

814 presented for nitrate (46NO_2^-, 62NO_3^-, 125H(NO_3)$_2^-$) and sulfate peaks (80SO_3^-, 97HSO_4^-) in

815 the lower panels in Figure 10. The general trends of peak intensities with GF in HTDMA-

816 ATOFMS dataset was preserved in estimated GF of ambient particles. The trends of nitrate and

817 sulfate peak intensities showed increases from NH to LH range and remained constant in the

818 MH mode. Similar to HTDMA-ATOFMS particles, stronger nitrate peaks were detected in SS

particles compared with the MH particles, while an opposite trend was observed for sulfate intensities. These results highlight the nonlinearity between GF and peak intensities of ATOFMS particles.

The nonlinearity of peak intensities with GF was also suggested by the different particle types presented in ATOFMS data. As shown in the lower panels in Figure 10, the distribution of ATOFMS individual particles showed enrichment in different areas in the GF-peak intensity diagram, suggesting the presence of particle groups of different compositions. To illustrate this character, we selected two areas with clear particle enrichments in GF-peak intensity diagram and their particle composition were analyzed (denoted as A and B in lower left panel in Figure 10). Obviously, particles in area A produced much larger nitrate signals than particles in area B. Particle numbers in the two areas suggested that Dust/ash dominated particles in area A (59%) while in area B the Dust/ash only accounted for 14% of particles (Figure S10). As a contrast, particles in area B were dominated by Aged EC type (53%) followed by 25% Dust/ash. Table 2 suggests that Aged EC and Dust/ash are the major types presented in the same MH mode. However, peak intensity responses to GF were indeed different for different particle types, suggesting the importance of particle types in describing peak intensities.

The particle distribution with sulfate intensities showed similar enrichment patterns to nitrate (lower right panel in Figure 11). Sulfate peak intensities were found to correlated with hygroscopicity in GF <1.2 range but in MH range no correlated with GF was observed. We note that except the larger peaks of nitrate and sulfate, some smaller peaks were also found to correlated with GF within specific particle type. We correlated peak intensities of Na_2Cl^+ and NO_3^- with the estimated GF of sea salt particles (Figure S11). The Na_2Cl^+ peaks were positively correlated with GF while the nitrate peaks were negatively correlated with GF. The observed correlation in sea salt particles are consistent with discussed trends in the HTDMA-ATOFMS dataset. These results demonstrate that the GF estimation method have effectively reflected the minor changes in particle mass spectra into the estimated hygroscopicity.

3.3.4 Comparing the estimated hygroscopicity with visibility

Particles with different hygroscopicity have different liquid water content and optical properties.

847 This fact can be demonstrated by correlating the concentrations of particles having different

848 hygroscopicity with atmospheric visibility (Liu et al., 2012;Qu et al., 2015;Chen et al., 2012).

849 We use the visibility data (https://www.wunderground.com/) logged in the Hongqiao airport

850 (31°12'N, 121°20'E) and Pudong airport (31°9.3'N, 121°49'E) during Sep-12 to Sep-28, 2012

851 (see the map in Figure S5). The contemporary visibility data of the two airports correlated

852 strongly (Figure S5), despite the 45 kilometers distance between the two airports. Fudan

853 campus locates roughly between the two airports, so that the average visibility between the two

854 airports was used to represent the visibility at Fudan site. We discriminated the particles into

855 less and more hygroscopic groups at splitting GF of 1.2, with their number concentrations

856 calculated with the same resolution of visibility data, as shown in the upper panel in Figure 5.

857 Except for P2 and P4 periods, when visibility were typically above 10km, an anti-correlation

858 was observed between visibility and particle numbers of more hygroscopic group than less

859 hygroscopic group. The fact could be further demonstrated by splitting particles into finer bins

860 of GF 0.9-1.1, 1.1-1.3, 1.3-1.55, whose number concentrations correlated with visibility (Figure

861 7). For particles in GF 0.9-1.1, there were actually no correlation between their concentrations

862 and visibility (R^2=0.08). For moderate hygroscopic particles (GF 1.1-1.3), the correlation

863 became stronger (R^2=0.34). MH mode particles (GF 1.3-1.55) were found to best anti-correlated

864 with visibility with R^2=0.58. Thus, these results clearly demonstrated that aerosol particles with

865 higher hygroscopicity could play more important role in affecting visibility.

866 **3.2.3 Sea salt type particles**

867 Sea salt type particles show a unique mode in the GF d_{va} diagram (Figure 6). We further

868 investigated the relation between characteristics of sea salt particles and the back trajectories of

869 ~~airmass (Figure 8) during period P1-P4 using HYSPLIT mode (Draxler, R.~~ Particle optical

870 properties were closely connected to hygroscopicity (Liu et al., 2012;Qu et al., 2015;Chen et

871 al., 2012). The hygroscopic growth increases particle volumes and cross sections and is

872 contributing to the visibility degradation. With the estimated hygroscopicity of ATOFMS

873 particles, we correlated atmospheric visibility with particle concentrations to study their

874 contributions to the visibility variation. The ATOFMS particle volume concentrations were

875 calculated for hygroscopicity modes of NH, LH, MH and SS based on ATOFMS particle

876 diameter and numbers. The particle volume concentrations was used because hygroscopic

877 growth change particle sizes rather than numbers (Chen et al., 2012). The visibility data was

878 obtained from (https://www.wunderground.com/) logged in the Hongqiao airport ($31°12'$ N,

879 $121°20'$ E) and Pudong airport ($31°9.3'$ N, $121°49'$ E) during the study period (see the map in

880 Figure S12). The temporal variations of visibility in two sites correlated strongly (Figure S12),

881 despite the 45 kilometers distance between two airports. The Fudan site is located roughly

882 between the two airports, and the two sets of visibility data were averaged to represent the study

883 site. In P2 and P4 the site was under the influences from ocean, resulting visibilities larger than

884 10 km (Figure 8). Apart from ATOFMS particles, contemporary $PM_{2.5}$ volume concentrations

885 were also correlated with visibility. The $PM_{2.5}$ volume concentrations were derived from $PM_{2.5}$

886 mass concentrations using particle density (1.4 gcm^{-3}). A strong correlation between ATOFMS

887 particle numbers and $PM_{2.5}$ was found (R^2=0.80).

888 An exponential relation between visibility and PM concentrations was found by the previous

889 study (Qu et al., 2015). After applying the exponential fitting to the visibility and particle

890 volume concentrations, we found a moderate correlation for ATOFMS particles (R^2=0.45) and

891 better correlations for $PM_{2.5}$ concentrations (R^2=0.64) (Figure S13). However, the fitting errors

892 were clearly dependent on ambient RH, with larger errors in higher humidity, indicating that

893 hygroscopicity might affect visibility degradations, which were consistent with other studies

894 (Chen et al., 2012;Liu et al., 2012). To further examine the effect of particle hygroscopicity on

895 visibility, we derived particle volumes in different RH using estimated κ values (Petters and

896 Kreidenweis, 2007). The κ values were calculated using the GF of individual particles at 85%

897 RH for ATOFMS data and the average GF of 1.36 for $PM_{2.5}$ volume data. With hygroscopicity

being considered, we found notable improvements of the correlations between PM concentrations and visibility, with the improved correlation observed for $PM_{2.5}$ concentrations (R^2=0.82) after applying correction for hygroscopicity (Figure 11). However, this improvement was barely the case for NH particles, probably due to the negligible hygroscopic growth. For the ATOFMS particles in different GF modes, we found the highest R^2 (0.65) for the MH particles. The correlation between SS particles and visibility was distorted due to the visibility reached its limit (10 km) when sea salt mode was pronounced (Figure 8). The R^2 between MH particles and visibility suggests that the variation of MH particles accounted for the major part of visibility changes (65%) during this period, which coincided with the major contribution of nitrate and sulfate to light extinction (61%) in eastern China areas (Qu et al., 2015). These results indicate the importance of discriminating particles by hygroscopicity in explaining the measured visibility.

R. and Rolph, G. D.,2003). During period P1, the airmass were relatively stable, and the airmass movement were relatively slow. The local circulation of airmass brought regional aerosol pollution to the sampling site, which was consistent with the elevated concentrations of more hygroscopic (MH) mode particles (Figure 5). During P2, the history of airmass exclusively passed over yellow sea without continental influence. The MH mode particles disappeared and only NH and GF 1.6 mode were detected in the predicated GF. Similar as P1, the back trajectories during P3 mainly stayed over continental regions in the mainland of China, resulting regional aerosol pollutions in MH particles to the site and GF 1.6 mode were barely present. During P4, the airmass mainly originated from northeastern part of East China Sea and GF 1.6 mode emerge again. Consequently, the back trajectories support the attribution of GF 1.6 mode to sea salt particles.

Figure 9 shows the differential mass spectra between sea salt particles during P1&P3 and during P2&P4, indicating that the sea salt particles, detected in P2 and P4, were relatively fresh, while

923 sea salt particles detected in P1 & P3 period were more aged. Clearly, sea salt particles in P1 &

924 P3 show stronger peaks of $Na(NO_3)_2^-$, $Na_2NO_3^+$, NO_3^-, while sea salt particles in P2 & P4 show

925 stronger NaCl related peaks (Figure 9). This result indicates that sea salt in P1&P3 experienced

926 more aging in the atmosphere. The right panel in Figure 9 compares the hygroscopicity

927 distributions of sea salt particles during P1&P3 and during P2&P4. As expected, the

928 hygroscopicity distribution during P1&P3 shifted slightly ($\Delta GF=-0.02$) to lower GF, suggesting

929 more aged sea salt particles had reduced hygroscopicity, consistent with the trend discussed

930 previously. These results also demonstrate that the hygroscopicity estimation method is

931 sufficiently sensitive to reflect the minor changes in particle mass spectra to the estimated

932 hygroscopicity.

933 **3.2.4 Particle type distributions in various hygroscopicity modes**

934 The particles analyzed by ATOFMS during the studied period were classified within the same

935 classification scheme as HTDMA-ATOFMS experiment. With the estimated hygroscopicity of

936 individual particles, Figure 10 shows the number contributions of each particle type as a

937 function of GF. In the GF 0.9-1.1 range, the fresh EC and HMOC particles were dominant with

938 biomass and cooking types. In the GF 1.1-1.3 range, the Ammonium/OC particles is the most

939 abundant type, which contributed to nearly 40% particle numbers in this GF range. The main

940 particle type in the higher GF range (1.3-1.55) was aged EC particles. Sea salt particles were

941 present mainly in the narrower range of GF 1.55-1.65. A previous HTDMA characterization

942 study (Swietlicki et al., 2008) has suggested that ambient submicron particles have four

943 hygroscopicity modes, namely near hydrophobic (NH), less hygroscopic (LH), more

944 hygroscopic (MH) and sea salt modes, with their GFs centered in 1.0-1.1, 1.11-1.33, >1.33

945 ~~and >1.85 ranges, respectively (at 90% RH). These hygroscopicity modes correspond well to~~
946 ~~the particle types analyzed in this study. Freshly emitted EC particles from combustion sources~~
947 ~~and organic particles with higher molecular weight were the major contributors of nearly~~
948 ~~hydrophobic (NH) mode in this study. Consistent with their particle mass spectra (Figure 2,~~
949 ~~Figure S2), more hygroscopic particles were hydrophilic due to condensation of nitrate and~~
950 ~~sulfate. For the chemical composition of less hygroscopic particles was rarely reported.~~
951 ~~However, the present study indeed identified a unique particle type that is specifically enriched~~
952 ~~in less-hygroscopic range. Both the HTDMA-ATOFMS experiment and ambient ATOFMS~~
953 ~~sampling have suggested that their mass spectra contained many organic, ammonium and~~
954 ~~sulfate signals. Temporal concentrations of this particle type indicate they were only enriched~~
955 ~~in specific days in P1 and P3 period, as suggested in Figure 5. Their real sources and production~~
956 ~~mechanisms deserve further investigations.~~

4. CONCLUSIONS

958 The hygroscopicity and composition of submicron particles were ~~simultaneously~~ characterized
959 in ~~urban atmosphere (Shanghai).~~a megacity in eastern China. A single particle mass
960 spectrometer, ~~ATOFMS,~~ was connected to the ~~downstream~~downflow of an HTDMA to analyze
961 particle composition of different hygroscopicity ~~segregated particles. A dataset linking~~ at 85%
962 RH. Direct connections between hygroscopicity and single particle ~~compositions and~~signatures
963 were established. The HTDMA-ATOFMS dataset suggested that particle types were distributed
964 differently in various hygroscopicity ~~was obtained~~ranges. Generally, ~~biomass particles,~~
965 ~~fresh~~Fresh EC particles, ~~organic~~ and organic particle types including Biomass, Cooking and
966 high molecular organic carbon (HMOC) were enriched in nearly-hydrophobic (NH) mode
967 (GF<1.1). The majority of particles in NH mode suggested characters of freshly emitted
968 particles from combustion sources. Particle types in the more-hygroscopic (MH) range (GF1.3-
969 1.5) include Aged EC, Amine-rich and Dust/ash particles ~~with high molecular weight (HMOC)~~

Formatted: Line spacing: 1.5 lines

were mostly present in NH particle mode. Hydrophilic particle types, including aged EC, amine rich . The mass spectra of MH particles, usually have a GF>1.3. Cooking particles suggested that they were mixed with significant fractions of secondary matters. The sea salt particles were exclusively detected in the higher GF< 1.1 range. Sea salt range (GF 1.5-1.7), with increasing detection probability at larger GF. In the moderate hygroscopicity range (GF 1.1-1.3), the Ammonium/OC particles were present in very hygroscopic range (GF>1.5). Atmospheric processing was shownwas identified with peak detection probability at GF 1.2.

Single particle spectra peak intensities were correlated with GF to reduce the disclose their possible connections. The peak intensities were nonlinearly correlated with GF. The peak intensities of nitrate and sulfate showed gradual increase from GF 0.9 to 1.2 while in larger GF range the same trends were not observed. Peak intensities showed opposite directions for nitrate and sulfate in GF 1.5-1.7 range with stronger nitrate peaks and smaller sulfate peaks. Except the general nonlinearity of peak intensities is subjected to variations with different particle types. The peak intensity analysis suggested the reduced hygroscopicity of sea salt particles. A unique Ammonium/OC particle type was identified to have a GF mode centered at 1.2, which is assumed to originate from coal combustion.after atmospheric aging.

In this study, basedBased on the obtained hygroscopicity established connections between composition relationsand composition, we developed a new statistical method to estimate particle hygroscopicity just from its single particle mass spectra. Individual The method was tested in a period of ATOFMS data in Shanghai. The estimated GF of individual particles suggested that ATOFMS particles were differentiated by the estimated hygroscopicity into various modes. Consistent with the HTDMApresent in similar hygroscopicity measurements, our estimatedmodes as HTDMA measurement on ambient aerosol. We discriminated particles into NH, LH, MH and SS mode by the GF of individual particles. Particle type contributions to the these hygroscopicity distribution shows three modes, namely near hydrophobic (NH) mode, more hygroscopic mode (MH) and sea salt mode. The temporal profiles of estimated suggested

40

996 consistent results with HTDMA-ATOFMS dataset. Based on the combined information on

997 particle composition, hygroscopicity ~~distributions can explain the variations of visibilities.~~

998 ~~This~~and airmass back trajectories, we inferred that the POA/EC, SOA, SIA and salts are the

999 characteristic compositions for particles in the NH, LH, MH, SS modes, respectively. The

1000 proposed method is a novel way of single particle mass spectrometry data analysis, which

1001 would provide ~~critical new~~additional information ~~on particulate water content,~~to the study of

1002 particle mixing states, source ~~apportionment and aging process.~~

identification**REFERENCES**

Andreae, M. O., and Rosenfeld, D.: Aerosol-cloud-precipitation interactions. Part 1. The nature and sources of cloud-active aerosols, Earth-Sci. Rev., 89, 13-41, 10.1016/j.earscirev.2008.03.001, 2008.

Angelino, S., Suess, D. T., and Prather, K. A.: Formation of aerosol particles from reactions of secondary and tertiary alkylamines: Characterization by aerosol time-of-flight mass spectrometry, Environmental Science & Technology, 35, 3130-3138, 10.1021/es0015444, 2001.

Buzorius, G., Zelenyuk, A., Brechtel, F., and Imre, D.: Simultaneous determination of individual ambient particle size, hygroscopicity and composition, Geophysical Research Letters, 29, 1974 10.1029/2001gl014221, 2002.

Chen, J., Zhao, C. S., Ma, N., Liu, P. F., Gobel, T., Hallbauer, E., Deng, Z. Z., Ran, L., Xu, W. Y., Liang, Z., Liu, H. J., Yan, P., Zhou, X. J., and Wiedensohler, A.: A parameterization of low visibilities for hazy days in the North China Plain, Atmospheric Chemistry and Physics, 12, 4935-4950, 10.5194/acp-12-4935-2012, 2012.

Chen, Y., Tian, M., Huang, R.-J., Shi, G., Wang, H., Peng, C., Cao, J., Wang, Q., Zhang, S., Guo, D., Zhang, L., and Yang, F.: Characterization of urban amine-containing particles in southwestern China: seasonal variation, source, and processing, Atmospheric Chemistry and Physics, 19, 3245-3255, 10.5194/acp-19-3245-2019, 2019.

Cheng, Y. F., Wiedensohler, A., Eichler, H., Heintzenberg, J., Tesche, M., Ansmann, A., Wendisch, M., Su, H., Althausen, D., Herrmann, H., Gnauk, T., Bruggemann, E., Hu, M., and Zhang, Y. H.: Relative humidity dependence of aerosol optical properties and direct radiative forcing in the surface boundary layer at Xinken in Pearl River Delta of China: An observation based numerical study, Atmospheric Environment, 42, 6373-6397, 10.1016/j.atmosenv.2008.04.009, 2008.

Crippa, M., DeCarlo, P. F., Slowik, J. G., Mohr, C., Heringa, M. F., Chirico, R., Poulain, L., Freutel, F., Sciare, J., Cozic, J., Di Marco, C. F., Elsasser, M., Nicolas, J. B., Marchand, N., Abidi, E., Wiedensohler, A., Drewnick, F., Schneider, J., Borrmann, S., Nemitz, E., Zimmermann, R., Jaffrezo, J. L., Prevot, A. S. H., and Baltensperger, U.: Wintertime aerosol chemical composition and source apportionment of the organic fraction in the metropolitan area of Paris, Atmospheric Chemistry and Physics, 13, 961-981, 10.5194/acp-13-961-2013, 2013.

Dall'Osto, M., Booth, M. J., Smith, W., Fisher, R., and Harrison, R. M.: A study of the size distributions and the chemical characterization of airborne particles in the vicinity of a large integrated steelworks, Aerosol Science and Technology, 42, 981-991, 10.1080/02786820802339587, 2008.

Dall'Osto, M., and Harrison, R. M.: Urban organic aerosols measured by single particle mass spectrometry in the megacity of London, Atmospheric Chemistry and Physics, 12, 4127-4142, 10.5194/acp-12-4127-2012, 2012.

Dall'Osto, M., Ovadnevaite, J., Ceburnis, D., Martin, D., Healy, R. M., O'Connor, I. P., Kourtchev,

I., Sodeau, J. R., Wenger, J. C., and O'Dowd, C.: Characterization of urban aerosol in Cork city (Ireland) using aerosol mass spectrometry, Atmos. Chem. Phys., 13, 4997-5015, 10.5194/acp-13-4997-2013, 2013.

Denkenberger, K. A., Moffet, R. C., Holecek, J. C., Rebotier, T. P., and Prather, K. A.: Real-time, single-particle measurements of oligomers in aged ambient aerosol particles, Environmental Science & Technology, 41, 5439-5446, 10.1021/es070329l, 2007.

Facchini, M. C., Mircea, M., Fuzzi, S., and Charlson, R. J.: Cloud albedo enhancement by surface-active organic solutes in growing droplets, Nature, 401, 257-259, 10.1038/45758, 1999.

Facchini, M. C., Rinaldi, M., Decesari, S., Carbone, C., Finessi, E., Mircea, M., Fuzzi, S., Ceburnis, D., Flanagan, R., and Nilsson, E. D.: Primary submicron marine aerosol dominated by insoluble organic colloids and aggregates, Geophysical Research Letters, 35, 2008.

Gard, E., Mayer, J. E., Morrical, B. D., Dienes, T., Fergenson, D. P., and Prather, K. A.: Real-time analysis of individual atmospheric aerosol particles: Design and performance of a portable ATOFMS, Analytical Chemistry, 69, 4083-4091, 10.1021/ac970540n, 1997.

Gard, E. E., Kleeman, M. J., Gross, D. S., Hughes, L. S., Allen, J. O., Morrical, B. D., Fergenson, D. P., Dienes, T., Galli, M. E., Johnson, R. J., Cass, G. R., and Prather, K. A.: Direct observation of heterogeneous chemistry in the atmosphere, Science, 279, 1184-1187, 10.1126/science.279.5354.1184, 1998.

Gysel, M., Crosier, J., Topping, D. O., Whitehead, J. D., Bower, K. N., Cubison, M. J., Williams, P. I., Flynn, M. J., McFiggans, G. B., and Coe, H.: Closure study between chemical composition and hygroscopic growth of aerosol particles during TORCH2, Atmospheric Chemistry and Physics, 7, 6131-6144, 2007.

Healy, R. M., Hellebust, S., Kourtchev, I., Allanic, A., O'Connor, I. P., Bell, J. M., Healy, D. A., Sodeau, J. R., and Wenger, J. C.: Source apportionment of PM2.5 in Cork Harbour, Ireland using a combination of single particle mass spectrometry and quantitative semi-continuous measurements, Atmospheric Chemistry and Physics, 10, 9593-9613, 10.5194/acp-10-9593-2010, 2010.

Healy, R. M., Evans, G. J., Murphy, M., Juranyi, Z., Tritscher, T., Laborde, M., Weingartner, E., Gysel, M., Poulain, L., Kamilli, K. A., Wiedensohler, A., O'Connor, I. P., McGillicuddy, E., Sodeau, J. R., and Wenger, J. C.: Predicting hygroscopic growth using single particle chemical composition estimates, Journal of Geophysical Research-Atmospheres, 119, 9567-9577, 10.1002/2014jd021888, 2014.

Herich, H., Kammermann, L., Gysel, M., Weingartner, E., Baltensperger, U., Lohmann, U., and Cziczo, D. J.: In situ determination of atmospheric aerosol composition as a function of hygroscopic growth, Journal of Geophysical Research-Atmospheres, 113, D16213 10.1029/2008jd009954, 2008.

Herich, H., Kammermann, L., Friedman, B., Gross, D. S., Weingartner, E., Lohmann, U., Spichtinger, P., Gysel, M., Baltensperger, U., and Cziczo, D. J.: Subarctic atmospheric aerosol

composition: 2. Hygroscopic growth properties, Journal of Geophysical Research-Atmospheres, 114, D13204 10.1029/2008jd011574, 2009.

Herich, H., Hueglin, C., and Buchmann, B.: A 2.5 year's source apportionment study of black carbon from wood burning and fossil fuel combustion at urban and rural sites in Switzerland, Atmospheric Measurement Techniques, 4, 1409-1420, 10.5194/amt-4-1409-2011, 2011.

Kamilli, K. A., Poulain, L., Held, A., Nowak, A., Birmili, W., and Wiedensohler, A.: Hygroscopic properties of the Paris urban aerosol in relation to its chemical composition, Atmospheric Chemistry and Physics, 14, 737-749, 10.5194/acp-14-737-2014, 2014.

Koehler, K. A., Kreidenweis, S. M., DeMott, P. J., Petters, M. D., Prenni, A. J., and Carrico, C. M.: Hygroscopicity and cloud droplet activation of mineral dust aerosol, Geophysical Research Letters, 36, L08805 10.1029/2009gl037348, 2009.

Laborde, M., Crippa, M., Tritscher, T., Juranyi, Z., Decarlo, P. F., Temime-Roussel, B., Marchand, N., Eckhardt, S., Stohl, A., Baltensperger, U., Prevot, A. S. H., Weingartner, E., and Gysel, M.: Black carbon physical properties and mixing state in the European megacity Paris, Atmospheric Chemistry and Physics, 13, 5831-5856, 10.5194/acp-13-5831-2013, 2013.

Li, H., Wang, Q. g., Yang, M., Li, F., Wang, J., Sun, Y., Wang, C., Wu, H., and Qian, X.: Chemical characterization and source apportionment of PM2.5 aerosols in a megacity of Southeast China, Atmospheric Research, 181, 288-299, 10.1016/j.atmosres.2016.07.005, 2016.

Li, K., Ye, X., Pang, H., Lu, X., Chen, H., Wang, X., Yang, X., Chen, J., and Chen, Y.: Temporal variations in the hygroscopicity and mixing state of black carbon aerosols in a polluted megacity area, Atmospheric Chemistry and Physics, 18, 15201-15218, 10.5194/acp-18-15201-2018, 2018.

Liu, H. J., Zhao, C. S., Nekat, B., Ma, N., Wiedensohler, A., van Pinxteren, D., Spindler, G., Muller, K., and Herrmann, H.: Aerosol hygroscopicity derived from size-segregated chemical composition and its parameterization in the North China Plain, Atmospheric Chemistry and Physics, 14, 2525-2539, 10.5194/acp-14-2525-2014, 2014.

Liu, P. F., Zhao, C. S., Gobel, T., Hallbauer, E., Nowak, A., Ran, L., Xu, W. Y., Deng, Z. Z., Ma, N., Mildenberger, K., Henning, S., Stratmann, F., and Wiedensohler, A.: Hygroscopic properties of aerosol particles at high relative humidity and their diurnal variations in the North China Plain, Atmospheric Chemistry and Physics, 11, 3479-3494, 10.5194/acp-11-3479-2011, 2011.

Liu, X. G., Zhang, Y. H., Cheng, Y. F., Hu, M., and Han, T. T.: Aerosol hygroscopicity and its impact on atmospheric visibility and radiative forcing in Guangzhou during the 2006 PRIDE-PRD campaign, Atmospheric Environment, 60, 59-67, 10.1016/j.atmosenv.2012.06.016, 2012degradation.

44

REFERENCES Lohmann, U., and Feichter, J.: Global indirect aerosol effects: a review, Atmospheric Chemistry and Physics, 5, 715-737, 2005.

Lohmann, U., Stier, P., Hoose, C., Ferrachat, S., Kloster, S., Roeckner, E., and Zhang, J.: Cloud microphysics and aerosol indirect effects in the global climate model ECHAM5 HAM, Atmospheric Chemistry and Physics, 7, 3425-3446, 2007.

Martin, M., Tritscher, T., Juranyi, Z., Heringa, M. F., Sierau, B., Weingartner, E., Chirico, R., Gysel, M., Prevot, A. S. H., Baltensperger, U., and Lohmann, U.: Hygroscopic properties of fresh and aged wood burning particles, Journal of Aerosol Science, 56, 15-29, 10.1016/j.jaerosci.2012.08.006, 2013.

Massling, A., Leinert, S., Wiedensohler, A., and Covert, D.: Hygroscopic growth of sub-micrometer and one-micrometer aerosol particles measured during ACE-Asia, Atmos. Chem. Phys., 7, 3249-3259, 10.5194/acp-7-3249-2007, 2007.

Pratt, K. A., Hatch, L. E., and Prather, K. A.: Seasonal Volatility Dependence of Ambient Particle Phase Amines, Environmental Science & Technology, 43, 5276-5281, 10.1021/es803189n, 2009.

Qiu, C., and Zhang, R. Y.: Multiphase chemistry of atmospheric amines, Physical Chemistry Chemical Physics, 15, 5738-5752, 10.1039/c3cp43446j, 2013.

Qu, W. J., Wang, J., Zhang, X. Y., Wang, D., and Sheng, L. F.: Influence of relative humidity on aerosol composition: Impacts on light extinction and visibility impairment at two sites in coastal area of China, Atmospheric Research, 153, 500-511, 10.1016/j.atmosres.2014.10.009, 2015.

Randles, C. A., Russell, L. M., and Ramaswamy, V.: Hygroscopic and optical properties of organic sea salt aerosol and consequences for climate forcing, Geophysical Research Letters, 31, 10.1029/2004gl020628, 2004.

Rissler, J., Vestin, A., Swietlicki, E., Fisch, G., Zhou, J., Artaxo, P., and Andreae, M. O.: Size distribution and hygroscopic properties of aerosol particles from dry season biomass burning in Amazonia, Atmospheric Chemistry and Physics, 6, 471-491, 2006.

Robinson, A. L., Subramanian, R., Donahue, N. M., Bernardo-Bricker, A., and Rogge, W. F.: Source apportionment of molecular markers and organic aerosol. 3. Food cooking emissions, Environmental Science & Technology, 40, 7820-7827, 10.1021/es060781p, 2006.

Shi, Y., Ge, M., and Wang, W.: Hygroscopicity of internally mixed aerosol particles containing benzoic acid and inorganic salts, Atmospheric Environment, 60, 9-17, http://dx.doi.org/10.1016/j.atmosenv.2012.06.034, 2012.

Silva, P. J., Liu, D. Y., Noble, C. A., and Prather, K. A.: Size and chemical characterization of individual particles resulting from biomass burning of local Southern California species, Environmental Science & Technology, 33, 3068-3076, 10.1021/es980544p, 1999.

Silva, P. J.: Source profiling and apportionment of airborne particles: A new approach using aerosol

time-of-flight mass spectrometry, Ph.D., University of California, Riverside, United States -- California, 428 428 p. pp., 2000.

Sjogren, S., Gysel, M., Weingartner, E., Alfarra, M. R., Duplissy, J., Cozic, J., Crosier, J., Coe, H., and Baltensperger, U.: Hygroscopicity of the submicrometer aerosol at the high alpine site Jungfraujoch, 3580 m a.s.l., Switzerland, Atmospheric Chemistry and Physics, 8, 5715-5729, 2008.

Song, X. H., Hopke, P. K., Fergenson, D. P., and Prather, K. A.: Classification of single particles analyzed by ATOFMS using an artificial neural network, ART 2A, Analytical Chemistry, 71, 860-865, 10.1021/ac9809682, 1999.

Su, Y. X., Sipin, M. F., Furutani, H., and Prather, K. A.: Development and characterization of an aerosol time-of-flight mass spectrometer with increased detection efficiency, Analytical Chemistry, 76, 712-719, 10.1021/ac034797z, 2004.

Swietlicki, E., Hansson, H. C., Hameri, K., Svenningsson, B., Massling, A., McFiggans, G., McMurry, P. H., Petaja, T., Tunved, P., Gysel, M., Topping, D., Weingartner, E., Baltensperger, U., Rissler, J., Wiedensohler, A., and Kulmala, M.: Hygroscopic properties of submicrometer atmospheric aerosol particles measured with H-TDMA instruments in various environments - a review, Tellus Series B-Chemical and Physical Meteorology, 60, 432-469, 10.1111/j.1600-0889.2008.00350.x, 2008.

Titos, G., Jefferson, A., Sheridan, P. J., Andrews, E., Lyamani, H., Alados-Arboledas, L., and Ogren, J. A.: Aerosol light-scattering enhancement due to water uptake during the TCAP campaign, Atmospheric Chemistry and Physics, 14, 7031-7043, 10.5194/acp-14-7031-2014, 2014.

Wang, X., Williams, B. J., Tang, Y., Huang, Y., Kong, L., Yang, X., and Biswas, P.: Characterization of organic aerosol produced during pulverized coal combustion in a drop tube furnace, Atmos. Chem. Phys., 13, 10919-10932, 10.5194/acp-13-10919-2013, 2013.

Wang, X., Shen, Y., Lin, Y., Pan, J., Zhang, Y., Louie, P. K. K., Li, M., and Fu, Q.: Atmospheric pollution from ships and its impact on local air quality at a port site in Shanghai, Atmos. Chem. Phys., 19, 6315-6330, 10.5194/acp-19-6315-2019, 2019.

Wang, X. F., Zhang, Y. P., Chen, H., Yang, X., Chen, J. M., and Geng, F. H.: Particulate Nitrate Formation in a Highly Polluted Urban Area: A Case Study by Single-Particle Mass Spectrometry in Shanghai, Environmental Science & Technology, 43, 3061-3066, 10.1021/es8020155, 2009.

Wang, X. N., Ye, X. N., Chen, H., Chen, J. M., Yang, X., and Gross, D. S.: Online hygroscopicity and chemical measurement of urban aerosol in Shanghai, China, Atmospheric Environment, 95, 318-326, 10.1016/j.atmosenv.2014.06.051, 2014.

Weingartner, E., Burtscher, H., and Baltensperger, U.: Hygroscopic properties of carbon and diesel soot particles, Atmospheric Environment, 31, 2311-2327, http://dx.doi.org/10.1016/S1352-2310(97)00023-X, 1997.

Ye, X., Tang, C., Yin, Z., Chen, J., Ma, Z., Kong, L., Yang, X., Gao, W., and Geng, F.: Hygroscopic

growth of urban aerosol particles during the 2009 Mirage-Shanghai Campaign, Atmospheric Environment, 64, 263-269, http://dx.doi.org/10.1016/j.atmosenv.2012.09.064, 2013.

Ye, X. N., Chen, T. Y., Hu, D. W., Yang, X., Chen, J. M., Zhang, R. Y., Khakuziv, A. F., and Wang, L.: A Multifunctional HTDMA System with a Robust Temperature Control, Advances in Atmospheric Sciences, 26, 1235-1240, 10.1007/s00376-009-8134-3, 2009.

Ye, X. N., Ma, Z., Hu, D. W., Yang, X., and Chen, J. M.: Size-resolved hygroscopicity of submicrometer urban aerosols in Shanghai during wintertime, Atmospheric Research, 99, 353-364, 10.1016/j.atmosres.2010.11.008, 2011.

Zelenyuk, A., Imre, D., Han, J. H., and Oatis, S.: Simultaneous measurements of individual ambient particle size, composition, effective density, and hygroscopicity, Analytical Chemistry, 80, 1401-1407, 10.1021/ac701723v, 2008.

Zhang, Q., Jimenez, J. L., Canagaratna, M. R., Allan, J. D., Coe, H., Ulbrich, I., Alfarra, M. R., Takami, A., Middlebrook, A. M., Sun, Y. L., Dzepina, K., Dunlea, E., Docherty, K., DeCarlo, P. F., Salcedo, D., Onasch, T., Jayne, J. T., Miyoshi, T., Shimono, A., Hatakeyama, S., Takegawa, N., Kondo, Y., Schneider, J., Drewnick, F., Borrmann, S., Weimer, S., Demerjian, K., Williams, P., Bower, K., Bahreini, R., Cottrell, L., Griffin, R. J., Rautiainen, J., Sun, J. Y., Zhang, Y. M., and Worsnop, D. R.: Ubiquity and dominance of oxygenated species in organic aerosols in anthropogenically-influenced Northern Hemisphere midlatitudes, Geophysical Research Letters, 34, L13801
10.1029/2007gl029979, 2007.

Zhang, Y. P., Wang, X. F., Chen, H., Yang, X., Chen, J. M., and Allen, J. O.: Source apportionment of lead-containing aerosol particles in Shanghai using single particle mass spectrometry, Chemosphere, 74, 501-507, 10.1016/j.chemosphere.2008.10.004, 2009.

Draxler, R. R. and Rolph, G. D.: HYSPLIT (Hybrid Single Particle Lagrangian Integrated Trajectory) model v 4.9, NOAA Air Resource Laboratory, Silver Spring MD, available at: http://www. arl.noaa.gov/ready/hysplit4.html, 2019.

AUTHOR CONTRIBUTION

Xinning Wang designed this study and conducted the experiments. Xiaofei Wang and Xin Yang supervised this study and help with experiment design. Xinning Wang, Xiaofei Wang and Xin Yang wrote the manuscript.

DATA AVAILABILITY

1219 Angelino, S., Suess, D. T., and Prather, K. A.: Formation of aerosol particles from reactions of
1220 secondary and tertiary alkylamines: Characterization by aerosol time-of-flight mass
1221 spectrometry, Environmental Science & Technology, 35, 3130-3138, 10.1021/es0015444, 2001.
1222 Ault, A. P., Gaston, C. J., Wang, Y., Dominguez, G., Thiemens, M. H., and Prather, K. A.:
1223 Characterization of the Single Particle Mixing State of Individual Ship Plume Events Measured
1224 at the Port of Los Angeles, Environmental Science & Technology, 44, 1954-1961,
1225 10.1021/es902985h, 2010.
1226 Ault, A. P., Williams, C. R., White, A. B., Neiman, P. J., Creamean, J. M., Gaston, C. J., Ralph,
1227 F. M., and Prather, K. A.: Detection of Asian dust in California orographic precipitation, Journal
1228 of Geophysical Research-Atmospheres, 116, 10.1029/2010jd015351, 2011.
1229 Buzorius, G., Zelenyuk, A., Brechtel, F., and Imre, D.: Simultaneous determination of
1230 individual ambient particle size, hygroscopicity and composition, Geophysical Research
1231 Letters, 29, 1974, 10.1029/2001gl014221, 2002.
1232 Chen, J., Zhao, C. S., Ma, N., Liu, P. F., Gobel, T., Hallbauer, E., Deng, Z. Z., Ran, L., Xu, W.
1233 Y., Liang, Z., Liu, H. J., Yan, P., Zhou, X. J., and Wiedensohler, A.: A parameterization of low
1234 visibilities for hazy days in the North China Plain, Atmospheric Chemistry and Physics, 12,
1235 4935-4950, 10.5194/acp-12-4935-2012, 2012.
1236 Chen, Y., Tian, M., Huang, R.-J., Shi, G., Wang, H., Peng, C., Cao, J., Wang, Q., Zhang, S.,
1237 Guo, D., Zhang, L., and Yang, F.: Characterization of urban amine-containing particles in
1238 southwestern China: seasonal variation, source, and processing, Atmospheric Chemistry and
1239 Physics, 19, 3245-3255, 10.5194/acp-19-3245-2019, 2019.
1240 Cheng, Y. F., Wiedensohler, A., Eichler, H., Heintzenberg, J., Tesche, M., Ansmann, A.,
1241 Wendisch, M., Su, H., Althausen, D., Herrmann, H., Gnauk, T., Bruggemann, E., Hu, M., and
1242 Zhang, Y. H.: Relative humidity dependence of aerosol optical properties and direct radiative
1243 forcing in the surface boundary layer at Xinken in Pearl River Delta of China: An observation
1244 based numerical study, Atmospheric Environment, 42, 6373-6397,
1245 10.1016/j.atmosenv.2008.04.009, 2008.
1246 Crippa, M., DeCarlo, P. F., Slowik, J. G., Mohr, C., Heringa, M. F., Chirico, R., Poulain, L.,
1247 Freutel, F., Sciare, J., Cozic, J., Di Marco, C. F., Elsasser, M., Nicolas, J. B., Marchand, N.,
1248 Abidi, E., Wiedensohler, A., Drewnick, F., Schneider, J., Borrmann, S., Nemitz, E.,
1249 Zimmermann, R., Jaffrezo, J. L., Prevot, A. S. H., and Baltensperger, U.: Wintertime aerosol
1250 chemical composition and source apportionment of the organic fraction in the metropolitan area
1251 of Paris, Atmospheric Chemistry and Physics, 13, 961-981, 10.5194/acp-13-961-2013, 2013.
1252 Dall'Osto, M., and Harrison, R. M.: Urban organic aerosols measured by single particle mass
1253 spectrometry in the megacity of London, Atmospheric Chemistry and Physics, 12, 4127-4142,
1254 10.5194/acp-12-4127-2012, 2012.
1255 Dall'Osto, M., Ovadnevaite, J., Ceburnis, D., Martin, D., Healy, R. M., O'Connor, I. P.,
1256 Kourtchev, I., Sodeau, J. R., Wenger, J. C., and O'Dowd, C.: Characterization of urban aerosol
1257 in Cork city (Ireland) using aerosol mass spectrometry, Atmos. Chem. Phys., 13, 4997-5015,
1258 10.5194/acp-13-4997-2013, 2013.

Draxler, R. R. and Rolph, G. D., HYSPLIT (Hybrid Single-Particle Lagrangian Integrated Trajectory) model v 4.9, NOAA Air Resource Laboratory, Silver Spring MD, available at: http://www. arl.noaa.gov/ready/hysplit4.html, 2019.

Facchini, M. C., Mircea, M., Fuzzi, S., and Charlson, R. J.: Cloud albedo enhancement by surface-active organic solutes in growing droplets, Nature, 401, 257-259, 10.1038/45758, 1999.

Facchini, M. C., Rinaldi, M., Decesari, S., Carbone, C., Finessi, E., Mircea, M., Fuzzi, S., Ceburnis, D., Flanagan, R., and Nilsson, E. D.: Primary submicron marine aerosol dominated by insoluble organic colloids and aggregates, Geophysical Research Letters, 35, 2008.

Gard, E. E., Kleeman, M. J., Gross, D. S., Hughes, L. S., Allen, J. O., Morrical, B. D., Fergenson, D. P., Dienes, T., Galli, M. E., Johnson, R. J., Cass, G. R., and Prather, K. A.: Direct observation of heterogeneous chemistry in the atmosphere, Science, 279, 1184-1187, 10.1126/science.279.5354.1184, 1998.

Gaston, C. J., Furutani, H., Guazzotti, S. A., Coffee, K. R., Bates, T. S., Quinn, P. K., Aluwihare, L. I., Mitchell, B. G., and Prather, K. A.: Unique ocean-derived particles serve as a proxy for changes in ocean chemistry, Journal of Geophysical Research: Atmospheres, 116, 10.1029/2010jd015289, 2011.

Gaston, C. J., Pratt, K. A., Suski, K. J., May, N. W., Gill, T. E., and Prather, K. A.: Laboratory Studies of the Cloud Droplet Activation Properties and Corresponding Chemistry of Saline Playa Dust, Environmental Science & Technology, 51, 1348-1356, 10.1021/acs.est.6b04487, 2017.

Gaston, C. J., Cahill, J. F., Collins, D. B., Suski, K. J., Ge, J. Y., Barkley, A. E., and Prather, K. A.: The Cloud Nucleating Properties and Mixing State of Marine Aerosols Sampled along the Southern California Coast, Atmosphere, 9, 52, 2018.

Gysel, M., Crosier, J., Topping, D. O., Whitehead, J. D., Bower, K. N., Cubison, M. J., Williams, P. I., Flynn, M. J., McFiggans, G. B., and Coe, H.: Closure study between chemical composition and hygroscopic growth of aerosol particles during TORCH2, Atmospheric Chemistry and Physics, 7, 6131-6144, 2007.

Hatch, L. E., Pratt, K. A., Huffman, J. A., Jimenez, J. L., and Prather, K. A.: Impacts of Aerosol Aging on Laser Desorption/Ionization in Single-Particle Mass Spectrometers, Aerosol Science and Technology, 48, 1050-1058, 10.1080/02786826.2014.955907, 2014.

Healy, R. M., Evans, G. J., Murphy, M., Juranyi, Z., Tritscher, T., Laborde, M., Weingartner, E., Gysel, M., Poulain, L., Kamilli, K. A., Wiedensohler, A., O'Connor, I. P., McGillicuddy, E., Sodeau, J. R., and Wenger, J. C.: Predicting hygroscopic growth using single particle chemical composition estimates, Journal of Geophysical Research-Atmospheres, 119, 9567-9577, 10.1002/2014jd021888, 2014.

Herich, H., Kammermann, L., Gysel, M., Weingartner, E., Baltensperger, U., Lohmann, U., and Cziczo, D. J.: In situ determination of atmospheric aerosol composition as a function of hygroscopic growth, Journal of Geophysical Research-Atmospheres, 113, D16213, 10.1029/2008jd009954, 2008.

Herich, H., Kammermann, L., Friedman, B., Gross, D. S., Weingartner, E., Lohmann, U., Spichtinger, P., Gysel, M., Baltensperger, U., and Cziczo, D. J.: Subarctic atmospheric aerosol composition: 2. Hygroscopic growth properties, Journal of Geophysical Research-Atmospheres, 114, D13204, 10.1029/2008jd011574, 2009.

Hu, D., Qiao, L., Chen, J., Ye, X., Yang, X., Cheng, T., and Fang, W.: Hygroscopicity of

1303 Inorganic Aerosols: Size and Relative Humidity Effects on the Growth Factor, Aerosol and Air
1304 Quality Research, 10, 255-264, 10.4209/aaqr.2009.12.0076, 2010.
1305 Huang, Y., Chen, H., Wang, L., Yang, X., and Chen, J.: Single particle analysis of amines in
1306 ambient aerosol in Shanghai, Environmental Chemistry, 9, 202-210, 10.1071/en11145, 2012.
1307 Koehler, K. A., Kreidenweis, S. M., DeMott, P. J., Petters, M. D., Prenni, A. J., and Carrico, C.
1308 M.: Hygroscopicity and cloud droplet activation of mineral dust aerosol, Geophysical Research
1309 Letters, 36, L08805, 10.1029/2009gl037348, 2009.
1310 Laborde, M., Crippa, M., Tritscher, T., Juranyi, Z., Decarlo, P. F., Temime-Roussel, B.,
1311 Marchand, N., Eckhardt, S., Stohl, A., Baltensperger, U., Prevot, A. S. H., Weingartner, E., and
1312 Gysel, M.: Black carbon physical properties and mixing state in the European megacity Paris,
1313 Atmospheric Chemistry and Physics, 13, 5831-5856, 10.5194/acp-13-5831-2013, 2013.
1314 Liu, H. J., Zhao, C. S., Nekat, B., Ma, N., Wiedensohler, A., van Pinxteren, D., Spindler, G.,
1315 Muller, K., and Herrmann, H.: Aerosol hygroscopicity derived from size-segregated chemical
1316 composition and its parameterization in the North China Plain, Atmospheric Chemistry and
1317 Physics, 14, 2525-2539, 10.5194/acp-14-2525-2014, 2014.
1318 Liu, P. F., Zhao, C. S., Gobel, T., Hallbauer, E., Nowak, A., Ran, L., Xu, W. Y., Deng, Z. Z., Ma,
1319 N., Mildenberger, K., Henning, S., Stratmann, F., and Wiedensohler, A.: Hygroscopic properties
1320 of aerosol particles at high relative humidity and their diurnal variations in the North China
1321 Plain, Atmospheric Chemistry and Physics, 11, 3479-3494, 10.5194/acp-11-3479-2011, 2011.
1322 Liu, X. G., Zhang, Y. H., Cheng, Y. F., Hu, M., and Han, T. T.: Aerosol hygroscopicity and its
1323 impact on atmospheric visibility and radiative forcing in Guangzhou during the 2006 PRIDE-
1324 PRD campaign, Atmospheric Environment, 60, 59-67, 10.1016/j.atmosenv.2012.06.016, 2012.
1325 Lohmann, U., and Feichter, J.: Global indirect aerosol effects: a review, Atmospheric Chemistry
1326 and Physics, 5, 715-737, 2005.
1327 Petters, M. D., and Kreidenweis, S. M.: A single parameter representation of hygroscopic
1328 growth and cloud condensation nucleus activity, Atmospheric Chemistry and Physics, 7, 1961-
1329 1971, 2007.
1330 Prather, K. A., Bertram, T. H., Grassian, V. H., Deane, G. B., Stokes, M. D., DeMott, P. J.,
1331 Aluwihare, L. I., Palenik, B. P., Azam, F., Seinfeld, J. H., Moffet, R. C., Molina, M. J., Cappa,
1332 C. D., Geiger, F. M., Roberts, G. C., Russell, L. M., Ault, A. P., Baltrusaitis, J., Collins, D. B.,
1333 Corrigan, C. E., Cuadra-Rodriguez, L. A., Ebben, C. J., Forestieri, S. D., Guasco, T. L., Hersey,
1334 S. P., Kim, M. J., Lambert, W. F., Modini, R. L., Mui, W., Pedler, B. E., Ruppel, M. J., Ryder,
1335 O. S., Schoepp, N. G., Sullivan, R. C., and Zhao, D.: Bringing the ocean into the laboratory to
1336 probe the chemical complexity of sea spray aerosol, Proceedings of the National Academy of
1337 Sciences, 201300262, 10.1073/pnas.1300262110, 2013.
1338 Pratt, K. A., Hatch, L. E., and Prather, K. A.: Seasonal Volatility Dependence of Ambient
1339 Particle Phase Amines, Environmental Science & Technology, 43, 5276-5281,
1340 10.1021/es803189n, 2009.
1341 Pratt, K. A., and Prather, K. A.: Real-Time, Single-Particle Volatility, Size, and Chemical
1342 Composition Measurements of Aged Urban Aerosols, Environmental Science & Technology,
1343 43, 8276-8282, 10.1021/es902002t, 2009.
1344 Qin, X. Y., Pratt, K. A., Shields, L. G., Toner, S. M., and Prather, K. A.: Seasonal comparisons
1345 of single-particle chemical mixing state in Riverside, CA, Atmospheric Environment, 59, 587-
1346 596, 10.1016/j.atmosenv.2012.05.032, 2012.

1347 Qiu, C., and Zhang, R. Y.: Multiphase chemistry of atmospheric amines, Physical Chemistry
1348 Chemical Physics, 15, 5738-5752, 10.1039/c3cp43446j, 2013.
1349 Qu, W. J., Wang, J., Zhang, X. Y., Wang, D., and Sheng, L. F.: Influence of relative humidity
1350 on aerosol composition: Impacts on light extinction and visibility impairment at two sites in
1351 coastal area of China, Atmospheric Research, 153, 500-511, 10.1016/j.atmosres.2014.10.009,
1352 2015.
1353 Randles, C. A., Russell, L. M., and Ramaswamy, V.: Hygroscopic and optical properties of
1354 organic sea salt aerosol and consequences for climate forcing, Geophysical Research Letters,
1355 31, 10.1029/2004gl020628, 2004.
1356 Rehbein, P. J. G., Jeong, C.-H., McGuire, M. L., and Evans, G. J.: Strategies to Enhance the
1357 Interpretation of Single-Particle Ambient Aerosol Data, Aerosol Science and Technology, 46,
1358 584-595, 10.1080/02786826.2011.650334, 2012.
1359 Rissler, J., Vestin, A., Swietlicki, E., Fisch, G., Zhou, J., Artaxo, P., and Andreae, M. O.: Size
1360 distribution and hygroscopic properties of aerosol particles from dry-season biomass burning
1361 in Amazonia, Atmospheric Chemistry and Physics, 6, 471-491, 2006.
1362 Shi, Y., Ge, M., and Wang, W.: Hygroscopicity of internally mixed aerosol particles containing
1363 benzoic acid and inorganic salts, Atmospheric Environment, 60, 9-17, 2012.
1364 Silva, P. J., Liu, D. Y., Noble, C. A., and Prather, K. A.: Size and chemical characterization of
1365 individual particles resulting from biomass burning of local Southern California species,
1366 Environmental Science & Technology, 33, 3068-3076, 10.1021/es980544p, 1999.
1367 Silva, P. J.: Source profiling and apportionment of airborne particles: A new approach using
1368 aerosol time-of-flight mass spectrometry, Ph.D., University of California, Riverside, United
1369 States -- California, 428-428 p. pp., 2000.
1370 Sjogren, S., Gysel, M., Weingartner, E., Alfarra, M. R., Duplissy, J., Cozic, J., Crosier, J., Coe,
1371 H., and Baltensperger, U.: Hygroscopicity of the submicrometer aerosol at the high-alpine site
1372 Jungfraujoch, 3580 m a.s.l., Switzerland, Atmospheric Chemistry and Physics, 8, 5715-5729,
1373 2008.
1374 Song, X. H., Hopke, P. K., Fergenson, D. P., and Prather, K. A.: Classification of single particles
1375 analyzed by ATOFMS using an artificial neural network, ART-2A, Analytical Chemistry, 71,
1376 860-865, 10.1021/ac9809682, 1999.
1377 Spencer, M. T., Shields, L. G., Sodeman, D. A., Toner, S. M., and Prather, K. A.: Comparison
1378 of oil and fuel particle chemical signatures with particle emissions from heavy and light duty
1379 vehicles, Atmospheric Environment, 40, 5224-5235, 10.1016/j.atmosenv.2006.04.011, 2006.
1380 Su, Y. X., Sipin, M. F., Furutani, H., and Prather, K. A.: Development and characterization of
1381 an aerosol time-of-flight mass spectrometer with increased detection efficiency, Analytical
1382 Chemistry, 76, 712-719, 10.1021/ac034797z, 2004.
1383 Sullivan, R. C., Guazzotti, S. A., Sodeman, D. A., and Prather, K. A.: Direct observations of the
1384 atmospheric processing of Asian mineral dust, Atmospheric Chemistry and Physics, 7, 1213-
1385 1236, 2007.
1386 Swietlicki, E., Hansson, H. C., Hameri, K., Svenningsson, B., Massling, A., McFiggans, G.,
1387 McMurry, P. H., Petaja, T., Tunved, P., Gysel, M., Topping, D., Weingartner, E., Baltensperger,
1388 U., Rissler, J., Wiedensohler, A., and Kulmala, M.: Hygroscopic properties of submicrometer
1389 atmospheric aerosol particles measured with H-TDMA instruments in various environments -
1390 a review, Tellus Series B-Chemical and Physical Meteorology, 60, 432-469, 10.1111/j.1600-

0889.2008.00350.x, 2008.

Toner, S. M., Shields, L. G., Sodeman, D. A., and Prather, K. A.: Using mass spectral source signatures to apportion exhaust particles from gasoline and diesel powered vehicles in a freeway study using UF-ATOFMS, Atmospheric Environment, 42, 568-581, 10.1016/j.atmosenv.2007.08.005, 2008.

Varutbangkul, V., Brechtel, F. J., Bahreini, R., Ng, N. L., Keywood, M. D., Kroll, J. H., Flagan, R. C., Seinfeld, J. H., Lee, A., and Goldstein, A. H.: Hygroscopicity of secondary organic aerosols formed by oxidation of cycloalkenes, monoterpenes, sesquiterpenes, and related compounds, Atmospheric Chemistry and Physics, 6, 2367-2388, 2006.

Wang, X. N., Ye, X. N., Chen, H., Chen, J. M., Yang, X., and Gross, D. S.: Online hygroscopicity and chemical measurement of urban aerosol in Shanghai, China, Atmospheric Environment, 95, 318-326, 10.1016/j.atmosenv.2014.06.051, 2014.

Weingartner, E., Burtscher, H., and Baltensperger, U.: Hygroscopic properties of carbon and diesel soot particles, Atmospheric Environment, 31, 2311-2327, 1997.

Ye, X., Tang, C., Yin, Z., Chen, J., Ma, Z., Kong, L., Yang, X., Gao, W., and Geng, F.: Hygroscopic growth of urban aerosol particles during the 2009 Mirage-Shanghai Campaign, Atmospheric Environment, 64, 263-269, 2013.

Ye, X. N., Chen, T. Y., Hu, D. W., Yang, X., Chen, J. M., Zhang, R. Y., Khakuziv, A. F., and Wang, L.: A Multifunctional HTDMA System with a Robust Temperature Control, Advances in Atmospheric Sciences, 26, 1235-1240, 10.1007/s00376-009-8134-3, 2009.

Ye, X. N., Ma, Z., Hu, D. W., Yang, X., and Chen, J. M.: Size-resolved hygroscopicity of submicrometer urban aerosols in Shanghai during wintertime, Atmospheric Research, 99, 353-364, 10.1016/j.atmosres.2010.11.008, 2011.

Zauscher, M. D., Wang, Y., Moore, M. J. K., Gaston, C. J., and Prather, K. A.: Air Quality Impact and Physicochemical Aging of Biomass Burning Aerosols during the 2007 San Diego Wildfires, Environmental Science & Technology, 47, 7633-7643, 10.1021/es4004137, 2013.

Zelenyuk, A., Imre, D., Han, J. H., and Oatis, S.: Simultaneous measurements of individual ambient particle size, composition, effective density, and hygroscopicity, Analytical Chemistry, 80, 1401-1407, 10.1021/ac701723v, 2008.

Zhang, G., Bi, X., Chan, L. Y., Li, L., Wang, X., Feng, J., Sheng, G., Fu, J., Li, M., and Zhou, Z.: Enhanced trimethylamine-containing particles during fog events detected by single particle aerosol mass spectrometry in urban Guangzhou, China, Atmospheric Environment, 55, 121-126, 10.1016/j.atmosenv.2012.03.038, 2012.

Zhang, Q., Jimenez, J. L., Canagaratna, M. R., Allan, J. D., Coe, H., Ulbrich, I., Alfarra, M. R., Takami, A., Middlebrook, A. M., Sun, Y. L., Dzepina, K., Dunlea, E., Docherty, K., DeCarlo, P. F., Salcedo, D., Onasch, T., Jayne, J. T., Miyoshi, T., Shimono, A., Hatakeyama, S., Takegawa, N., Kondo, Y., Schneider, J., Drewnick, F., Borrmann, S., Weimer, S., Demerjian, K., Williams, P., Bower, K., Bahreini, R., Cottrell, L., Griffin, R. J., Rautiainen, J., Sun, J. Y., Zhang, Y. M., and Worsnop, D. R.: Ubiquity and dominance of oxygenated species in organic aerosols in anthropogenically-influenced Northern Hemisphere midlatitudes, Geophysical Research Letters, 34, L13801, 10.1029/2007gl029979, 2007.

~~COMPETING INTERESTS~~

~~The authors declare that they have no conflict of interest.~~

TABLES

Table 1. Statistics of the DRH, GF, sampling duration and the number of chemically analyzed particles by ATOFMS (D_{dry} = 250 nm, RH = 85%).

D_{RH} (nm)	225	250	275	300	325	350	375	400	425
Growth Factor	0.9	1.0	1.1	1.2	1.3	1.4	1.5	1.6	1.7
Duration (hours)	42	67	11	20	8	11	34	20	11
Number of particle spectra	742	1665	709	1401	2330	4469	6399	723	262

Table 2. Statistics on particle number contributions of ATOFMS particle types to different GF modes. The statistics are the average contributions and variation ranges (in brackets) based on temporal data in daily resolution.

Contribution (%)	NH (GF <1.1)	LH (GF 1.1-1.3)	MH (GF 1.3-1.5)	SS (GF >1.5)
Fresh EC	14 (7-17)	2 (1-4)	0 (0-3)	0 (0-1)
Cooking	3 (0-7)	1 (0-3)	0 (0-0)	0 (0-0)
Biomass	18 (7-35)	9 (2-17)	0 (0-1)	0 (0-0)
HMOC	40 (30-68)	8 (2-15)	0 (0-1)	0 (0-0)
Ammonium/OC	11 (3-21)	32 (20-45)	2 (1-5)	0 (0-0)
Aged EC	2 (1-5)	12 (5-20)	47 (15-72)	13 (1-42)
Dust/ash	3 (1-6)	13 (9-22)	27 (13-53)	26 (4-44)
Amine-rich	3 (1-5)	12 (2-41)	13 (4-39)	11 (1-44)
Sea salt	0 (0-1)	0 (0-1)	1 (0-4)	40 (7-78)

FIGURES

Figure 1. The schematic of HTDMA-ATOFMS characterization setup showing the major parts

of HTDMA (left), ATOFMS (right). The humidifier in HTDMA was maintained at 85% RH.
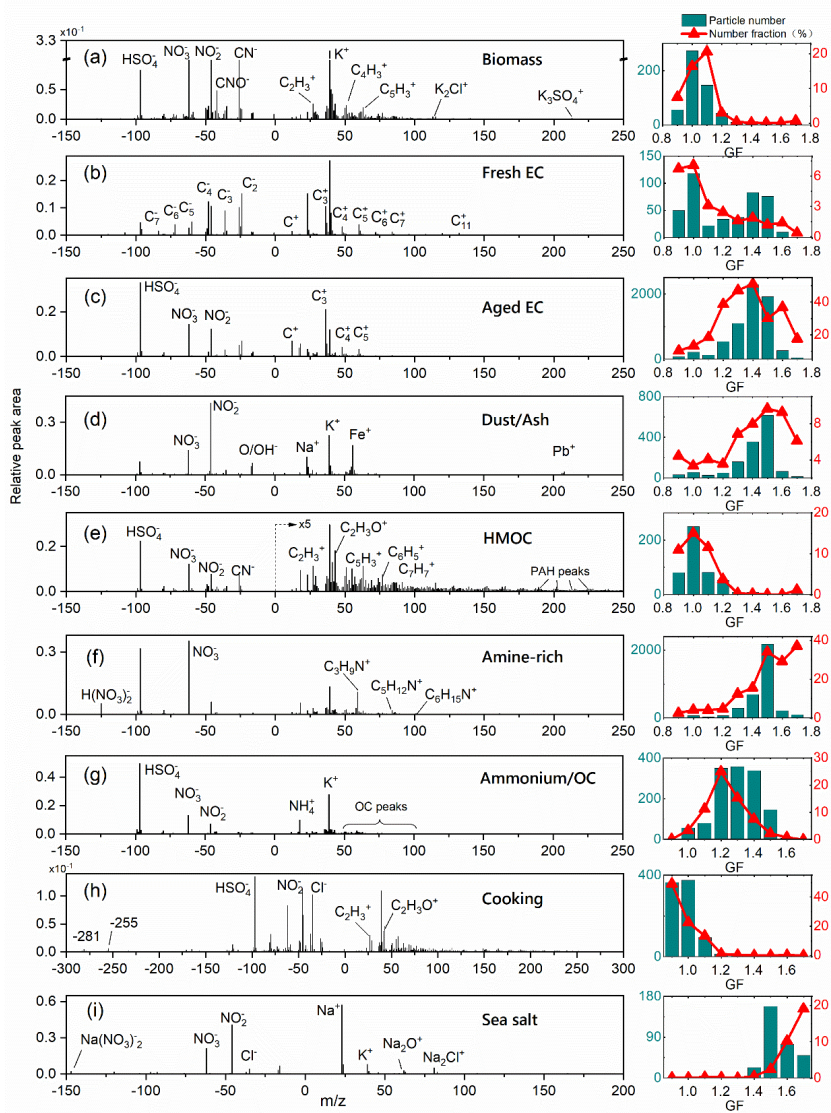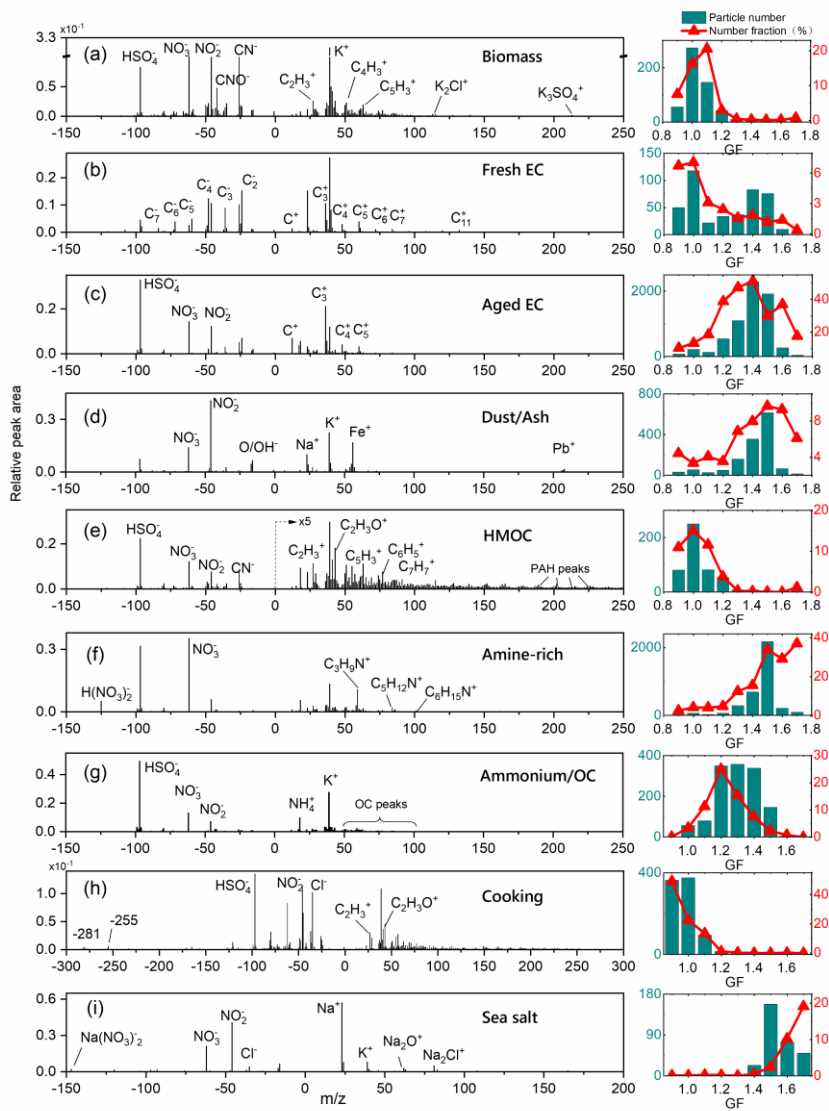
Figure 2. (Left panel) Averaged particle mass spectra of the major particle types detected in HTDMA-ATOFMS characterization. Peaks of significance were labelled. Right panels show the particle numbers of each type (left-axis) and their relative number fractions in total particles (right-axis) as a function of GF.
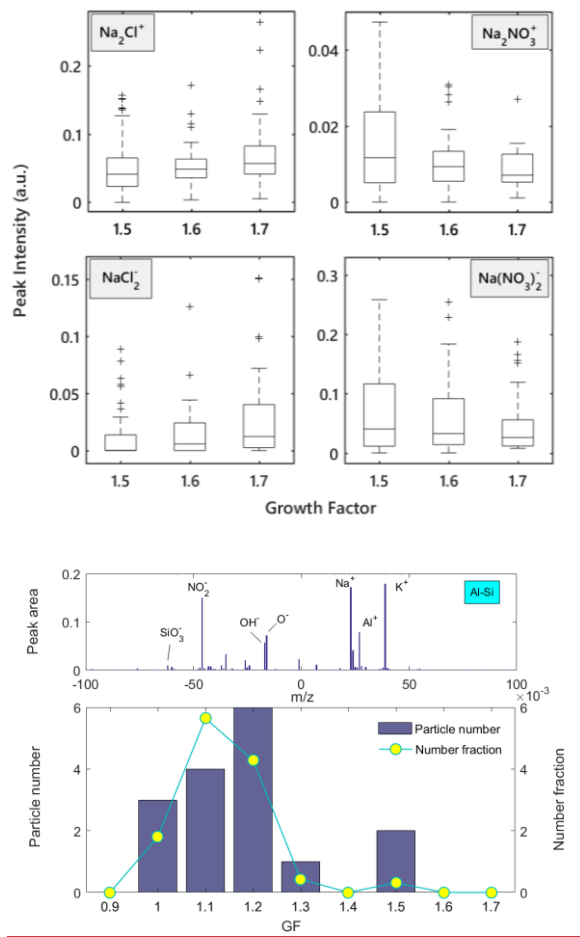
1461

1462

1463   Figure 3. Average mass spectra and hygroscopicity distribution of Al-Si particles.

1464
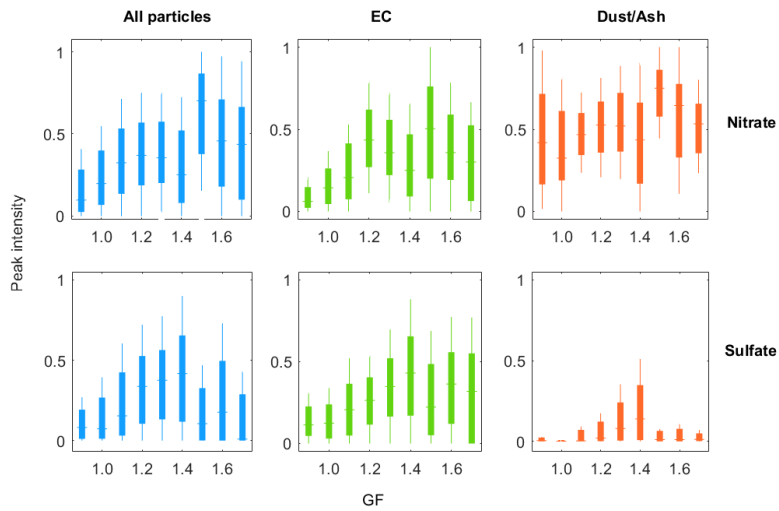
Figure 4. Statistics of ~~relevant~~nitrate and sulfate peak intensities (minimum, 25th percentile, median, 75th percentile, maximum) with GF in HTDMA-ATOFMS experiment. The intensity statistics were calculated for All particles, EC particles and Dust/Ash particles separately.
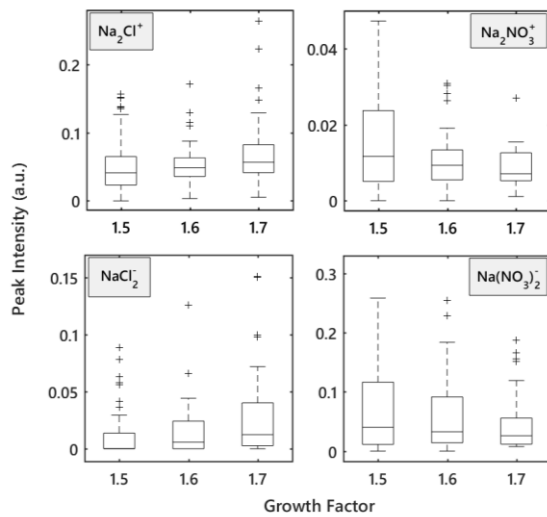
Figure 5. Statistics of peak intensities in sea salt particle mass spectra ~~detected at~~in GF 1.5-1.7 range. The statistics ~~are (from bottom to top): the~~include minimum, 25th percentile, median,

1472   75th percentile, maximum and outliers for each GF bin.

1473
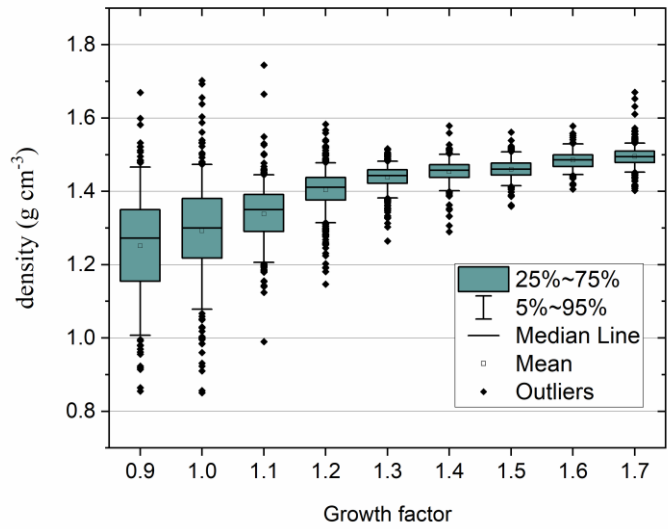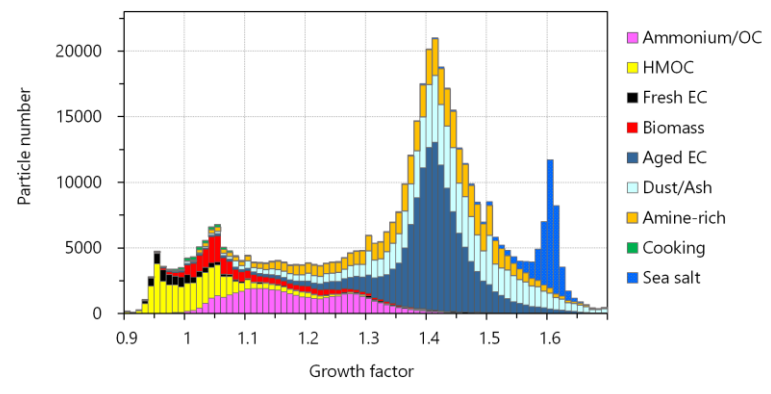
Figure ~~4~~6. Particle ~~effective densities~~number distribution of ~~particles~~different particle types as a function of ~~growth factor. The statistics are (from bottom~~estimated GF during Sep-12 to ~~top):~~ ~~the 5th percentile, 25th percentile, median, 75th percentile, 95th percentile and outliers~~Sep-28, 2012.

1481

1482
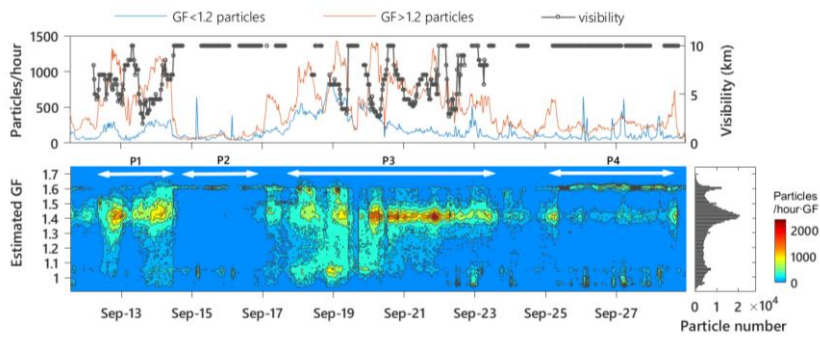
1483
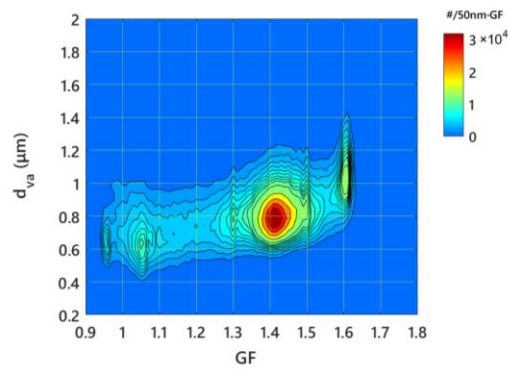
1484   ~~Figure 5. (Upper)~~

1485   Figure 7. The distribution of ATOFMS particles as a bivariate function of estimated GF and

1486   aerodynamic diameter.

1487
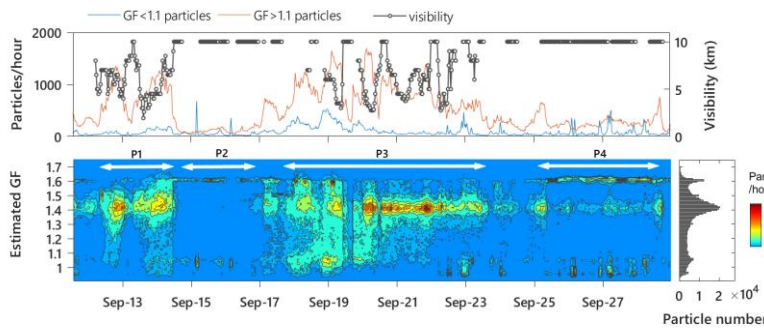
Figure 8. Temporal ~~variation~~variations of atmospheric visibility and ~~particle~~number concentrations of ~~Near Hydrophobic~~nearly-hydrophobic (estimated GF < 1.~~25~~1) and ~~More Hygroscopic~~hygroscopic (GF >1.~~25) mode. (Lower)~~1) particles (Upper). The ~~contour plot illustrates~~lower panel show the temporal variation of estimated GF from Sep-12 to Sep-28, 2012. ~~The~~In the lower-right panel ~~denotes~~is the particle number distribution ~~as a function of estimated~~with GF during the period.
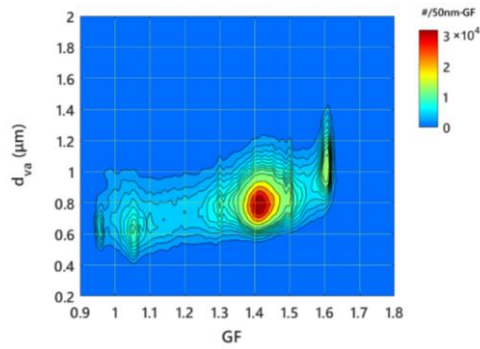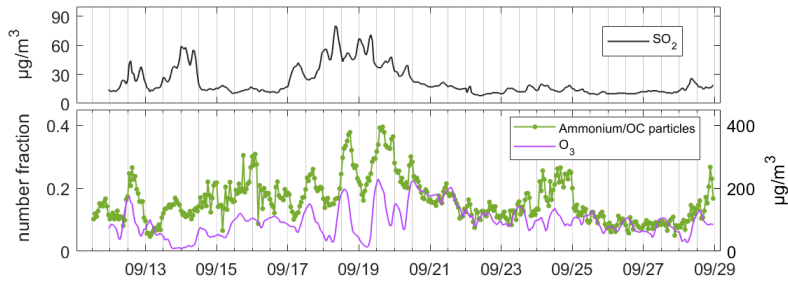
1497

Figure ~~6. Contour plot~~9. Temporal traces of ~~particle~~ Ammonium/OC relative number concentrations, ambient O_3 and SO_2 concentrations during Sep-12 to Sep-28, 2012

1500
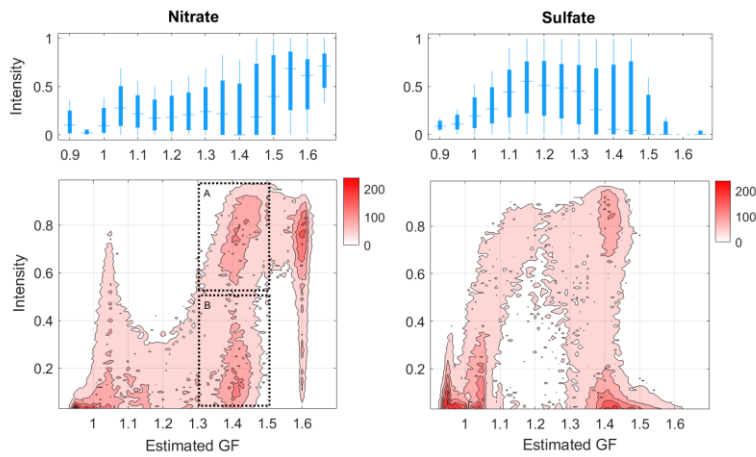
1501

1502 Figure 10. Statistics (minimum, 25th percentile, median, 75th percentile, maximum) on the nitrate

1503 and sulfate peak intensities of ambient particles at different GFs (upper). The lower panels show

1504 particle distributions as a bivariate function of estimated GF and ~~aerodynamic diameter measured~~

1505 ~~by ATOFMS.~~peak intensities of nitrate and sulfate.
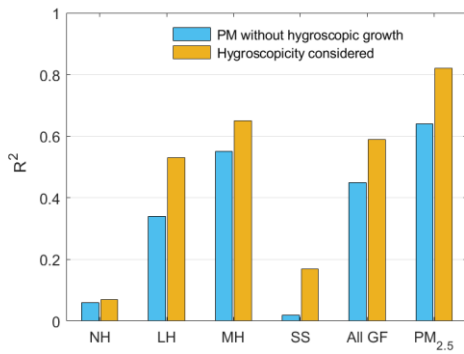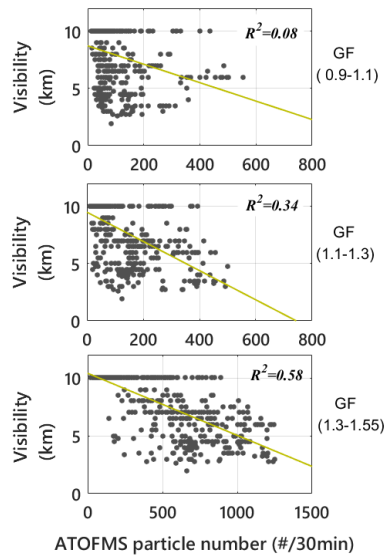
Figure ~~7. Correlation plots~~11. The R-squares between visibility and ~~ATOFMS~~ PM volume concentrations with and without considering particle ~~numbers with the estimated GF in 0.9-1.1, 1.1-1.3 and 1.3-1.55 range.~~
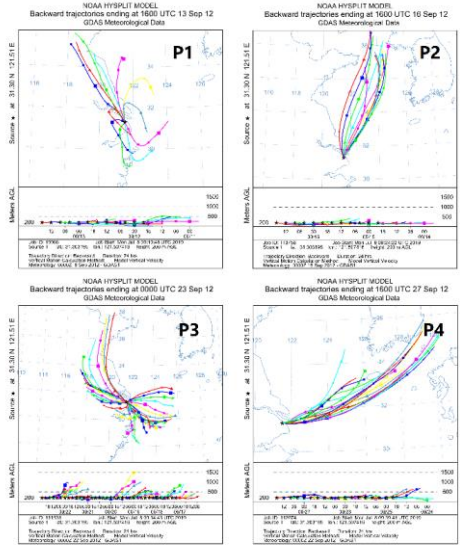
1512

1513 Figure 8. The 24 hour backward trajectories during P1 - P4 periods of the sampling site (by

1514 HYSPLIT model).
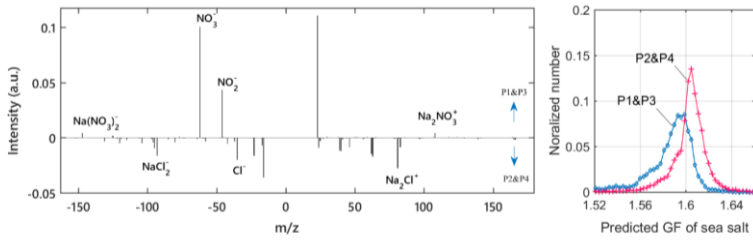
1515

1516 Figure 9. The differential mass spectrum between sea salt particles in (P1&P3) and (P2&P4).

1517 Positive peaks indicate they are larger in P1&P3 than P2&P4. The right figure shows the

1518 distributions of the predicted GF of sea salt in (P1&P3) and (P2&P4). Sea salt numbers were

1519 normalized by their total numbers.

1520
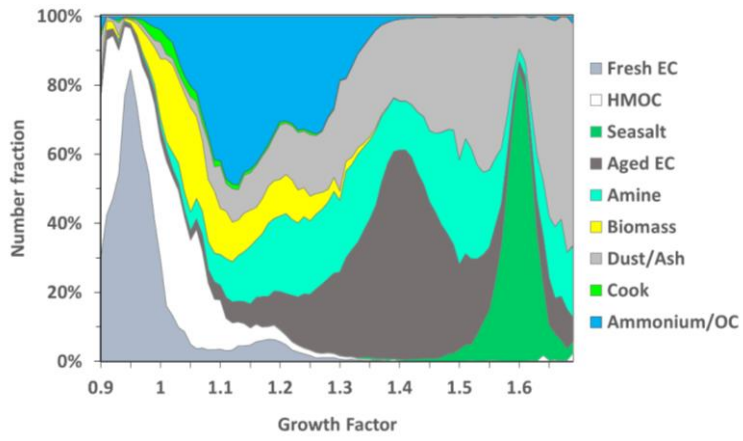
1521

Figure 10. The number fractions of ATOFMS particle types as a function of estimated
hygroscopicity during Sep 12 to Sep 28, 2012.

hygroscopicity